

**DEVELOPMENT OF AN IN VITRO PUMP:
MECHANICAL CHARACTERIZATION AND
SURFACE ENGINEERING OF ELASTOMERIC
MEMBRANES**

ISHA PAIK

**Thesis submitted to the University of Nottingham
for the degree of Doctor of Philosophy**

July 2013

Abstract

In vitro modelling offers the potential of recapitulating human degenerate tissue for physiological studies and pharmacological screening. Yet, few systems have been developed to date, primarily due to the lack of vascularisation in engineered tissue. Here, the development of an *in vitro* pump is addressed. This will be the first component of a long term strategy to build internal circulatory systems for *in vitro* engineered tissue. Firstly, mechanical characterisation and surface biocompatibility of spin coated poly(dimethylsiloxane) (PDMS) elastomeric membranes was investigated to assess whether PDMS could be used as a structural constituent. Results showed that spin coating speed defines both film thickness and specific mechanical properties since tensile testing revealed that PDMS membranes exhibit thickness-dependent mechanical properties. Plasma polymerisation of allylamine was used to surface engineer the hydrophobic PDMS surface to promote cell adhesion and proliferation. Surface characterisation revealed that PDMS surfaces became hydrophilic and nitrogen enriched as a result of plasma polymerised allylamine (ppAAm) deposition. Additionally, a thick ppAAm deposition (92 nm) is required to minimise hydrophobic recovery of PDMS. Cell culture studies showed that cells readily attached to ppAAm (92 nm)

deposited PDMS and that these surfaces were best suited to cultivating cells compared to other surface treatments.

Secondly, a method was developed to control cell positioning on the PDMS surface, since cell alignment is required to generate directional and contractile force. The deposition of ppAAm (92 nm) and airbrushing of extracellular matrix (ECM) aerosols can be spatially restricted using a micro-stencil. Individual and multiple cell line patterns were achieved that remained faithful for ≤ 10 days. Importantly, this technique micropatterned cells at high resolution over macro scales. External mechanical stimulation was used to influence cell alignment and cytoskeletal organisation on ppAAm (92 nm)/ Fibronectin (Fn) micropatterned PDMS. Results showed that incorporating substrate strain with surface micropatterning can be used to control site- and alignment- specific cell attachment.

Publications and presentations

The work presented in this thesis has given rise to the following publications and presentations.

Publications in peer-reviewed journals

Paik I., Scurr D.J., Morris B., Hall G., Denning C., Alexander M., Shakesheff K.M., Dixon J.E. (2012) Rapid micropatterning of cell lines and human pluripotent stem cells on elastomeric membranes. *Biotech. Bioeng.* 109(10), pp 2630-2641

Oral Presentations

Paik I., Dixon J.E., Muscular Tissue Engineering for Functional Force-generating Biological Devices. Presented at the BOSE user group annual conference, London (UK), April, 2011

Poster Presentations

Paik I., Dixon J.E., Shakesheff K. & Rivett P. Surface Modification of an Elastomeric Membrane for the Purpose of Cardiac Tissue Engineering (CTE). Presented at the Tissue & Cell Engineering Society Conference, Glasgow (UK),

July, 2010 and Leeds (UK), 2011. Also presented at the UK Pharmaceutical Sciences Conference, East Midlands Conference Centre, September, 2010

Paik I., Scurr D.J., Morris B., Hall G., Denning C., Alexander M., Shakesheff K.M., Dixon J.E. Rapid micropatterning of cell lines and human pluripotent stem cells on elastomeric membranes. Presented at the Tissue & Cell Engineering Society Conference, Liverpool (UK), July, 2012. Also presented at the UK Pharmaceutical Sciences Conference, July 2012

Acknowledgements

Throughout the years of my PhD, I have received exceptional support from many people in the School of Pharmacy. Firstly, I would like to thank my supervisor Professor Kevin Shakesheff for providing me with the opportunity to work on the in vitro living pump grant. Kevin's support and guidance as a supervisor has allowed me to maximise the potential of my research, he has given me excellent opportunities that have equipped me with invaluable skills for my future ahead. Also, thanks to Biotechnology and Biological Sciences Research Council and Regentec® for funding. I would like to thank Professor Donal McNally and Dr. David Chau for their assistance with my lab work when I started my PhD. I also thank Dr James Edward Dixon for both his input in to the research presented in this thesis and his dedication to the field, which provided me with a source of motivation.

Many thanks to the Tissue Engineering group at the Centre for Biomolecular Sciences, particularly Dr Cheryl Rahman and Dr Catherine Rogers who have been extremely supportive, especially when I was faced with difficulties in my PhD, they have become more than work colleagues and I wish them the very best for the

future. Thanks to my peers to include Gemma Gaw, Manali Mukherjee and Tanvi Garg.

Special thanks to my family; my parents for supporting me in all my endeavours, I am so very lucky to have them and my brother Taran, who has always been there for me, I wish him the best of luck for the final year of his degree. Thanks also to my friends Bayode and Vanisha, especially Tirupa and Hiten. Finally, I want to thank Henry who has been a firm pillar throughout and has given me the happiest memories that I will keep with me for a lifetime.

Abbreviations

ACGM	<u>A</u> dvisory <u>C</u> ommittee on <u>G</u> enetic <u>M</u> odification
ATCC	<u>A</u> merican <u>T</u> ype <u>C</u> ulture <u>C</u> ollection
bFGF	<u>B</u> asic <u>F</u> ibroblast <u>G</u> rowth <u>F</u> actor
b-PEI	<u>b</u> ranch <u>e</u> d- <u>P</u> oly <u>e</u> th <u>e</u> ny <u>i</u> mi <u>n</u> e
CMS	<u>C</u> yclic <u>M</u> echanical <u>S</u> train
CTE	<u>C</u> ardiac <u>T</u> issue <u>E</u> ngineering
DMA	<u>D</u> ynamic <u>M</u> echanical <u>A</u> nalys <u>e</u> r
DMEM	<u>D</u> ul <u>b</u> ecco's <u>M</u> odified <u>E</u> agle's <u>M</u> edium
DMEM-F12	<u>D</u> ul <u>b</u> ecco's <u>M</u> odified <u>E</u> agle's <u>M</u> edium- <u>H</u> am <u>F</u> - <u>1</u> <u>2</u> medium
DMSO	<u>D</u> im <u>e</u> thyl <u>S</u> ulph <u>o</u> xide
ECM	<u>E</u> xtrac <u>e</u> llular <u>M</u> atrix
EDTA	<u>E</u> thylene <u>d</u> iamine <u>t</u> etraacetic <u>a</u> cid
eGFP	<u>E</u> nhanced <u>G</u> reen <u>F</u> luorescent <u>P</u> rotein
emm	<u>E</u> mission
ex	<u>E</u> xcitation
FCS	<u>F</u> oetal <u>C</u> alf <u>S</u> erum
Fn	<u>F</u> ibronectin
FWHM	<u>F</u> ull <u>W</u> idth <u>H</u> alf <u>M</u> aximum

g	Centrifugal <u>G</u> Force (Tilting Strain)
GAG(s)	<u>G</u> lycosaminoglycan(s)
HA	<u>H</u> yaluronic
HBSS	<u>H</u> ank's <u>B</u> alanced <u>S</u> alt <u>S</u> olution
HESC	<u>H</u> uman <u>E</u> mbryonic <u>S</u> tem <u>C</u> ell
HEMA	2- <u>h</u> ydroxyethyl <u>m</u> ethacrylate
Hz	<u>H</u> ertz
iHMSC(s)	<u>I</u> mmortalised <u>H</u> uman <u>M</u> esenchymal <u>S</u> tem <u>C</u> ell(s)
LMW	<u>L</u> ow- <u>M</u> olecular- <u>W</u> eight
β -ME	β - <u>m</u> ercaptoethanol
MEF(s)	<u>M</u> ouse <u>E</u> mbryo <u>F</u> ibroblast(s)
MMC	<u>M</u> itomycin <u>C</u>
mRFP	<u>M</u> onomeric <u>R</u> ed <u>F</u> luorescent <u>P</u> rotein
MSC(s)	<u>M</u> esenchymal <u>S</u> tem <u>C</u> ell(s)
NEAA	<u>N</u> on- <u>e</u> ssential <u>a</u> mino <u>a</u> cid
Pa	Pascal
PBS	<u>P</u> hosphate- <u>b</u> uffered <u>s</u> aline
PCL	<u>P</u> olycaprolactone
PCLA	ϵ -caprolactone- <i>co</i> -L-lactide/ <u>P</u> oly-L-lactide
P(CL+LLA)	ϵ -caprolactone/ L-lactic acid
PDMS	<u>P</u> oly <u>d</u> imethyl <u>s</u> iloxane
PEG	<u>P</u> olyethylene <u>G</u> lycol
PEUU	<u>P</u> olyester <u>U</u> rethane <u>U</u> rea
PGA	<u>P</u> olyglycolic <u>A</u> cid

PGS	<u>P</u> oly(<u>g</u> lycerol <u>s</u> ebecate)
PIPAAm	<u>P</u> oly(<u>N</u> - <u>i</u> sopropyl <u>a</u> cryl <u>a</u> mide)
PLA	<u>P</u> oly <u>l</u> actic <u>A</u> cid
PLCL	<u>P</u> oly(<u>l</u> actide-co- <u>ε</u> - <u>c</u> aprolactone)
PLGA	<u>P</u> oly <u>l</u> actic-co- <u>G</u> lycolic <u>A</u> cid
PLLA	<u>P</u> oly- <u>L</u> - <u>L</u> actic <u>A</u> cid
POC	<u>P</u> oly(1,8- <u>o</u> ctanediol-co- <u>c</u> itric acid)
ppAAm	<u>P</u> lasma polymerised <u>a</u> llyl <u>a</u> mine
PU	<u>P</u> olyurethane
PVA	<u>P</u> oly <u>V</u> inyl <u>A</u> lcohol
RF	<u>R</u> adio <u>F</u> requency
RPM	<u>R</u> evolutions per <u>m</u> inute
QCM	<u>Q</u> uartz <u>c</u> rystal <u>m</u> icrobalance
TCPS	<u>T</u> issue <u>C</u> ulture <u>P</u> olystyrene
ToF-SIMS	<u>T</u> ime of <u>F</u> light- <u>S</u> econdary Ion <u>M</u> ass <u>S</u> pectroscopy
TS	<u>T</u> ensile <u>S</u> train
UV	<u>U</u> ltraviolet
UVO	<u>U</u> ltraviolet/ <u>o</u> zone
v/v	<u>V</u> olume per <u>V</u> olume
WCA	<u>W</u> ater <u>c</u> ontact <u>a</u> nge
w/v	<u>W</u> eight per <u>V</u> olume
XPS	<u>X</u> -ray <u>P</u> hotoelectron <u>S</u> pectroscopy

Table of contents

<u>Abstract</u>	I
<u>Publications and presentations</u>	III
<u>Acknowledgements</u>	V
<u>Abbreviations</u>	VII
<u>Chapter 1: General Introduction</u>	1
1.1 Brief definition of regenerative medicine	1
1.2 Importance of <i>in vitro</i> modelling	1
1.2.1 Limiting factors of <i>in vitro</i> modelling	1
1.3 Cardiac anatomy	2
1.3.1 The heart	2
1.3.2 Myocardium	3
1.4 Cardiac tissue engineering	5
1.4.1 Design criteria for substrate preparation	5
1.4.2 Mechanical compatibility	6
1.5 Cells used in cardiac tissue engineering	8
1.5.1 Skeletal myoblasts	8
1.5.2 Somatic muscle cells	9

1.5.3	Stem cell derived cardiomyocytes	9
1.6	Biomaterial selection	11
1.6.1	Naturally occurring polymers	11
1.6.2	Synthetic polymers	15
1.6.3	Elastomers	18
1.7	External stimulation	20
1.7.1	Bioreactors	21
1.7.2	Mechanical stimulation	21
1.7.3	Electrical stimulation	22
1.7.4	Micro-patterning	22
1.8	Engineering a 3-D <i>in vitro</i> pump	23
1.9	Aims	25
<u>Chapter 2:</u>	<u>Materials and methods</u>	27
2.1	Materials	27
2.1.1	Cell lines	27
2.1.2	General chemicals	27
2.1.3	Apparatus and Consumables	27
2.2	Methods	28
2.2.1	Polymer Preparation	28
2.2.2	Spin Coating PDMS on glass	29
2.2.3	Spin coating PDMS on metal	31
2.2.4	Culture conditions	31
	2.2.4.1 <i>Calculating desired cell density</i>	33

2.2.4.2	<i>Genetic labelling of cell lines</i>	34
2.2.5	Alamar blue assay	34
2.2.6	Surface engineering	35
2.2.7	Surface characterization	36
2.2.7.1	<i>Sessile drop technique</i>	36
2.2.7.2	<i>Ellipsometry</i>	36
2.2.7.3	<i>XPS</i>	37
2.2.7.4	<i>ToF-SIMS analysis</i>	37
2.2.8	Micropatterning	38
Chapter 3:	<u>Mechanical compatibility of poly(dimethylsiloxane) for cardiac tissue engineering</u>	40
3.1	Introduction	40
3.2	Materials and Methods	42
3.2.1	Sample Preparation	42
3.2.2	Measuring PDMS membrane thickness	42
3.2.3	Uniaxial tensile tests	43
3.2.4	Cyclic Mechanical Testing	43
3.3	Results and Discussion	44
3.3.1	Stress-strain behaviour of PDMS membranes	44
3.3.2	Effect of spin coating speed on PDMS membrane thickness, tensile strength and ultimate elongation	48
3.3.3	Effect of fatigue on PDMS membrane stiffness	55

3.3.4	Mechanical compatibility of PDMS for CTE	58
3.4	Conclusion	58
<u>Chapter 4: Surface engineering of PDMS membranes to encourage cell adhesion and proliferation</u>		60
4.1	Introduction	60
4.2	Materials and Methods	63
4.2.1	Substrate Preparation	63
4.2.2	Surface Engineering	63
4.2.3	Ellipsometry	63
4.2.4	Surface Wettability	63
4.2.5	XPS	63
4.2.6	Cell Culture	64
4.3	Results and Discussion	64
4.3.1	Ellipsometry	65
4.3.2	Surface Wettability	65
4.3.3	XPS	70
4.3.4	Cell attachment, proliferation and viability on ppAAm coated PDMS	72
4.4	Conclusion	74
<u>Chapter 5: Surface micropatterning of PDMS to create spatially ordered cell monolayers</u>		76
5.1	Introduction	76
5.2	Materials and Methods	78
5.2.1	Membrane fabrication	78
5.2.2	Surface micropatterning	78

5.2.3	Surface characterisation	78
5.2.4	Cell culture	79
5.2.5	Imaging	79
5.3	Results and Discussion	80
5.3.1	Plasma-stencilling of ppAAm (92 nm) on PDMS	80
5.3.2	ECM aerosol microstencilling of ppAAm coated PDMS	82
5.3.3	Micropatterned cell culture	85
5.3.4	Patterning complex geometries	87
5.3.5	Patterning of cell co-cultures	93
5.4	Conclusion	96
<u>Chapter 6: Effect of substrate strain and geometric constraints on cell alignment and cytoskeletal organisation</u>		98
6.1	Introduction	98
6.2	Materials and Methods	102
6.2.1	Membrane fabrication	102
6.2.2	Surface micropatterning	102
6.2.3	Subjecting micropatterned PDMS membranes to uniaxial strain	102
6.2.4	Surface characterisation	102
6.2.5	Cell culture and immunofluorescent staining	104
6.2.6	Imaging	104
6.3	Results and Discussion	105
6.3.1	Surface characterisation of ppAAm micropatterned PDMS subjected to strain	105

6.3.2	Cell attachment, alignment and cytoskeletal organisation on unstrained/ strained micropatterned PDMS	114
6.4	Conclusion	125
<u>Chapter 7: General discussion, conclusions and future development</u>		127
7.1	Manufacturing scaffolds and investigating mechanical compatibility and biocompatibility	128
7.1.1	General discussion and conclusions	128
7.1.2	Future development	129
7.2	Control of cell positioning on PDMS using micropatterning and external stimulation	129
7.2.1	General discussion and conclusions	129
7.2.2	Future development	130
References		133
Appendix		148
1	Media and Supplements	148
1.1.	Media A	148
1.2	Media B	148
1.3	Media C	149
1.4	Phosphate buffered saline (PBS) (0.01 M pH 7.4)	149
1.5	Ethylenediaminetetraacetic acid (EDTA) stock solution (2 %)	149
1.6	Trypsin/EDTA solution	149
1.7	Freezing medium (Sigma-Aldrich, Poole, UK)	150
2	Other Solutions	150
2.1	Triton-X 100 solution (0.1 % v/v)	150

2.2	Poly vinyl acetate (PVA) solution (30 %)	150
3	General cell maintenance	150
3.1	Cryopreservation	150
3.2	Cell revival from storage	151
3.3	Trypan blue exclusion assay	151
4	Standard curve derivation	151
4.1	Alamar blue assay	151
5	Sample Preparation for CMS testing on BOSE	153
5.1	Membrane preparation	153
5.2	Fatigue bath containing PDMS membrane	154

List of figures

Chapter 1: General Introduction

- Figure 1.1 Illustration of the heart 4
- Figure 1.2 Schematic outlining the key steps involved towards engineering a 3-D in vitro pump system 24

Chapter 2: Materials and methods

- Figure 2.1 Cross-linking reaction of poly(dimethylsiloxane) (PDMS) 30

Chapter 3: Mechanical compatibility of poly(dimethylsiloxane) for cardiac tissue engineering

- Figure 3.1 Stress-strain curves of PDMS membranes spin coated at 250, 500, 1000 and 2000 RPM 46
- Figure 3.2 Key regions of stress strain curves illustrated using PDMS membranes spin coated at low (250 RPM) and high (500 rpm) speed 47
- Figure 3.3 Effect of spin coating speed on membrane thickness, ultimate elongation and tensile strength of PDMS membranes 49
- Figure 3.4 Effect of spin coating speed on the Young modulus of PDMS membranes 52

Figure 3.5	The effect of cyclic mechanical strain (CMS) on PDMS membranes spin coated at 2000 RPM	57
Chapter 4:	Surface engineering of PDMS membranes to encourage cell adhesion and proliferation	
Figure 4.1	Time-dependent plasma polymerized allylamine (ppAAm) deposition analysis on PDMS membranes	66
Figure 4.2	Images showing the interaction of a water droplet with the untreated PDMS (PDMS), oxygen etched PDMS (PDMS*), ppAAm (13 nm) and ppAAm (92 nm) surface during 14 days	68
Figure 4.3	Hydrophobicity analyses of ppAAm deposited PDMS. A) Average WCA values for PDMS, PDMS*, ppAAm (13 nm) and ppAAm (92 nm) treated surfaces during 14 days	69
Figure 4.4	Atomic analyses of ppAAm-coated PDMS to assess surface coverage of deposited ppAAm over a 14 day period	71
Figure 4.5	Cell number on PDMS, oxygen etched PDMS (PDMS*) and ppAAm deposited surfaces during 14 days	73
Chapter 5:	Surface micropatterning of PDMS to create spatially ordered cell monolayers	
Figure 5.1	ToF SIMS analysis of ppAAm-coated PDMS	81
Figure 5.2	Accuracy of ppAAm deposition through Microstencils	83
Figure 5.3	Aerosol deposition of fibronectin (Fn) on ppAAm-coated PDMS	84
Figure 5.4	Testing media conditions for micropatterned PDMS membranes	86

Figure 5.5	Micropatterning of cell lines	88
Figure 5.6	Morphology of NIH-3T3 cells during micropatterning	89
Figure 5.7	Micropatterning of HUES7 HESC line	90
Figure 5.8	Micropatterning of HUES7 HESC cell line	91
Figure 5.9	Micropatterning of Complex Designs	92
Figure 5.10	Three-dimensional structures of micropatterned PDMS sheets	94
Figure 5.11	Co-culture Micropatterning	95
 Chapter 6: Effect of substrate strain and geometric constraints on cell alignment and cytoskeletal organisation		
Figure 6.1	Image of PDMS membrane mounted on strain rig	103
Figure 6.2	ToF SIMS analyses of ppAAm-coated PDMS	107
Figure 6.3	ToF SIMS analyses of ppAAm-coated PDMS	108
Figure 6.4	Line scan of CN ⁻ ion intensity across 500 μm^2 area of ppAAm micropatterned PDMS subjected to 0% and 95% tensile strain (TS)	110
Figure 6.5	Intensity of molecular ions from ppAAm (92 nm) micropatterned PDMS surfaces subjected to 0% and 95% TS	111
Figure 6.6	Aerosol deposition of Fn on ppAAm deposited PDMS	113
Figure 6.7	Micropatterning of cell lines	115

Figure 6.8	Fluorescent images of eGFP labeled iHMSC micropatterns on PDMS membranes.	117
Figure 6.9	Images showing actin stress fiber and nuclei orientation of iHMSCs 48 hours post seeding.	118
Figure 6.10	Actin stress fiber orientation of iHMSCs	119
Figure 6.11	Nuclei orientation of iHMSCs	122
Figure 6.12	Box and whisker plot to show effect of surface condition on iHMSC nuclei aspect ratio (elongation)	123
Appendix		
5.1	Sample Preparation for CMS testing on BOSE	153
5.2	Fatigue bath containing PDMS membrane	154
5.3	Stress-strain plots of PDMS membranes subjected to uniaxial tension	155
5.4	Cyclic mechanical strain of PDMS membranes spin coated at 2000 rpm (10 s duration)	156

1

General Introduction

1.1 Brief definition of regenerative medicine

Regenerative medicine is the process of repairing or regenerating human cells, tissues or organs to restore or establish normal tissue function¹. The aim of this field is to engineer tissue constructs to use for transplantation or *in vitro* test systems to meet present clinical demands^{2,3}.

1.2 Importance of *in vitro* modelling

At present, the ability to disrupt the progression or reverse degenerative disease mechanisms remains at a primitive stage. Molecular pathways that lead to human diseases have been researched using animal models or two-dimensional (2-D) cell monolayers, not entirely mimicking human physiology. *In vitro* modelling would offer a precise recapitulation of human degenerate tissue for physiological studies and pharmacological screening⁴. Yet, very few test systems have been developed to date.

1.2.1 Limiting factors of *in vitro* modelling

The main limitation hindering the development of *in vitro* modeling is the lack of a

sufficient blood vessel system⁵. This is required to provide a constant source of oxygen/ nutrients to the tissue engineered construct. This lack of vascularization undoubtedly leads to cell necrosis.

The work outlined in this thesis focuses on engineering heart tissue for the purpose of creating a functional three-dimensional (3-D) pump (mini-heart). This is part of a long term strategy to build internal circulatory systems for *in vitro* engineered tissue, thereby bridging the major divide between *in vitro* engineered tissue and *in vivo* vascularised tissue. Since the function of this engineered device is to mimic the heart it is important to consider the native architecture.

1.3 Cardiac anatomy

1.3.1 The heart

The image in figure 1.1 shows a diagram of the heart which consists of four chambers. These chambers are connected by valves and can be grossly divided into two pumps on the lower left and right; the ventricles. The ventricles act in synchrony to pump blood to and from the body, maintaining systemic and pulmonary circulation, respectively. The passage of blood through the ventricles during systemic and pulmonary circulation is illustrated by red and blue arrows respectively in figure 1.1. The upper right and left of the heart contain the atria, responsible for collecting blood returning to the heart and to facilitate filling of the ventricles^{6,7}. The cardiac wall chambers are composed of three layers, the outer visceral epicardium, central contractile myocardium and the endocardium (see

figure 1.1.). The composition of these layers varies for each ventricle since they both carry out different functions. The left ventricle has a dense, thick muscular wall (8-15 mm), approximately double the muscular wall thickness of the right ventricle (4-5 mm) in healthy adults. Contraction of the left and right ventricular myocardium forces blood to pressurize and subsequently expel from the heart. However, myocardium in the left ventricle must exert stronger muscular contractions compared to the right ventricle in order to maintain systematic circulation, thus left ventricular myocardium is thicker than the right ventricular myocardium. The pressure of blood being expelled from the left ventricle is generally one order of magnitude higher than the right ventricle^{6,8}.

1.3.2 Myocardium

Myocardium is highly vascularised tissue with cardiomyocytes that constitute one third of the myocardial cell population in adults⁹. Fibroblasts are responsible for creating a network of cells interconnecting cardiomyocytes to the extracellular matrix (ECM)¹⁰.

Myocardial architecture is highly ordered with cardiomyocytes and capillaries embedded in a net of connective tissue that is organized into different levels. These include respectively: endomysium that surrounds and connects each individual muscular cell, undulated perimysium fibers surrounding groups of myocytes (cardiac muscle fibers) and the epimysium, the layer of connective tissue encapsulating the myocardium¹¹. Kanzaki et al. conducted a qualitative study using scanning electron microscopy to observe the connective tissue skeleton of

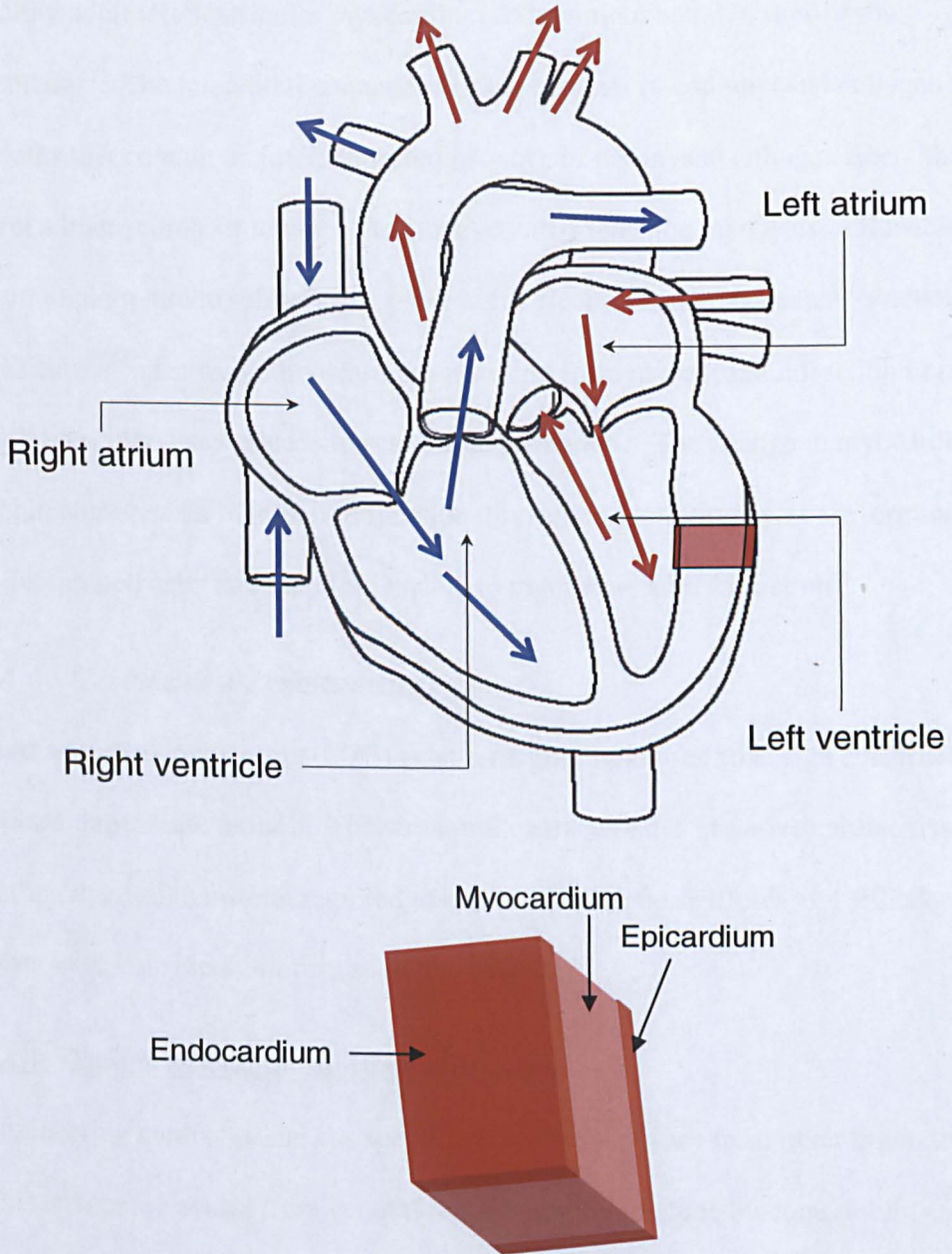


Figure 1.1 Illustration of the heart. Image showing the location of the four chambers (atria, ventricles), and illustrating the passage of oxygenated blood and deoxygenated blood in to and out of the heart, identified by the red and blue arrows, respectively. Inset shows the composition of the cardiac wall chamber.

healthy adult left ventricular myocardium following removal of non-fibrous elements¹². The interstitial connective tissue consists of endomyosial collagen sheaths that contain an interconnected network of perimysial collagen fibers that form a honeycomb structure. The honeycomb orients the myocytes, influencing them to align into myofibers that provide for electrical and mechanical function of the heart^{13,14}. Damaged myocardium resulting from myocardial infarction or other cardiovascular disease leads to scar tissue formation. The change in myocardial architecture results in impaired functionality, since cardiomyocytes are terminally differentiated cells and therefore unable to regenerate after infarction¹⁵.

1.4 Cardiac tissue engineering

Cardiac tissue engineering (CTE) is an emerging field used to design constructs to replace degenerate tissue¹⁶. The structural characteristics of native cardiac tissue outline the design criteria required to create biomimetic scaffolds and will also be taken in to consideration for use in this project.

1.4.1 Design criteria for substrate preparation

Engineering cardiac tissue has specific requisites that vary from other organ tissue. This is because besides from general requirements to include biocompatibility, immunogenicity and biodegradability, cardiac tissue requires high rates of oxygen and nutrient exchange to support high levels of metabolic activity. Thus, the engineered tissue construct must encourage angiogenesis for the vascularisation of the engineered myocardium. Furthermore, cardiac tissue is subjected to ongoing

cyclic stresses and strain, therefore mechanical compatibility is a crucial factor especially when selecting biomaterials, since the substrate will constitute the main structural component of the engineered cardiac tissue⁶.

1.4.2 Mechanical compatibility

The micro-mechanical environment is an important regulator in stem cell lineage specification and cell function, controlled either through the specific mechanical properties of the substrate to which the cells adhere, or the exposure to external forces^{17,18}. Engler et al found that embryonic cardiomyocytes extracted from 4 to 10 day old quail only maintained contractile function when adhered to polyacrylamide gels that mimic the elasticity of the developing myocardial microenvironment¹⁹. Myocytes exhibited actomyosin striation and 1 Hz beating, mimicking physiological contraction of healthy contracting myocardium. Myocytes adhered to stiffer matrices overstrained themselves, characterized by lack of striated myofibrils and loss in contractile force. The method and analyses in this study are useful for the assessment of cardiogenesis of embryonic stem cells/ pluripotent stem cells. Jacot et al. also investigated the effects of extracellular stiffness on cardiomyocyte maturation²⁰. Neonatal rat cardiomyocytes were plated on collagen-coated polyacrylamide gels with varying stiffness. Cells on gels mimicking stiffness of native myocardium (10 kPa) generated greater contractile force than cells on stiffer or softer gels. Cardiomyocytes on 10 kPa gels also exhibited aligned sarcomeres, this was not evident for cardiomyocytes seeded on stiffer/softer substrates. Other studies have

investigated the effect of varying the stiffness of the scaffold over time to mimic the developmental changes in the native ECM in the first postnatal week²¹. This is the stage where cardiomyocytes develop from mesoderm, resulting in a 9-fold increase in stiffness attributed to a change in collagen expression and localization. Recently, Young et al. fabricated thiolated-hyaluronic (HA) hydrogels crosslinked with poly(ethylene glycol) diacrylate and seeded chick embryonic cardiomyocytes²². The stiffness of these gels was modulated by changing the molecular weight of the crosslinker. Incorporating appropriate tuning to the hydrogels resulted in cardiomyocytes expressing a 3-fold increase in mature cardiac specific markers and formation of up to 60% more mature muscle fibers compared to cells on compliant hydrogel following a 2 week period. These results suggest that temporally changing material properties may enhance cell maturation *in vitro*. The studies outlined above demonstrate the significance that micro-mechanical properties have on regulating pre-cardiac cell development to cardiomyocytes and cardiomyocyte contractile force.

The control of engineered myocardium's bulk mechanical properties is also critical to ensuring that biomimetic function is sustained, particularly when *in situ* CTE is intended. This is because *in vivo*, the substrate's macro-mechanical properties must meet the cyclic haemodynamic demands of the cardiovascular system. Thus, the engineered construct must be elastic to respond to constant cyclic strain and prevent from deforming permanently as a result of mechanical fatigue (creep behavior)²³. Engelmayr et al. investigated the native macro-mechanical properties

of ventricular myocardium²⁴. Tissue sections were extracted with defined circumferential and longitudinal axes that respectively corresponded to the epicardial surface of the heart. Uniaxial tensile testing was used to measure the Young modulus of left ventricular myocardium. Results showed that mechanical stiffness is dictated by muscle fiber orientation, termed ‘cardiac anisotropy’. Conceptually appealing would be a scaffold that mimics the native structure-function dependency of the myocardium, as well as the capability of supporting physiological loads. To achieve this, careful consideration must be taken to select the biomaterial, processing method and cell type.

1.5 Cells used in cardiac tissue engineering

Although the work within this thesis focuses on biomaterial development it is important to consider the cell sources available for cardiac therapy since ultimately, the cell type is responsible for imitating physiological function of the engineered myocardium.

1.5.1 Skeletal myoblasts

Skeletal myoblasts have been considered for cardiac regeneration because they have electromechanical properties similar to cardiomyocytes. Skeletal myoblast satellite cells are mononuclear progenitor cells found in mature cells. These cells have the capacity to become activated, differentiate and fuse to augment existing muscle fibres or form new fibres. Therefore, skeletal myoblast satellite cells can be isolated from autologous sources preventing immunogenicity, and can be

rapidly expanded in an undifferentiated state *in vitro*²⁵. However, it has been established that when implanted in to myocardium, these cells remain committed to form only mature skeletal muscle cells and thus have different electromechanical properties to the surrounding cardiac tissue. As a result, there is no improvement in contractile behavior of the host tissue²⁶.

1.5.2 Somatic muscle cells

Somatic cell lines to include foetal or neonatal (rat or mouse) cardiomyocytes are widely used to create engineered myocardium. This is because these cells have the inherent structural, contractile and electrophysiological properties of cardiomyocytes and still exhibit some proliferative capacity²⁷. Soonpaa et al. published a pioneering study demonstrating that foetal cardiomyocytes could be transplanted and integrated within the myocardium of healthy mice²⁸. The surviving donor cells were aligned with recipient cells and integrated with the host tissue. Results from other studies also indicate that early-stage cardiomyocytes can be successfully implanted in to diseased heart models and are more suitable candidates for CTE than mature cardiac cell lines²⁹⁻³¹. Yet, these cell lines are only useful for proof of concept work since neonatal human or rat cardiomyocytes cannot be used for clinical application. An alternative approach is to use stem cells²⁵.

1.5.3 Stem cell derived cardiomyocytes

Stem cell derived cardiomyocytes offer more potential for tissue regeneration

compared to the cell lines stated above for several reasons²⁵. These include the lifetime ability to self replicate, thus allowing for expansion of stem cells with similar properties *in vitro*. Furthermore, stem cells are clonogenic, providing each cell with the capability of forming a colony in which all cells are derived from this single cell with identical genetic constitution. Following expansion stem cell lines can be directed to differentiate into the cardiomyogenic lineage. Research has shown the embryonic stem cells hold greater translational potential compared to adult stem cells. This is because embryonic stem cells are pluripotent; they have a broader multilineage profile. Embryonic stem cell lines are useful for *in vitro* work because they are robust cell lines. They exhibit long-term proliferative ability with limited karyotypic instability and can be cryopreserved^{32,33}. Previous work indicates that human embryonic stem cells (HESCs) differentiated in to cardiomyocytes *in vitro* mimics normal development *in vivo* indicated by expression of cardiac transcription factors and identifiable ultrastructural elements³⁴⁻³⁷. These include Z-line, A (dark) and (I) light bands of the sarcomere³⁸. Moreover, hESC-cardiomyocytes within beating clusters exhibit well coupled gap junctions and continue to spontaneously contract for at least 5 months in culture. Functional integration into the myocardium of animal models including pigs, guinea-pigs, rats and mice have also been shown³⁹⁻⁴¹. Therefore, HESC-cardiomyocytes could provide a suitable cell source for construction of an *in vitro* cardiac pump. This is providing that a suitable structural component is incorporated. Below, both natural and synthetic materials including the processing

methods used to fabricate scaffolds used for cardiac tissue regeneration are discussed.

1.6 Biomaterial selection

1.6.1 Naturally occurring polymers

Natural polymers mimic the ECM environment of healthy myocardium more closely than synthetic alternatives. Moreover, retaining ECM components provides the opportunity to encourage cell adhesion, proliferation and differentiation in the native state²⁵. ECM derivatives to include collagen, gelatin, fibronectin, glycosaminoglycans (GAGs) and Matrigel (commercially available basement membrane matrix) have been explored with conflicting results⁴². This is largely due to differences in composition and processing methods which dictate the physical properties of the scaffold. Most often, these scaffolds are designed to engineer cardiac patches. Cardiac patch therapy involves engineering a patch which is populated with cells *in vitro* and later implanted *in vivo* serving the purpose of cell delivery and mechanical support to infarct regions²⁵. Van Luyn et al. compared the level of organization and contractile behavior of neonatal rat cardiomyocytes and fibroblasts cultured in 2-D (confluent monolayer) and 3-D, consisting of neonatal rat cardiomyocytes embedded within a collagen I matrix⁴³. The 3-D co-cultures incorporating collagen more closely resembled intact cardiac tissue demonstrated by cell organization and unison contractile behavior. Zimmerman et al. cast circular molds comprising neonatal rat cardiomyocytes,

collagen I and matrigel⁴⁴. The engineered tissue displayed important hallmarks of engineered myocardium resembling adult, rather than immature native tissue from which the cells were harvested. Collagen-GAG scaffolds have also been explored as a cell delivery device to infarct areas of the heart. Xiang et al demonstrated that using different cross-linking methods to process collagen-GAG scaffolds has a marked response on the tissue response in situ⁴⁵. Implantation into infarct regions of rats revealed that the engineered tissue integrated with native ventricular myocardium and exhibited contractile function. However, whether the engineered tissue improved left ventricular function could not be determined. Zhong et al. used electrospinning to develop collagen-GAG scaffolds for soft tissue application⁴⁶. The study showed that the electrospun scaffolds exhibited a uniform nanofibrous and porous structure with a mean diameter of 260 nm, similar to that found in native ECM and supported cell adhesion and proliferation.

Electrospinning is a process whereby polymer solution in a needle-syringe is exposed to high voltage. Subsequent charging of the polymer solution creates an electrostatic force in the form of charge repulsion within the solution, resulting in ejection of polymer fibers from the needle. The potential of electrospinning ECM constituents is promising because the nanodimension fibers within the constructs closely mimic the native ECM myocardial architecture⁴⁷.

The studies mentioned above have focused on cellular integration with the scaffold. Less consideration has been paid to the effect of material composition and cross-linking on the physical attributes of the scaffold. Recently, Best's lab

addressed this issue investigating the physical properties of scaffolds comprising collagen, gelatin and elastin⁴⁸. Importantly, the study showed that the composition of these polymers alongside crosslinking using carbodiimides, (via carboxylic acids and amine groups on collagen and elastin), can be used to tailor specific mechanical and degradation properties. Furthermore, the study revealed that the tensile properties of collagen and elastin scaffolds closely matched native myocardium.

Cell sheet technology is another strategy used to engineer cardiac patches. Rather than incorporating cells with ECM constituents, these processes rely on cell-cell junctions and adhesive proteins within confluent cultured cell monolayers to preserve structure. Shimizu et al. cultured neonatal rat cardiomyocytes on a synthetic temperature-responsive polymer, poly(N-isopropylacrylamide) (PIPAAm) from which cell sheets detached by reducing temperature without any enzymatic treatments⁴⁹. This work demonstrated 4 cell sheets layered together to form a cardiac patch were electrically communicative, displaying spontaneous beating both *in vitro* and *in vivo*. The same group later published a study on the formation of tubes of neonatal rat cardiomyocytes using their cell sheet technology⁵⁰. The construct successfully generated inner pressure changes but fluid movement and longer timescale elasticity of the structure was not demonstrated.

More recently, there has been growing interest in decellularised matrices in CTE to imitate both the structural and biochemical environments of myocardium. Taylor's lab at the University of Minnesota described a method to decellularize cadaveric rat hearts via enzymatic digestion⁵¹. The underlying matrix remained intact and the cadaveric hearts were reseeded with cardiac or endothelial cells to mimic cardiac cell population. Constructs were maintained *in vitro* for 28 days. By day 8, the constructs could generate pump function under external stimulation. Non-cardiac tissue to include small intestinal sub mucosa and bladder matrix have also been used to engineer cardiac patches because the ECM is retained following decellularisation^{47,52}. Injectable hydrogels are becoming an increasingly popular niche within CTE as they provide a minimally invasive route for cell delivery to the heart compared to cardiac patch therapy. The first explored natural materials were collagen and fibrin⁵³. Huang et al. attempted to engineer an *in vitro* 3-D structure using neonatal rat cardiomyocytes from rats to form tethered cylinders of cells in a biodegradable fibrin gel⁵⁴. Encouragingly, the cells could be stimulated to contract the gel. Matrigel and powdered decellularised matrix have also been investigated as they offer a more complex extracellular environment compared to using single constituents of ECM. Non-mammalian alternatives to include alginate and chitosan have also been explored. The main limitation of these injectable systems is their inability to provide mechanical support *in vivo*. This also limits their capabilities to create functional constructs *in vitro*⁶.

Radisic and Vunjak-Novakovic stated that natural polymers exhibited limited and non-adaptable mechanical properties, as well as batch-to-batch variation between scaffolds⁵⁵. This limits the use of naturally derived polymers as biomaterials for CTE. As a result, material scientists have turned to synthetic polymers as an alternative.

1.6.2 Synthetic polymers

Amongst the first synthetic materials aliphatic polyesters including hydrolytically biodegradable polymers composed of polylactic acid (PLA), polyglycolic acid (PGA) and their co-polymer polylactic-co-glycolic acid (PLGA) were investigated⁶. These polymers were used to fabricate synthetic ECM structures and processed into a variety of configurations to include fibres, porous sponges and tubular structures⁵⁶. These polymers are hydrolytically biodegradable making them favorable for *in vivo* purposes. However, these constructs were not suitable for CTE since the scaffolds lost mechanical strength as a result of material degradation. Loss in mechanical strength could lead to scaffolds that are not able to sustain the mechanically dynamic environment of the heart. Thus, researchers focused on different synthetic and/ or natural polymers as an alternative to mimic the elastic properties of cardiac tissue⁵⁷. Material elasticity provides a good measure to assess whether scaffolds mimic the mechanical elasticity of native tissue and thus resist material fatigue as a result of long term cycling *in vivo*. Researchers identify specific material properties including Young modulus, tensile

strength and ultimate elongation to measure material elasticity. These properties will be discussed further in Chapter 3.

Amongst the various processing techniques, electrospinning is widely used to fabricate nanofibrous synthetic structures. This is because electrospun scaffolds exhibit nano-scale morphology of the native ECM, which aids cell adhesion and proliferation. Furthermore, Young modulus, tensile strength and ultimate elongation can be tailored by controlling both the orientation and geometry of the electrospun fibres⁴⁷. Importantly, the orientation of fibres provides nano-architecture anisotropy to cells, assisting adhered cells to form a functional syncytium. Polycaprolactone (PCL) is another aliphatic polyester and has been electrospun to form nanofibrous scaffolds for CTE. Shin et al. cultured neonatal rat cardiomyocytes on PCL meshes that exhibited ECM like-topography⁵⁸. The fibres were suspended across a wire ring that acted as a passive load to contracting cardiomyocytes. Cell contraction was observed after 3 days. Following 14 days, protein expression of cardiac specific-proteins was evident. These included connexin43, cardiac troponin I and α -myosin heavy chain. The same group also constructed scaffolds consisting of 5 layers of PCL nanofibrous mesh laminated together and seeded with neonatal rat cardiomyocytes⁵⁹. Electrical communication was established between layers creating synchronized cell beating. Most recently Fozdar et al. developed scaffolds with a novel architecture⁶⁰. Unlike other constructs developed for CTE, auxetic structures with tunable negative Poisson's ratio were fabricated with polyethylene glycol (PEG) using a stereolithography

technique. Digital micromirror device projection printing was used to construct single, double and multiple-layer PEG scaffolds with interconnected porosity and the ability to support external forces imposed by the external environment. The unique characteristic about these scaffolds was that mechanical stiffness was influenced by scaffold geometry and not porosity.

Composites have also been developed to include sponges based on ϵ -caprolactone-co-L-lactide reinforced with knitted poly-L-lactide fabric (PCLA). The novel feature of this composite being that the spongy portion composed of 50% ϵ -caprolactone and 50% L-lactic acid (P(CL+LLA)) is absorbed within 2 months *in vivo*, where as the knitted fibrous component poly-L-lactic acid (PLLA) persists for 1-2 years. Ozawa et al. seeded rat aortic smooth muscle cells on PCLA and PGA patches *in vitro* and subsequently implanted into infarct rat models for 8 weeks⁶¹. Histology revealed that PCLA patches had increased cell numbers and presence of anti- α -smooth muscle actin compared to PGA patches. Zong et al. electrospun PLLA as well as PLLA-PLGA-PEG based scaffolds of different compositions⁶². Results showed that pure PLLA scaffolds supported the growth and proliferation of rat cardiomyocytes better than the composite scaffolds. Composites of natural and synthetic polymers have also been explored including poly(lactide-co- ϵ -caprolactone/collagen) (PLCL/collagen) electrospun nanofibres to which rabbit cardiomyocytes adhered and integrated⁴⁷.

Injectable gels incorporating synthetic polymers have also been investigated including variations of PEG. Dobner et al. injected PEG-vinyl sulfone as a non-degradable option without any long-term functional benefit⁶³. Variations of the temperature sensitive polymer PIPAAm mentioned earlier have been developed. The advantage of incorporating of PIPAAm being that such hydrogels undergo a phase transition just below physiological temperature, causing gel formation at 37°C but remaining liquid at room temperature. Research on PIPAAm based injectables have either shown stable or improved cardiac function when implanted in to small animal infarct models^{64,65}. The main drawback of using synthetic materials as an alternative to natural polymers for injectable hydrogel application is that they lack inherent bioactivity. Moreover, scaffolds composed of polyester based polymers have been found to undergo plastic deformation and failure on exposure to long term strain⁶⁶. To overcome this, elastomers have been considered.

1.6.3 Elastomers

An elastomer is defined as a polymeric material that can be stretched several times and return to its original dimensions without permanent deformation. This makes elastomers desirable for CTE because they possess inherent elasticity to sustain the *in vivo* cyclic loading of the heart. Furthermore, Young's modulus, tensile strength and ultimate elongation of elastomers can be finely tuned by varying the extent of cross linking during fabrication⁶⁷. Polyurethane (PU) polymers are elastomeric and have tunable degradation rates making them suitable for *in vivo*

application. Mcdevitt et al. fabricated solvent cast elastomeric PU films patterned with laminin moieties by microcontact printing which were subsequently seeded with neonatal rat cardiomyocytes⁶⁸. Secondary and tertiary populations were later seeded to form a multi-layered organized tissue. Cardiomyocytes displayed highly aligned monolayers and were capable of contracting the thin solvent cast film. This demonstrated the potential of patterned PU constructs to engineer organized cardiac tissue. Contrarily, Alperin et al. found that embryonic stem cell derived cardiomyocytes seeded on ECM protein-coated PU films exhibited similar behavior as cardiomyocytes seeded on gelatin coated tissue culture polystyrene (TCPS)⁶⁹. This included myofibrillar organization and contractile behavior. However, unlike TCPS the PU construct was deformed by the contracting cardiomyocytes. This maximized cardiomyocyte force generation thus emphasizing the importance of using substrates that could be deformed by the contraction of cardiomyocytes. As an alternative, polyester urethane urea (PEUU) was used to develop a cardiac patch without seeding cells and implanted in to rat infarct models⁷⁰. Following 8 weeks implantation, histology analysis showed the presence of contractile smooth muscle fibers, this also improved cardiac remodeling. Bastida et al. processed elastomeric scaffolds comprised of Poly(1,8-octanediol-co-citric-acid) (POC) by salt leaching and investigated the effect of modifying the porosity on the mechanical properties of the scaffold⁷¹. Young's modulus increased as the porosity increased. The scaffolds were pre-coated with fibronectin, collagen and laminin and subsequently seeded with HL-1

cardiomyocytes. Results showed that cell attachment was dictated by protein-type and concentration. Therefore illustrating that POC porous film could be tailored to meet specific mechanical and biological requirements for cardiac culture. In 2008, Chen et al. developed a biocompatible, degradable and elastic cardiac patch synthesized by polycondensation of glycerol and sebacic acid at 110, 120 and 130°C to form poly(glycerol sebacate) (PGS)⁶⁶. The processing conditions determined the Young's moduli of the patch, which ranged from 0.056-1.2 MPa. The study showed the potential of tailoring the mechanical properties of this elastomer to accommodate for the varied stiffness of myocardium of different animal groups for the purpose of *in vivo* testing. Engelmayr et al. synthesized PGS scaffolds with an accordion-like honeycomb microstructure, borrowing more closely from the native myocardial architecture²⁴. These constructs overcame principal structural-mechanical limitations of previously researched scaffolds. Furthermore, these scaffolds promoted the formation of grafts with aligned neonatal rat cardiomyocytes and mechanical properties more closely resembling native myocardium. The research above explicitly demonstrates how scaffold geometry orientates cell positioning. However in many cases, external stimulation is necessary to facilitate cardiac tissue development.

1.7 External stimulation

External stimuli are used as an aid to assemble differentiated cardiac cell populations and induce contractile and electrophysiological functionality in tissue engineered constructs⁷². External stimuli have previously shown to encourage

parallel cell orientation in structurally and mechanically incompatible scaffolds, which would otherwise yield isolated regions of cardiomyocyte alignment^{73,74}.

1.7.1 Bioreactors

Bioreactors are frequently used as they provide biophysical stimuli such as cyclic stretch, hydrodynamic forces and electrical stimulations. Furthermore, bioreactors enable control and monitoring of oxygen, growth factors and nutrients⁶.

1.7.2 Mechanical stimulation

Mechanical stimulation is an important regulator of cell function and plays a critical role during tissue development and repair⁷⁵. Akhyari et al. seeded cells isolated from children on gelatin-matrix scaffolds and subjected the constructs to cyclic mechanical stress (80 cycles/ minute for 14 days)⁷⁶. Control scaffolds were maintained under identical conditions without stretch. Results showed the cyclic mechanical stretch regimen increased cell proliferation and distribution throughout the construct. Collagen matrix formation and organization was also enhanced.

Similarly, Zimmerman et al, found that collagen matrix scaffolds seeded with neonatal rat cardiomyocytes and subsequently exposed to cyclic stretch displayed important hallmarks of differentiated myocardium⁴⁴. This was illustrated by cell morphological features and the change in composition of the basement membrane surrounding the cardiomyocytes. Cyclic loading is known to play a regulatory role in ECM synthesis. Cardiomyocytes sense changes in mechanical strain applied to them through cell-surface receptors. As a result, cells adjust their expression and

synthesis of ECM molecules in order to adapt their environment to these changes. Collagen is secreted by cardiomyocytes to provide tensile strength and serve as an organizational scaffold, it the most abundant protein in cardiovascular tissue⁷⁵.

1.7.3 Electrical stimulation

Although cyclic mechanical stretch substantially improves cell differentiation and alignment it has been stated that electrical stimulation is required for further development and function of engineered myocardium. This includes the distribution of gap junction proteins to include connexin-43, responsible for orderly coupling between electrical pacing signals and macroscopic contractions. There are detailed protocols available for the development of engineered myocardium with the application of pulsatile electric fields^{77,78}. Radisic et al. subjected neonatal rat cardiomyocytes seeded on collagen scaffolds to electrical pulses mimicking electrophysiological conditions⁷⁹. Following 8 days, electrical field stimulation alone induced cell alignment and coupling, increased the amplitude of synchronous contraction and resulted in a remarkable level of ultrastructural characterisation. This included elevated levels of connexin-43 and other gap junction proteins.

1.7.4 Micro-patterning

Patterning techniques can be used to create non-homogenous boundary constraints. These are also a physical stimulus used to encourage cell alignment^{68,80}. Feinberg et al. published a Science paper on the formation of thin films seeded with

neonatal rat cardiomyocytes capable of biomimetic function⁸¹. This was achieved using a microprinting technique to fabricate elastomeric films with Fibronectin lines. Careful consideration of the substrate material and cell patterning led these films to perform other functions as diverse as gripping, pumping, walking and swimming.

1.8 Engineering a 3-D *in vitro* pump

The present literature can be used to determine the key requirements for engineering a functional three-dimensional pump. Figure 1.2 shows a schematic, outlining the key steps involved. Gene modification techniques are incorporated to derive cardiomyocytes from human embryonic stem cells (HESCs) (Note: this is not the focus for the work presented here). These cardiomyocytes can be assembled to form a device that can harness the contraction of cells and create a system that can pump liquid. The key requirements for engineering such a system are to form flexible tubes of a polymer that have adequate mechanical properties such that the cardiomyocytes can contract the polymer sheet. When the cardiomyocytes relax, the polymer film must be able to recover its original surface area. Surface patterning can be exploited to position the cardiomyocytes in an assembly that will best utilize the force generated by cell contraction.

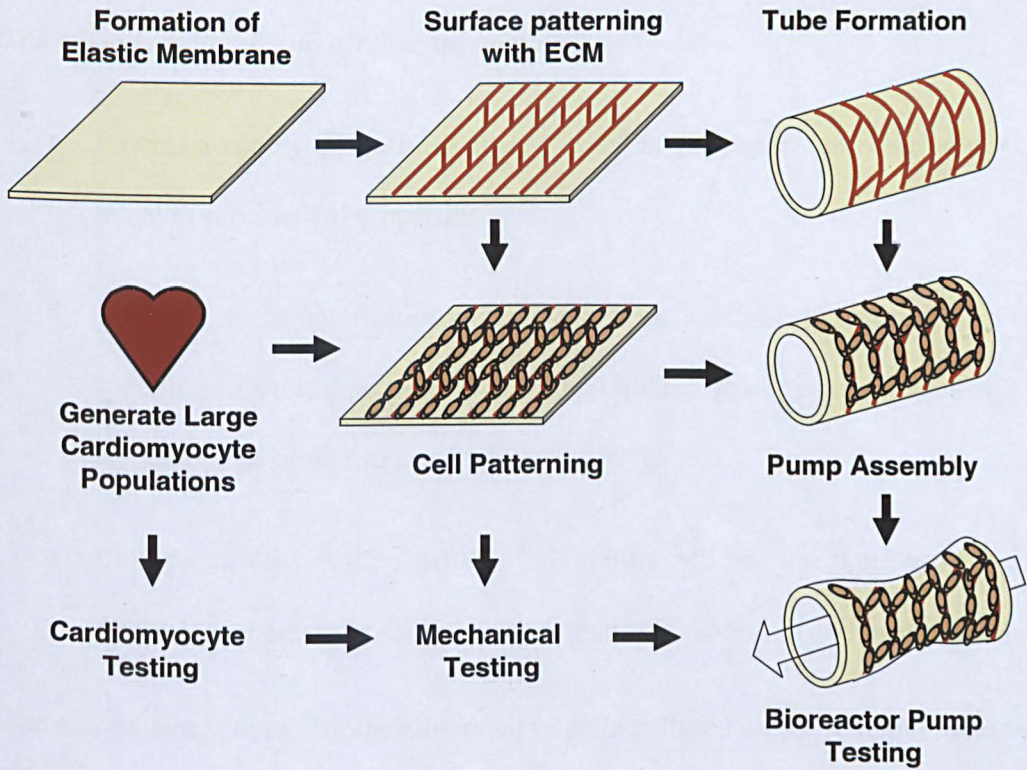


Figure 1.2 Schematic outlining the key steps involved towards engineering a 3-D *in vitro* pump system. The work in this thesis focuses on formation of the elastic membrane, mechanical testing and surface patterning.

1.9 Aims

There are two distinct aims of the research presented in this thesis. The first aim is to develop a method to manufacture scaffolds, which will constitute the structural component of the 3-D *in vitro* pump.

The objectives in order to achieve this aim are:

- Process a variety of scaffolds composed of an elastomeric polymer with a range of mechanical properties.
- Mechanical characterisation of the elastomeric scaffolds to determine specific mechanical properties. This will include loading the samples at physiological strain rates and stresses at 37°C.
- Biocompatibility of the scaffold. Cell culture will be carried out to determine whether the scaffold can support cell adhesion and proliferation.

The second aim is to encourage alignment of cells cultured on the scaffold surface since aligned cardiomyocytes generate directional contraction and more force.

The objectives in order to achieve this aim are:

- Investigate a micropatterning technique and assess whether the technique can be used to control the positioning of cells on the scaffold.
- Plating cells on the micropatterned surface. Determine whether cell alignment is maintained over time i.e. faithfulness of the pattern.

- Apply external stimulation. Compare cell seeded scaffolds exposed to external stimulation to cell seeded scaffolds maintained in static culture. This will determine whether external stimulation will aid cell alignment alongside the micropatterning technique.

2

Materials and methods

2.1 Materials

2.1.1 Cell lines

C2C12, NIH-3T3, BJ6 and HL1 cell lines were purchased from ATCC at passage

1. The HUES7 human embryonic stem cell (HESC) line was a kind gift from

Harvard University¹. These cells were received at passage 11. The human

mesenchymal stem cell line was obtained from TCS CellWorks, Buckingham, UK.

On receipt the cells were at passage 1. Cells were genetically modified in house to

create the immortalised human mesenchymal stem cell (iHMSC) line and kindly

provided by Dr. J E Dixon.

2.1.2 General chemicals

All chemicals were sourced from Sigma-Aldrich (Poole, UK) unless otherwise

stated. Stock solutions were sterile filtered using a 0.22 µm Whatman sterile filter.

Details of other reagents can be found in the appendix.

2.1.3 Apparatus and Consumables

Primaria 6-well culture dishes, 1 ml 5 ml and 50 ml syringes were purchased from

Falcon, Becton and Dickinson Ltd., Oxford, UK. Tissue culture flasks (25 cm², 75 cm² and 175 cm²) were purchased from Nunclon, Denmark. Costar 96-well flat bottom, non-treated, black polystyrene assay plates were purchased from Corning, NY, USA. Sterilin® petri dishes, 15 and 50 ml sterile centrifuge tubes, 5 ml 10 ml 20 ml and 50 ml plugged serological pipettes, sterile glass pasteur pipettes, 1 ml 200 µl and 20 µl pipette tips, 0.22 µm filters, 1 ml cryovials, 500 µl and 1 ml eppendorfs were purchased from Fisher Scientific, Loughborough, UK. The improved Neubauer haemocytometer, parafilm, weighing boats and 100 ml beakers were purchased from Scientific Laboratory supplies, Nottingham, UK. 20 ml universals and 7 ml bijoux were purchased from Sarstedt Ltd., Leicestershire, UK. Tissue culture Incusafe® incubators were bought from Sanyo, Loughborough, UK. The Leica DM-IRB/E inverted microscope was purchased from Leica Microsystems Ltd., Milton Keynes, UK.

2.2 Methods

2.2.1 Polymer Preparation

Poly(dimethylsiloxane) (PDMS) was prepared using the Sylgard® 184 elastomer kit (Dow Corning, South Wales, UK) which comes in two parts; a base and a cross-linker. Both constituents are mixed together in a 10:1 ratio, respectively, to initiate the cross-linking reaction. The base/ cross-linker was stirred thoroughly to create a homogenous solution and degassed under ambient conditions prior to spin coating.

The PDMS cross-linking reaction is illustrated in figure 2.1. The siloxane base contains oligomers with vinyl groups (C=C), an example of an oligomer is shown in figure 2.1.A. The low-molecular-weight (LMW) cross-linking agent contains oligomers which contain silicon hydride (Si-H) bonds (see figure 2.1.B) and a platinum (Pt) based catalyst. When base and curing agent are mixed together, the platinum based catalyst catalyses the addition of the Si-H bond across the vinyl groups as illustrated in figure 2.1.C. This reaction proceeds to create a cross-linked network. Increasing the ratio of curing agent to base will increase the number of cross-links. Elevated temperatures will accelerate the cross-linking reaction.

2.2.2 Spin Coating PDMS on glass

Spin coating is a process used to form membranes on to flat substrate surfaces. Briefly, an excess volume of polymer is deposited on the substrate surface which is secured on a stage. The stage is rotated at a specified speed, continued rotation allows spread of the polymer fluid on the substrate surface by centrifugal force. The speed at which the stage rotates determines the final thickness of the spin coated layer on the substrate.

PDMS membranes were fabricated via a multi-step spin coating process. Glass microscope slides (76 x 26 mm) were soaked in acetone for 15 minutes and air dried. 30% (w/v) solution of poly(vinyl acetate) (PVA) in phosphate buffered saline (PBS) was spin coated on to the glass slides at 1000 revolutions per minute (rpm) using a 400 Lite Spinner (Laurell Technologies, North Wales, UK).

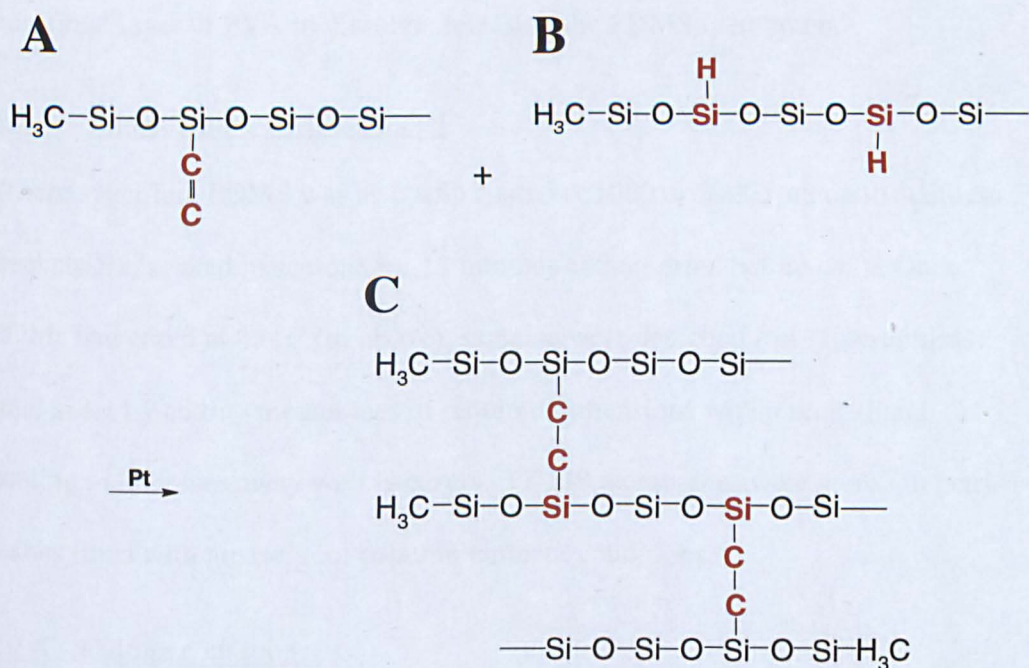


Figure 2.1 Cross-linking reaction of poly(dimethylsiloxane) (PDMS). Illustration showing the cross linking reaction of PDMS. The siloxane base contains vinyl groups (**A**) and the low-molecular-weight (LMW) cross-linker contains Si-H functional groups (**B**) and a Pt catalyst. Mixing base and cross-linker together forms a cross linked network (**C**). Methyl groups bonded to silicon (Si) have been omitted to make the figure comprehensible. This illustration has been adapted from Lue et al².

Samples were left for at least one hour to air dry the PVA. PDMS was then spin coated at 250, 500, 1000 or 2000 rpm for two minutes and left to cure at 65°C overnight. Samples were subsequently immersed in deionised water allowing the sacrificial layer of PVA to dissolve, releasing the PDMS membrane.

2.2.3 Spin coating PDMS on metal

Where specified, PDMS was also spin coated at 1000 or 2000 rpm on to stainless steel sheets (soaked in acetone for 15 minutes and air dried before use). Once PDMS had cured at 65 °C (as above), samples were detached from the stainless steel sheet by cutting membranes of required dimensions with a scalpel and peeling membranes away with tweezers. PDMS membranes were stored in petri dishes lined with greaseproof paper in ambient conditions.

2.2.4 Culture conditions

All cell lines were cultured and maintained as monolayers in tissue culture flasks stored in a humidified-atmosphere tissue culture incubator at 37 °C with 5 % CO₂, ensuring that cells never reached greater than 80% confluence at any one time. C2C12 myoblasts, NIH-3T3 and BJ6 fibroblasts and iHMSCs were grown in media A (appendix 1.1).

HL1 cardiomyocytes were maintained in media B (appendix 1.2) on gelatin and fibronectin (Fn)- coated T25 flasks as previously described³. Flasks were coated by adding 25 µg of Fn in 2 ml of 0.02% gelatin in water to each flask and

incubating at 37 °C overnight. The medium was changed daily. At confluence, cells were split and re-plated (1:3 ratio).

The HUES7 HESC line was maintained as previously described⁴. To prepare conditioned medium, mouse embryo fibroblasts (MEFs) (strain CD1, 13.5 days post coitum) were mitotically inactivated with mitomycin C (MMC) (10 µg/ml) for 2.5 hours and seeded at 6×10^4 cells/ cm². Following 24 hours, inactivated MEFs were incubated in a T75 flask and incubated with 25 ml of media C (appendix 1.3) for 24 hours. Conditioned media was subsequently harvested and made ready for use by supplementing with an additional 4 ng/ml bFGF. Each flask of inactivated MEFs was used to condition the medium for 7 consecutive days. HUES7 HESCs were cultured on Matrigel™ coated tissue culture flasks with daily media changes. Tissue culture flasks were coated by adding Matrigel diluted in DMEM (1:100) and leaving for 1 hour under ambient conditions. Matrigel/DMEM was aspirated prior to plating HUES7 HESC's. Cells were subcultured at confluence (1:3-5 re-plating ratio).

The C2C12, NIH-3T3, BJ6 and HL1 cell lines were routinely passaged using a standard trypsinisation protocol. This included gentle rinsing of the cells with phosphate buffered saline (PBS) (appendix 1.4), followed by treatment with trypsin/EDTA solution (appendix 1.5 and 6) at 37 °C for at least three minutes (based on visual detachment). Following cell detachment, trypsin was inactivated by addition of the appropriate complete medium for the cell line (2:3 ratio of trypsin/EDTA to complete medium). The cell suspension was transferred to a

centrifuge tube and centrifuged at 250 g for 5 minutes. HUES7 HESC's were detached by incubating with 0.05% trypsin/EDTA solution in PBS for less than one minute at 37 °C. Single cells/ small clumps were liberated by tapping the flasks and transferring to a centrifuge tube. Cells were centrifuged at 200 g for two minutes, re-suspended in fresh complete medium and re-plated. All cell pellets were re-suspended in the appropriate volume of conditioned medium. The cell pellet was gently agitated before re-seeding cells at the desired cell density. Cells were either transferred to tissue culture flasks or used for further experiments.

Cell stocks were made and stored in liquid nitrogen for later use (appendix 3).

Cell lines were passaged up to a maximum of 20 times. However cells were discarded if there were any noticeable differences in cell doubling times or morphology.

All aseptic techniques used were performed in accordance with the ATCC guidelines. All cell culture tasks were confined to class II safety cabinets in accordance with ACGM Containment level 2 regulations. Biological waste was disinfected and or/ autoclaved in accordance with ACGM requirements.

2.2.4.1 Calculating desired cell density

Following detachment of cells using trypsin/EDTA solution, the trypan blue exclusion technique (appendix 3.3) was used to determine cell counts and cell viability. Cells were spun down at either 250 or 200 g for five minutes, the

supernatant was removed and cells re-suspended in an appropriate volume of growth media to provide the required cell density. The final cell concentration was used to plate directly onto samples or wells of a tissue-culture plate.

2.2.4.2 Genetic labelling of cell lines

Genetically labelled cell lines were kindly provided by Dr. James Dixon. Briefly, cell lines were genetically labelled using transduction of lentiviruses expressing either enhanced green fluorescent protein (eGFP) or monomeric red fluorescent protein (mRFP). Details of methodology and reagents can be found elsewhere⁵. Cell lines were selected with Puromycin (NIH-3T3: 3 µg/ ml; HL1: 2 µg/ ml; BJ6: 1 µg/ ml and HUES7: 0.3 µg/ ml) for three passages.

2.2.5 Alamar blue assay

The Alamar Blue assay (Invitrogen®, Paisley, UK) was used to measure cell proliferation and viability on sample surfaces. This is a colorimetric assay containing a REDOX indicator that fluoresces when reduced within the alamar blue solution in contact with a metabolising cell population. The advantage of using this assay was that Alamar Blue is non toxic and did not infiltrate the cells so samples could be maintained and used for further time points.

Within a 6-well plate, medium was aspirated from sample containing wells and replaced with Alamar Blue (1:9 in Hank's Balanced Salt Solution (HBSS)) (appendix 4.1). Alamar Blue was also kept in blank wells. Plates were wrapped in aluminium foil and incubated for 90 minutes at 37 °C. Aliquots (200 µl) were

taken from each well and transferred to 96 well polystyrene plate for fluorometric analysis (ex 560 nm/ emm 590 nm) using the InfiniteTM M200 plate reader (Tecan). Average blank values were subtracted from sample measurements and a standard curve was used to correlate fluorescence to cell number (appendix 4.1)

2.2.6 Surface engineering

PDMS surface chemistry was modified using a plasma reactor under vacuum conditions as previously described⁶. The plasma reactor consists of a T-shaped borosilicate chamber enclosed by stainless steel endplates and sealed with Viton O-rings. Plasma was initiated by a 13.56 MHz radiofrequency generator (Coaxial Power Systems Ltd., Sussex, UK) connected to an external deposition chamber by two copper band electrodes and matched manually such that the reflected power was <1 W. Allylamine was degassed by two freeze-pump-thaw cycles prior to use. Allylamine vapour and oxygen gas flow in to the deposition chamber was monitored and controlled manually by needle valves (BOC Edwards, Crawley, UK).

PDMS membranes were oxygen etched for three minutes at a power of 20W and pressure of 300 mTorr. Following this, PDMS surfaces were deposited with plasma polymerised allylamine (ppAAM) for a length of time (specified further on) at a power of 20W and pressure of 300 mTorr. Deposition thickness was monitored using a quartz crystal microbalance (QCM) located inside the reactor.

2.2.7 Surface characterization

2.2.7.1 Sessile drop technique

The sessile drop technique uses a liquid sample to deposit a droplet on to a surface from a syringe that is located above the sample pointing vertically down. A goniometer is a measurement tool used to measure the contact angle of the droplet with the surface. The contact angle is defined as the interaction of the angle at the solid/ liquid interface and the liquid/ air interface. A high contact angle is characteristic of a low wetting or hydrophobic surface. Conversely, a low contact angle is characteristic of a high wetting or hydrophilic surface. The method described in this work used a CAM 200 goniometer (KSV Instruments Ltd., Helsinki, Finland) to measure the static water contact angle (WCA) on each surface type as previously described⁶. Images were captured using a Basler A602f camera and contact angles were measured using CAM 200 image analysis software.

2.2.7.2 Ellipsometry

Ellipsometry was used to determine the deposition thickness of plasma polymerized allylamine (ppAAm) on PDMS surfaces. The method involves initiating a beam of polarized light on to the sample surface. Ellipsometry measures a change in polarization as the light reflects or transmits from the material. The measured response depends on the optical properties and thickness of the material. The technique is restricted to using materials of known optical properties to fit mathematical models used to determine film thickness. Silicon

wafers deposited with ppAAm were used instead of PDMS membranes to determine film thickness. The 'Si with transparent film' model which incorporates the Cauchy dispersion equation was used ⁷.

2.2.7.3 XPS

Surface elemental species of PDMS membranes were determined using X-ray Photoelectron Spectroscopy (XPS) (AXIS ULTRA Kratos, UK) 48 hours post plasma treatment. Briefly, the sample surface is irradiated with monochromatic x-rays causing emission of photoelectrons from a surface depth of 1-10 nm. An electron energy analyzer is used to measure the binding energy and intensity of the photoelectrons. This determines the elemental identity, chemical state and quantity of an element at the surface. A monochromatic Al K α X-ray source with energy of 1487 eV was used, operated at 15 mA emission current and 10 kV anode potential. The pass energy was 80 eV for wide scans with a step size of 0.1 eV. The take off angle of the photoelectron analyzer was 90° for the data shown (quantified using empirically modified relative sensitivity factors).

2.2.7.4 ToF-SIMS analysis

Time of flight secondary ion mass spectroscopy (ToF SIMS) is a surface analytical instrument that irradiates the sample surface with a pulsed primary ion beam to desorb and ionize molecules from a surface depth of ~ 1nm. The resulting secondary ions are accelerated into a mass spectrometer where they are analysed according to mass by measuring their time of flight from the sample surface to the detector. Three different modes of analysis can be employed, these are: surface

mass spectroscopy, surface imaging and depth profiling. Surface imaging was used to detect the distribution of ppAAm on the PDMS surface. Imaging mode is where the pulsed ion beam is rastered across the surface to acquire the entire mass spectrum/ per pixel. The local mass spectrum can be used to identify the presence and distribution of surface molecular species through secondary ion images or ‘chemical mapping.’

ToF-SIMS data were acquired using a ToF-SIMS IV instrument (ION-TOF GmbH., Münster, Germany) equipped with a bismuth liquid metal ion gun and a single-stage reflectron analyzer. Operating conditions utilized a Bi_1^+ primary ion energy of 25 kV and a pulsed target current of approximately 1.0 pA. Low-energy electrons (20 eV) were used to compensate for surface charging caused by the positively charged primary ion beam on the insulating surfaces. Rastered areas of $500 \times 500 \mu\text{m}^2$ were analyzed at a resolution of 256×256 pixels. The total primary ion beam dose for each analyzed area was kept below 1×10^{12} ions cm^{-2} , ensuring static conditions. Preliminary and preparative data analysis was carried out using IONTOF Surfacelab6 software.

2.2.8 Micropatterning

Stainless steel stencils with laser cut micro-features were provided by Tannlin Ltd, UK. Patterns covered a total area of 1.1 cm^2 . These micro-stencils acted as masks to selectively deposit ppAAm (see 2.2.6) and extracellular matrix (ECM) aerosols on the PDMS surface.

Liquid fibronectin (Fn), (Sigma, UK) was used as the prototype ECM protein. Fn was fluorescently labelled and purified using the AlexaFluor568 Labelling Kit (Invitrogen, UK). Fn (4 μ l of 500 μ g/ml in PBS) was airbrushed using a ECL4500 HP-CS gravity fed airbrush connected to an IWATA Studio Silver Jet Compressor (The Airbrush Company Ltd., UK). Aerosols were deposited at a working pressure of 20 psi. Matrigel (BD Biosciences, UK) was airbrushed diluted 1:1 in DMEM. Matrigel was kept on ice to prevent polymerisation before deposition.

3

Mechanical compatibility of poly(dimethylsiloxane) for cardiac tissue engineering

3.1 Introduction

Native myocardium exhibits unique biomechanical behaviour which acts as a stimulus for cardiomyocyte development and function⁷⁵. Thus, to engineer functional tissue equivalents it is essential to mimic the physiological environment. Biomaterials used to engineer myocardium must be capable of sustaining constant mechanical loads. Previous studies have shown how cardiomyocytes cultured on substrates with inadequate mechanical properties result in non-contractile engineered tissue⁸⁸.

In this chapter, the mechanical compatibility of a biomaterial is analysed by tensile testing to yield specific material properties including tensile strength, ultimate elongation, Young modulus and long term stiffness. These properties are considered most relevant because physiologically, myocardial tissue is subjected to long term tension beating cyclically and constantly⁸⁹. The native left ventricular myocardium consists of a collagen fibrous matrix and in its healthy state is soft

and elastic, the Young modulus ranges from 0.01-0.02 MPa at the beginning of diastole and 0.5 MPa at the end of diastole. These values have previously been used as the lower and upper bounds of stiffness when selecting biomaterials²⁵.

As discussed in depth within the general introduction (1.6.3), elastomers have become widely recognised in the CTE field because they can be manufactured to match the criteria outlined above^{25,90}. Importantly, the mechanical properties of an elastomer can be finely tuned by varying the extent of cross linking. This work focuses on poly(dimethylsiloxane) (PDMS) as a potential substrate for engineering cardiac tissue. PDMS comes from a large elastomer family of polysiloxanes or silicones, generally having numerous applications in the form of coatings and thin films⁹¹. Both chemical structure and cross linking density contribute to the intrinsic elastic properties of PDMS. PDMS has a flexible and mobile macromolecular structure. Abou-Hessein et al. found that this is the result of a very open silicon-oxygen-silicon bond angle ($\sim 130^\circ$) and almost zero rotational energy for the silicone-oxygen (Si-O) bond⁹². The macromolecular structure of PDMS consists of polymer chains with a small diameter of approximately 0.7 nm. The cross linking of these chains contributes to PDMS having large ultimate elongation and low stiffness⁹³. Previous work showed that PDMS fabricated in to membranes could be used as a substrate for engineering myocardium⁸¹. However, the mechanical properties of these membranes needs to be better understood. The objective of this work is to use spin coating to manufacture PDMS membranes of

different thickness and subsequently investigate how membrane thickness affects the mechanical response to tensile testing.

3.2 Materials and Methods

3.2.1 Sample Preparation

PDMS was prepared and spin coated at 250, 500, 1000 and 2000 rpm as previously described in 2.2.1 and 2.2.2. Die cutting was used to create dog bone shaped samples from the PDMS membranes. Sample dimensions complied with the ASTM D412 test for standardised vulcanized rubber and thermoplastic elastomers and were used for uniaxial tensile testing.

For cyclic mechanical testing, PDMS membranes spin coated at 2000 rpm were used. These samples were cut in to rectangles (26 x 18 mm) using a scalpel. An acetate frame (18 x 36 mm, border thickness of 5 mm) was attached to each PDMS membrane using freshly made PDMS to provide support. Samples were left for 48 hours at room temperature for the PDMS adhesive to cure. A stencil was used to mark the 'five dot dice pattern' on one side of the PDMS membrane using a permanent marker (appendix 5.1).

3.2.3 Measuring PDMS membrane thickness

PDMS is inherently hydrophobic, this meant that spin coated PDMS membranes readily sealed themselves to microscope glass slides. A permanent marker was used to mark three areas on the glass slide close to the PDMS membrane, (see appendix 1.2). Each of these three areas was viewed using a Nikon Optiphot

microscope (Nikon, UK); the magnification (x40), light intensity and coarse focus remained fixed. The fine focus control knob on the microscope was marked with a micrometer scale. This scale was used to determine the difference in focal distance between the glass microscope slide and the PDMS membrane. The average difference of the three areas determined the final PDMS membrane thickness. Data was statistically analysed using a one-way ANOVA test with the Bartlett's post test to evaluate whether the linear trend was statistically significant at a 95% confidence level ($p < 0.01$).

3.2.4 Uniaxial tensile tests

Dog bone shaped PDMS membranes were mounted in to standard manufactured tensile grips of an Instron Universal (Sercal Materials Testing Machines Services Ltd, Worcestershire, UK) controlled with Instron Bluehill software. A 5kg load cell was used to monitor load. Samples were strained to failure at a rate of 1 mm/second. PDMS membrane stiffness was measured by mounting samples in a Q800 Dynamic Mechanical Analyser (DMA), (TA Instruments, Hertfordshire, UK). Samples were subjected to a maximum force of 0.02 N and the Young modulus of the stress strain curves was measured using associated software. Tensile testing was carried out twice; at room temperature and 37°C.

3.2.5 Cyclic Mechanical Testing

To assess long term mechanical stiffness, PDMS membranes were placed in a fatigue bath consisting of custom made stainless steel tensile grips (see appendix 5.2). The fatigue bath was mounted on to an Electroforce ELF 3200 mechanical

tester (BOSE, UK) controlled by WinTest software (Ver 2.51). Samples were subjected to cyclic mechanical strain (CMS) at 1 Hz and peak strain of 10% to mimic physiological conditions for 72 hours. All testing was carried out in a tissue culture incubator at 37°C and 5% CO₂. PDMS membrane strain was controlled using a camera extensometer. The camera monitored the distance between the five dots of the dice pattern marked on the membranes; this determined the sample strain (see appendix 5.1). Each sample was strained to 10% before and after CMS was applied.

3.3 Results and Discussion

Tissue engineered myocardium must incorporate a biomaterial that offers minimal resistance to cardiomyocyte-mediated contraction. Although the mechanical properties of native tissue are used as a guideline when selecting biomaterials, the correct mechanical properties for creating biomimetic tissue engineered myocardium remain unknown. Thus, it was necessary to manufacture a range of PDMS membranes so that cell function could be studied at a later stage. The effect of spin coating speed on physical and mechanical properties of PDMS membranes was assessed.

3.3.1 Stress-strain behaviour of PDMS membranes

There is limited information available on the tensile properties of spin coated PDMS membranes. Therefore, it was necessary to investigate the mechanical response of spin coated PDMS membranes to tensile testing to gain knowledge of how these elastomeric membranes may respond in physiological conditions.

Uniaxial tensile testing was used to derive stress-strain curves and investigate material behaviour. PDMS membranes were mounted in to an Instron and subjected to uniaxial tension at a constant strain rate of 1 mm/ second. The stress-strain behaviour of PDMS membranes spin coated at 250, 500, 1000 and 2000 rpm is illustrated in figure 3.1.

The graphs in figure 3.1 show that the stress-strain curve of a spin coated PDMS membrane follows the same non-linear profile at all spin coating speeds. Figure 3.2 shows the stress-strain curve of a PDMS membrane spin coated at low (250 rpm) and high speed (2000 rpm). Both stress-strain curves show elastomeric behaviour. This is characteristic of elastomers, where the membrane initially deforms reversibly before it yields and flows under the applied force, failing as a result of strain hardening⁹⁶. Key regions of the stress-strain curves have been highlighted, the three regions provide values for the Young modulus, tensile strength and ultimate elongation of each membrane. The linear elastic region remained within 0-10% strain of the stress-strain curve for each spin coated PDMS membrane. However, figure 3.1 shows that there is no trend in the data. Next, the film thickness of membranes spin coated at each speed were measured and the effect of spin coating speed on tensile strength and ultimate elongation was investigated.

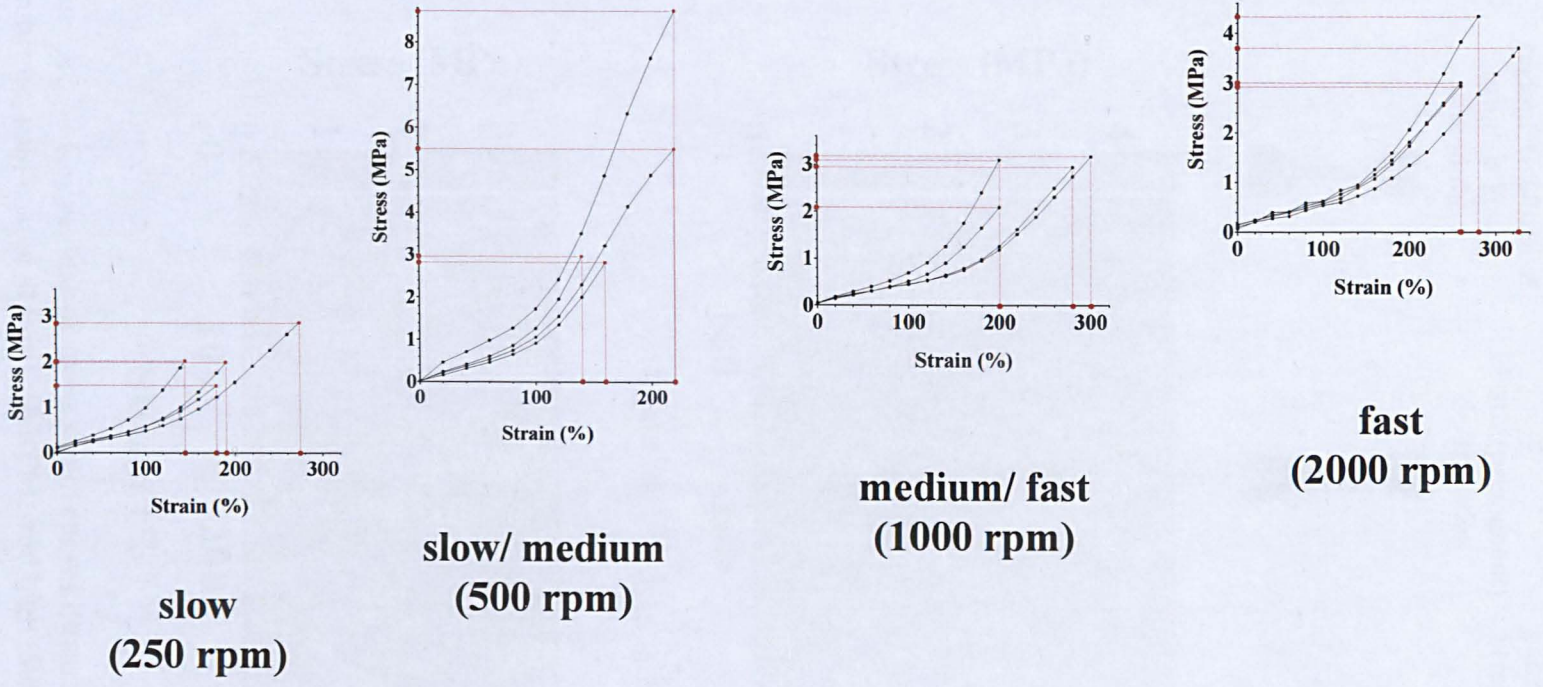


Figure 3.1 Stress-strain curves of PDMS membranes spin coated at 250, 500, 1000 and 2000 RPM. Red lines highlight the maximum stress and strain of each stress-strain curve.

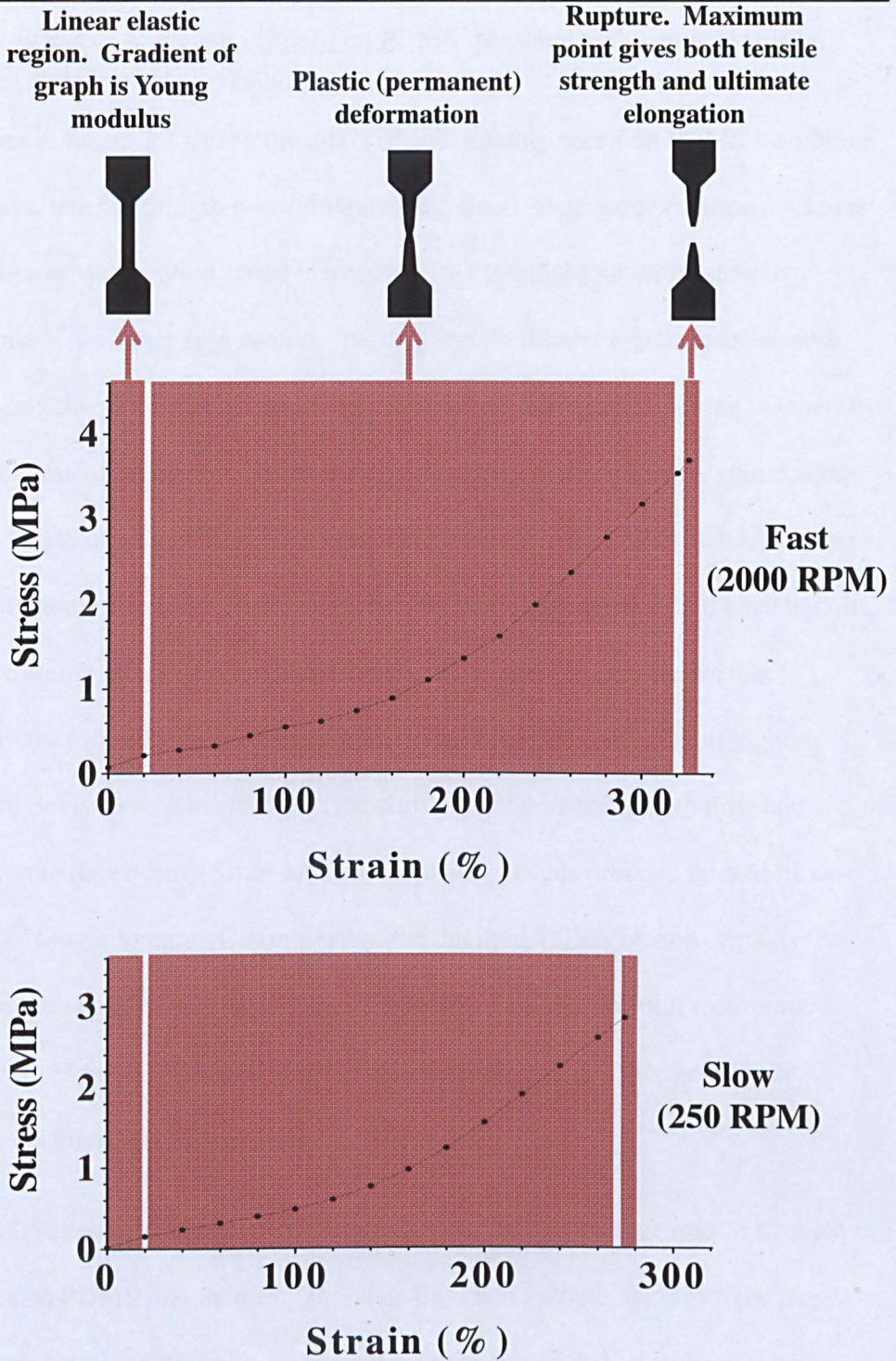


Figure 3.2 Key regions of stress strain curves illustrated using PDMS membranes spin coated at low (250 RPM) and high (500 rpm) speed.

3.3.2 Effect of spin coating speed on PDMS membrane thickness, tensile strength and ultimate elongation

The data in figure 3.3 shows the effect of spin coating speed on PDMS membrane thickness, tensile strength and ultimate elongation. Average membrane thickness decreases as spin coating speed increases. This is consistent with previous literature^{93,94}. Higher spin coating speeds generate thinner membranes because higher angular velocities act on the viscous PDMS during spin coating. Generally, the thickness of membranes formed by spin coating is controlled by spin coating speed, length of spin coating time and polymer viscosity⁹⁵. In this case, polymer viscosity and time remained constant, thus spin coating speed would have had the most profound effect on membrane thickness. Figure 3.3 also shows that membranes formed at lower spin coating speeds (<1000 rpm) exhibit higher standard deviations. This is due to the curing of PDMS being both time and temperature dependent. Since lower spin coating speeds produce thicker films, they take longer to cure. Consequently, the uncured PDMS is more sensitive to flow on the substrate due to gravity. This results in a non-uniform membrane thickness. However, the size of the error bars indicates that the variance in membrane thickness is negligible.

Figure 3.3 shows the effect of spin coating speed on the average tensile strength of spin coated PDMS membranes. This data has been extrapolated from the stress-strain curve of each PDMS membrane plotted in figures 3.1, it is the maximum stress that the membrane can withstand prior to failure. Tensile strength increases

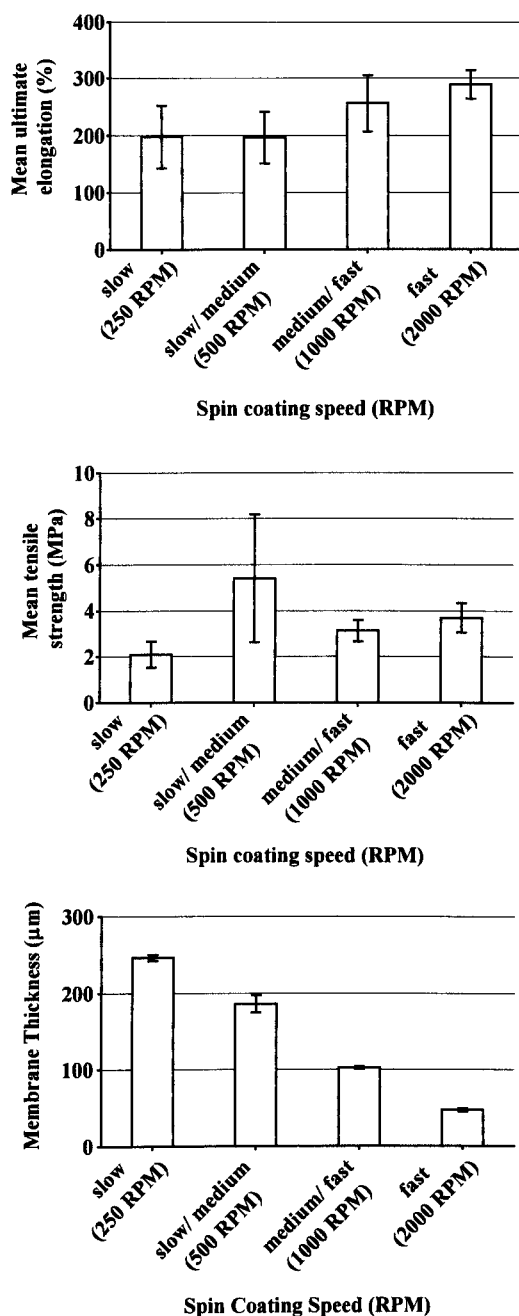


Figure 3.3 Effect of spin coating speed on membrane thickness, ultimate elongation and tensile strength of PDMS membranes. Mechanical testing was carried out on the Instron (Sercal Materials Testing Machines Services Ltd, Worcestershire, UK).

from 2.1 to 3.68 MPa as spin coating speed increased from 250 rpm to 2000 rpm. Membranes spin coated at 500 rpm do not follow this trend, exhibiting the highest tensile strength (5.4 MPa), however this value is less accurate illustrated by a large SEM (± 2.5 MPa). The tensile strength of spin coated PDMS membranes (2.1-3.68 MPa) is an order of magnitude higher than the tensile strength of human myocardium (3-15 kPa)⁹⁷. This shows that PDMS membranes are capable of sustaining higher mechanical loads.

Figure 3.3 shows the effect of spin coating speed on the ultimate elongation of spin coated PDMS membranes. Again, this data has been extrapolated from the stress-strain curve of each PDMS membrane plotted in figure 3.1. The ultimate elongation is the maximum strain that the membrane can withstand prior to failure. The ultimate elongation increases from 198 to 290 % as spin coating speed increased from 250 rpm to 2000 rpm. This shows that PDMS membranes exceeded twice their original length prior to failure, characteristic of elastomeric behaviour⁹⁸.

Further to investigating the end point mechanical response of PDMS membranes, dynamic mechanical analysis was used to re-measure the Young modulus. This is because the dynamic mechanical analyser (DMA) is more appropriate than the Instron for measuring the Young modulus of polymeric materials⁹⁹. Furthermore, unlike the Instron, the preload on each membrane tested on the DMA was defined prior to stretch, ensuring that the initial stress acting on each membrane remained constant. Each of six PDMS membranes was initially subjected to a uniaxial

tensile test, first at room temperature and secondly at 37 °C (data not shown).

Membranes were stretched within their linear elastic region to ensure that no permanent deformation occurred. The stress-strain curves derived from the Instron determined that PDMS membranes remained linear elastic between 0-10% strain, thus membranes were subjected to a maximum of 8% tensile strain. Stress-strain curves of PDMS membranes in both conditions were identical indicating that the mechanical response of PDMS membranes *in vivo* is the same as that in ambient conditions. Subsequently, all further tensile testing in the DMA was carried out at 37°C. Quintets of PDMS membranes spin coated at 250, 500, 1000 and 2000 rpm were subjected to a maximum of 8% strain. The Young modulus was automatically determined by Q800 DMA software by measuring the gradient of the stress strain line. An example of the primary data is shown in Appendix 5.3

Figure 3.4 shows the effect of spin coating speed on the average Young modulus of PDMS membranes. Young modulus decreases from 1.74 to 0.79 MPa as spin coating speed increases from 250 rpm to 2000 rpm. The thickest membranes spin coated at the lowest speed (250 rpm) exhibit a lower Young modulus of 1.46 MPa. However, this value is less precise illustrated by the large error bar for this data set. Since Young modulus is an indicator of mechanical stiffness, these results show that the thinnest PDMS membranes (spin coated at 2000 rpm) exhibit the least stiffness.

Average tensile strength, ultimate elongation and the Young modulus of spin coated PDMS membranes vary according to the spin coating speed used. Since

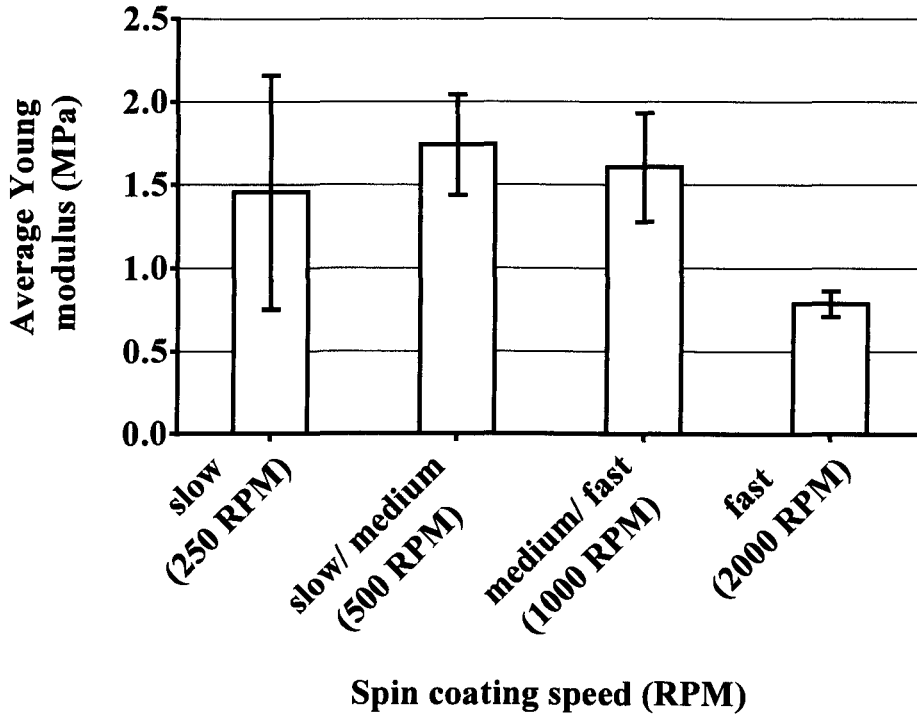


Figure 3.4 Effect of spin coating speed on the Young modulus of PDMS membranes. Membranes were elongated to a maximum force of 0.02 N using the dynamic mechanical analyser (DMA), (TA Instruments, Hertfordshire, UK).

spin coating speed controls membrane thickness the data suggests that the mechanical properties of PDMS membranes are thickness-dependant, a phenomenon that has previously been described¹⁰⁰. Tensile strength and ultimate elongation decreases, whilst the Young modulus increases as PDMS membrane thickness increases from 50 to 200 μm . Liu et al. also showed that the Young modulus and tensile strength of spin coated PDMS membranes became thickness dependant beyond a critical membrane thickness ($< 200 \mu\text{m}$)¹⁰⁰. However, Young modulus and tensile strength increased as membrane thickness decreased, contrary to the findings in this work. They defined an equation relating the radius of the wafer substrate, the angular velocity and the shear stress acting on PDMS during spin coating. At higher spin coating speeds ($>1000 \text{ rpm}$), a higher angular velocity is required creating a greater shear stress between PDMS and the substrate. This shear stress causes the polymer chains within the bulk PDMS to preferentially align in a direction that gives the PDMS membrane a higher Young modulus and tensile strength⁹⁴. It is difficult to ascertain why the trend between Young modulus and film thickness in this work differs. Known differences between both studies include the substrate (PVA coated glass) and substrate dimensions on which PDMS was spin coated. This could have affected the shear stress between the PDMS and the substrate. It is also possible that the length of curing time had a more profound effect on Young modulus compared to the spin coating speed. As previously mentioned, thicker PDMS membranes take longer to cure. Longer curing time induces a higher cross linking density resulting in an increased Young

modulus. However, further work is required to fully understand the true mechanism behind this. These results demonstrate that the mechanical response of PDMS membranes to uniaxial tensile strain is dependent on the spin coating speed used to manufacture the membrane.

Having gained better understanding of the mechanical response of spin coated PDMS membranes to tensile strain, it was necessary to make a decision about which membrane thickness should be used for further developmental work. Since the correct mechanical properties for biomaterials used in CTE remain unknown, previous work by Feinberg et al. was used to come to an informed conclusion⁸¹. Feinberg et al showed that rat cardiomyocytes seeded on PDMS membranes with a thickness of <50 μm were capable of deforming the membrane during contraction. Furthermore, this work demonstrated that membrane thickness is a crucial factor for engineering tissue with contractile function. In this work, the aim is to seed a higher cell density of cardiomyocytes than used by Feinberg et al. Thus, it is reasonable to presume that a higher cardiomyocyte density is capable of inducing a stronger contraction and deforming PDMS membranes of 50 μm thickness. Furthermore, during practical work it was found that spin coated PDMS membranes with a thickness of <50 μm were very difficult to handle at the size that is required for this project, so employing 50 μm thick membranes would present fewer difficulties. Thus, for all future developmental work in this thesis, PDMS membranes spin coated at 2000 rpm will be used.

Next PDMS membranes spin coated at 2000 rpm were subjected to cyclic loading mimicking physiological conditions to investigate the effect of fatigue on PDMS membrane stiffness.

3.3.3 Effect of fatigue on PDMS membrane stiffness

Cyclic mechanical testing is used to measure mechanical property degradation as a result of material fatigue. Four PDMS membranes spin coated at 2000 rpm were subjected to 72 hours of cyclic mechanical strain (CMS) (0-10%) at 1 Hz, with a triangular waveform to mimic the cardiac environment²⁴. Each membrane was submerged in DMEM within the fatigue bath during testing to mimic the wet conditions *in vivo*. Once each PDMS membrane was mounted in to the bioreactor, the extensometer incorporated with the BOSE was used to detect the extent of strain using the five dot dice pattern, eliminating the requirement to determine the sample strain manually.

The line graph in appendix 5.4 shows the cyclic strain applied to a rectangular PDMS membrane for a 10 second duration to illustrate the regime detailed above. The effect of CMS on the stiffness of PDMS membranes was assessed by measuring the Young modulus of each membrane before and after CMS was applied. The Young modulus was automatically derived using WinTest software by subjecting each membrane to a uniaxial tensile test to a maximum of 8% at a strain rate of 1 mm/10 seconds. Again, the extensometer was used to monitor sample strain to a maximum of 8%.

Figure 3.5 is a line graph showing the effect of CMS on four PDMS membranes spin coated at 2000 rpm. The data shows that an increase in membrane thickness generally results in an increase in Young modulus. The effect of CMS on mechanical stiffness of each PDMS membrane varies, resulting in either an increase or decrease in mechanical stiffness. The thinnest membrane (47 μm) exhibits the greatest variation in stiffness as a result of applying CMS, the Young modulus decreased by 78 kPa. Although the adequate mechanical response of biomaterials to CMS for CTE is unknown, there is a previous study that examined the effect of CMS on the stiffness of PGS, an established elastomer in the field of CTE²⁴. Engelmayr et al. used the same cyclic test conditions as the work in this thesis to test material fatigue of both PGS and rat myocardium. The study found that applying CMS caused a change in mechanical stiffness of PGS and rat myocardium; the Young modulus decreased by 30-50 kPa in both materials, the same order of magnitude of change that CMS had on PDMS.

The Young modulus of PDMS membranes before CMS was applied ranged from 1.25 to 1.5 MPa. This value is higher than the Young modulus of 50 μm thick PDMS membranes tested on the DMA (0.79 MPa). This may be a direct influence of changing sample dimensions and should be taken in to consideration for future work. Rectangular shaped PDMS membranes were used for cyclic testing. Standard dog bone shaped specimens (used for uniaxial tensile testing), were not used because future work will involve applying CMS to cells cultured on PDMS membranes, requiring a larger surface area to accommodate the cell monolayer.

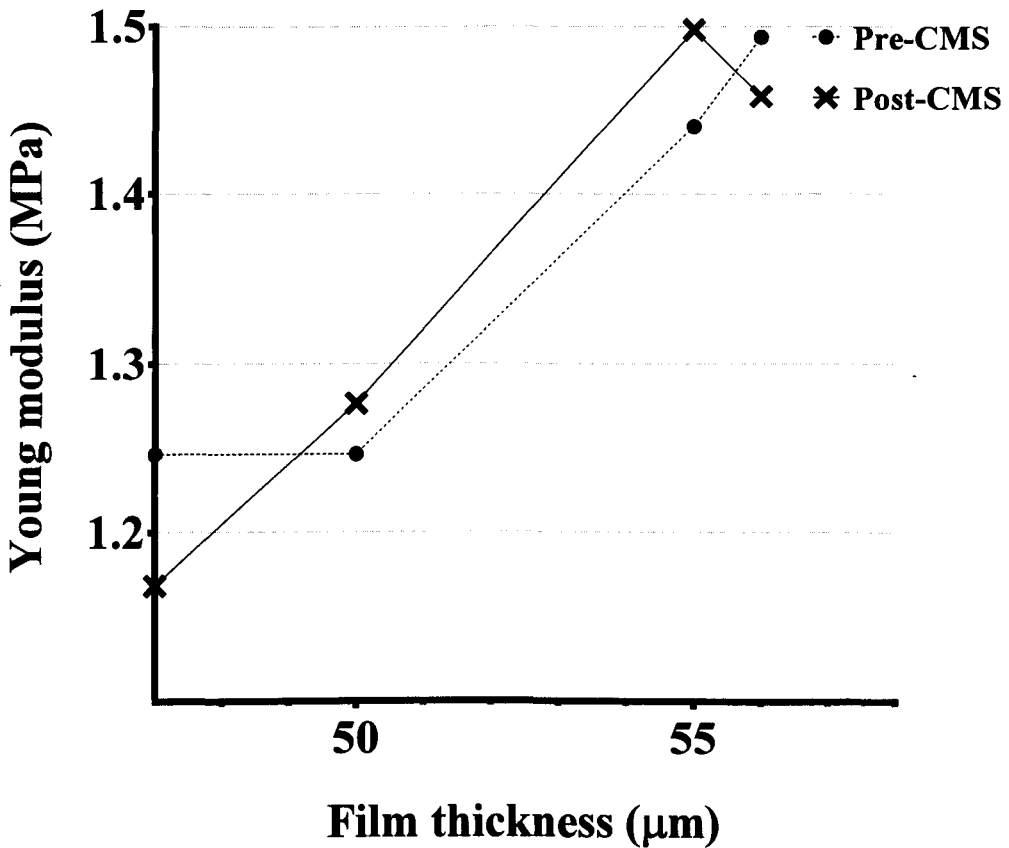


Figure 3.5 The effect of cyclic mechanical strain (CMS) on PDMS membranes spin coated at 2000 RPM. The Young modulus of four membranes was measured using extensometer / WinTest software before and after application of CMS on the BOSE Electroforce 3200 (Bose, UK).

3.3.4 Mechanical compatibility of PDMS for CTE

PDMS fabricated in to membranes with a thickness ranging from 50 to 250 μm exhibit a mechanical stiffness that is the same order of magnitude as established elastomers within the field of CTE. For example, PGS and POC membranes exhibit a Young modulus of 2.6 and 2.1 MPa respectively^{24,71}. However, the Young modulus of healthy native myocardium is 10-50 kPa, this is a difference of two orders of magnitude. Although the correct mechanical properties for biomaterials used in CTE remain unknown, the study by Feinberg et al. demonstrated the capability of PDMS membranes to create engineered myocardium⁸¹. Furthermore, this paper contains important quantitative information that can be used to investigate the physical and mechanical properties on cardiomyocyte contractile function at a later stage.

3.4 Conclusion

The practical work included in this chapter explored the feasibility of the spin coating process to create membranes from the elastomer PDMS and subsequently, the effect of this process on the mechanical properties of the membranes. Results showed that spin coating successfully created PDMS membranes with inherent elasticity and demonstrated the versatility of this technique to manufacture membranes of different thickness. Further analysis showed that membrane thickness is dependent on the spin coating speed used. Uniaxial tensile testing of PDMS membranes spin coated at 250, 500, 1000 and 2000 rpm showed that the linear elastic region remained within 0-10% for all membranes. This elastic limit

will be used for future work to ensure that PDMS membranes do not permanently deform or exceed this limit. The data revealed that there is a trend between tensile properties (tensile strength, ultimate elongation, Young modulus) and the spin coating speed used. Fatigue testing showed that there was no trend to draw a conclusion on how CMS affects the mechanical stiffness of PDMS membranes.

The results from this chapter provide broader knowledge on the tensile behaviour of spin coated PDMS membranes and the data will be used for future reference. For the meantime, membranes spin coated at 2000 rpm will be used for further developmental work.

Further work will be required at a later stage to understand the relationship between PDMS membrane stiffness, membrane dimensions and contractile activity, once cardiomyocytes are successfully seeded and aligned on the membrane surface.

4

Surface engineering of PDMS membranes to encourage cell adhesion and proliferation

4.1 Introduction

The mechanical properties of spin coated PDMS membranes have been established in the previous chapter, the next step is to develop a method to make the PDMS surface cell adhesive. The inherent surface chemistry of PDMS inhibits cell adhesion. This is attributed to a hydrophobic surface and low surface energy¹⁰¹. Therefore, it is necessary to modify the PDMS surface to encourage cell adhesion.

Various methods to encourage cell attachment to the PDMS surface have been previously reported. De Silva et al deposited adhesive proteins on PDMS using micro-contact printing and precision aerosol spraying of laminin through a mask^{102,103}. Both processes mediated cell adhesion via the adhesive protein, effectively masking the surface rather than altering surface chemistry. One popular method to render the PDMS surface hydrophilic is using oxygen plasma treatment, however the chemically modified surface does not remain stable for more than 24 hours^{104,105}. This is a result of hydrophobic recovery, a phenomenon

that can occur as a result of diffusion of low-molecular-weight (LMW) chains from the bulk to the surface. Thus, there has been growing interest in developing methods to create hydrophilic PDMS surfaces that remain stable for a longer period of time.

Bodas et al. used higher levels of oxygen etching to preserve surface hydrophilicity by using a higher RF power (150 W) and longer treatment time (15 minutes)¹⁰⁶. Eddington et al. found that thermal aging of oxygen plasma activated PDMS surfaces reduced the effect of hydrophobic recovery¹⁰⁴. Kim et al. used radio frequency (RF) plasma treatment at atmospheric pressure rather than at vacuum pressure to oxygen etch the PDMS surface¹⁰⁷. This resulted in a hydroxyl rich PDMS surface that remained stable for twenty days. An alternative to oxygen etching has been to use ultraviolet (UV) treatment to first reduce hydrophobic recovery followed by an ultraviolet/ozone (UVO) treatment to generate hydrophilic groups on the PDMS surface¹⁰⁸. Functional group implantation using polymer grafting following oxygen plasma treatment is a controlled and uniform method to change the surface chemistry of a polymer. Mashwari et al. and Bodas et al. used oxygen plasma treatment followed with a chemical derivatization step, using branched- polyethylenimine (b-PEI) and 2-hydroxyethyl methacrylate (HEMA), respectively^{109,110}. Both techniques showed that incorporating b-PEI and HEMA retained PDMS surface hydrophilicity for at least ten days. However, the main drawback of the above mentioned studies is that these surface modification techniques change the local mechanical properties of

PDMS. This affects the behaviour of cells adhered to the surface since mechanical stiffness is important for cell proliferation, differentiation and physiology. The nature of this work requires that the mechanical properties of PDMS are able to influence the cells attached.

Plasma polymers have been used in addition to oxygen etching to prepare different surface chemistries^{86,111}. They provide smooth coatings and do not alter topography. They can be deposited on to any substrate independent of surface chemistry. This chapter focuses on plasma polymerising the PDMS surface with allylamine. Allylamine is an amine containing organic monomer which can be plasma polymerised creating a poly(allylamine) surface. The linear formula of poly(allylamine) is $[\text{CH}_2\text{CH}(\text{CH}_2\text{NH}_2)]_n$ (chemical structure is illustrated in figure 5.1). Plasma polymerised allylamine (ppAAm) has previously been used to create hydrophilic, cell adhesive surfaces^{86,112,113}. The advantage of using allylamine is that it is a non-saturated monomer so less energy is required for the polymerisation. Furthermore, a higher amount of primary amine can be retained in the plasma polymer consequently creating an amine rich plasma polymerised surface. This work incorporates light oxygen plasma treatment to activate the PDMS surface and ensure good coating adhesion of ppAAm. Surface characterisation techniques have been used to monitor surface stability and the effect of this surface modification technique on cell adhesion and proliferation is also investigated.

4.2 Materials and Methods

4.2.1 Substrate Preparation

Elastomeric membranes of 50 μm thickness were formed by spin coating PDMS on to stainless steel sheets as described in 2.2.3.

4.2.2 Surface Engineering

PDMS surfaces were oxygen etched and deposited with plasma polymerised allylamine (ppAAm) for either 5 or 25 minutes as described in 2.2.6. Triplicates of each surface were created.

4.2.3 Ellipsometry

Ellipsometry was used to measure ppAAm deposition thickness as described in 2.2.7.2.

4.2.4 Surface Wettability

Static water contact angle (WCA) measurements were made on each surface type 48 hours after plasma treatment of PDMS membranes as described in 2.2.7.1. using a CAM 200 Optical Contact Angle Meter and software (KSV Instruments Ltd., Helsinki, Finland) as previously described⁸⁶. Images were taken using a Basler A602f camera. All contact angle measurements were made 48 hours after plasma treatment of the PDMS membranes unless stated otherwise.

4.2.5 XPS

Surface elemental species of PDMS and ppAAm deposited PDMS membranes was

determined using X-ray Photoelectron Spectroscopy (XPS) (AXIS ULTRA Kratos, UK) 48 hours post plasma treatment as described in 2.2.7.3.

4.2.6 Cell Culture

C2C12 myoblasts were cultured and plated on to engineered PDMS membranes in non-tissue culture plastic (TCP) 6 well plates as described in 2.4 and 2.2.4.1 respectively. Cell suspensions of 5×10^5 cells (in 4mls/well) were used. Cell viability was assessed using the Alamar Blue assay (see 2.2.5). Data was statistically analysed using the two-way ANOVA test. The post Bonferonni test was used to evaluate the statistical significance between the positive control (TCP) and treated samples at a 95% confidence level ($p < 0.05$). Statistically significant data is represented with a (****).

4.3 Results and Discussion

Oxygen etching and surface deposition of plasma polymerised allylamine (ppAAm) were used to change the surface chemistry of hydrophobic PDMS to a hydrophilic state and encourage cell attachment. Oxygen etching was used to break bonds at the PDMS surfaces such that the interface with the ppAAm coating would be strong and durable. As previously mentioned, higher levels of oxygen etching have been used to change PDMS surface chemistry without the need for further polymer deposition¹⁰⁶. These approaches used high powered environmental plasma systems which would result in conversion of PDMS to surface Silica by oxidation and affect local mechanical properties. PpAAm is

stable under flexing, thus a nanometre (nm) scale coating on PDMS with this polymer offers an alternative to high-level surface oxygen etching.

4.3.1 Ellipsometry

Ellipsometry was used to measure ppAAm surface deposition thickness on oxygen etched silicon wafers. Deposition thickness increases with exposure time to plasma treatment as shown in Figure 4.1. Ellipsometry readings were significantly lower than values provided by the QCM measurement made in the plasma chamber. This is similar to previous work¹¹⁴.

Two ppAAm surface deposition thicknesses on PDMS membranes were used for further surface modification studies [13 and 92 nm, abbreviated to ppAAm (13 nm) and ppAAm (92 nm) respectively]. These are similar thicknesses used by studies depositing a ppAAm coating to aid the attachment of cells¹¹³. Oxygen etched PDMS membranes were also used, these have been abbreviated to PDMS*.

4.3.2 Surface Wettability

The next stage of this work assessed the change in surface hydrophobicity of PDMS membranes by ppAAm deposition. Surface analysis was carried out 48 hours after plasma treatment allowing sufficient time for any radical species trapped in the ppAAm film to equilibrate with the ambient environment and to match the time after production which samples were used in cell experiments. The WCA between a sessile water droplet and the surface directly demonstrates the

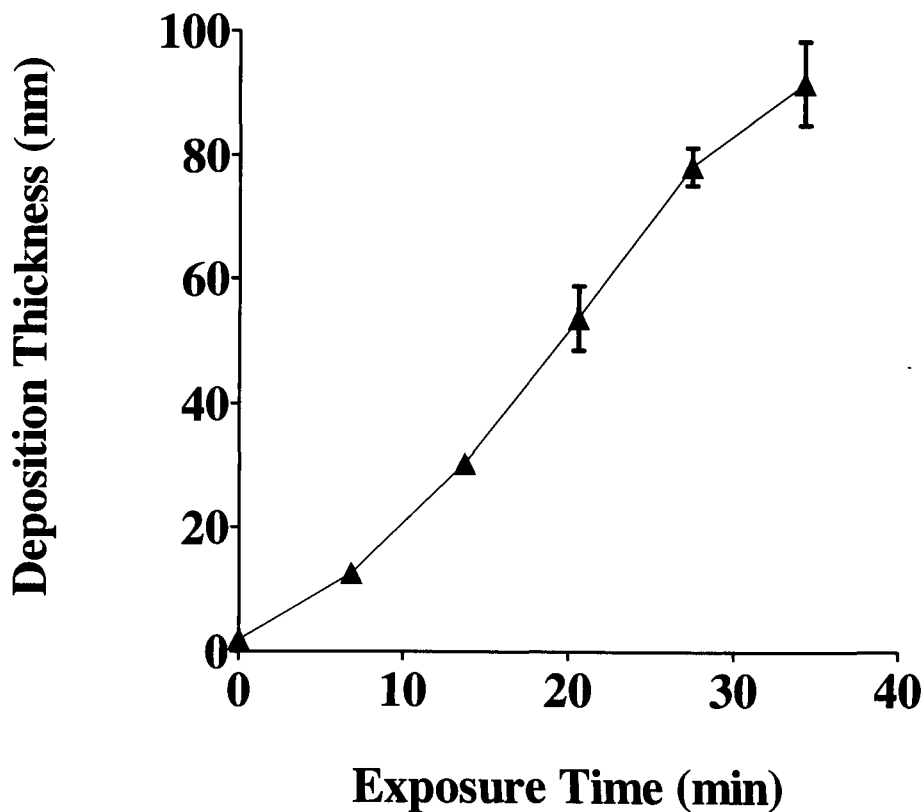


Figure 4.1 Time-dependent plasma polymerized allylamine (ppAAm) deposition analysis on PDMS membranes. Deposition thickness was measured using an ellipsometer (J.A. Woollam Co. Inc., Lincoln, USA). Results represent mean deposition thickness \pm SEM.

hydrophobic/philic properties of the surface. The WCA values were measured over two weeks during which PDMS samples were stored at room temperature. Figure 4.2 shows images of a water droplet as it first came in to contact with the PDMS surfaces. Untreated PDMS (PDMS) shows no change in shape of the water droplet during 14 days. Oxygen etched PDMS (PDMS*), ppAAm (13 nm) and (92 nm) surfaces show that the shape of the water droplet on contacting the surface changed over the two week period. At day 1, the water droplet covers a larger surface area on PDMS*, ppAAm (13 nm) and (92 nm) surfaces compared to days 7 and 14. This suggests that these surfaces are hydrophilic at day 1 but retain surface hydrophobicity. These images were used to measure WCA values to evaluate how surface hydrophobicity changed over time, the data is shown in Figure 4.3. The surface wettability of untreated PDMS surfaces remained uniform at 110° demonstrating hydrophobicity. PDMS* surfaces were least stable, the WCA was decreased by the treatment compared to PDMS, and then increased from 78 to 95° from day 0 to 14. This hydrophobic recovery is as a result of the diffusion of oligomers from the PDMS to the plasma oxidised silicone surface. PDMS surfaces deposited with ppAAm (13 nm) and ppAAm (92 nm) had the lowest WCA values at day 0, these being 70 and 71° , respectively showing that surfaces have been made more hydrophilic. These values are in the range as those previously reported for ppAAm^{86,113}. However, by day 14, the WCA values increased to 87 and 77° for ppAAm (13 nm) and ppAAm (92 nm), respectively. The thicker ppAAm deposit reduced hydrophobic recovery, presumably by

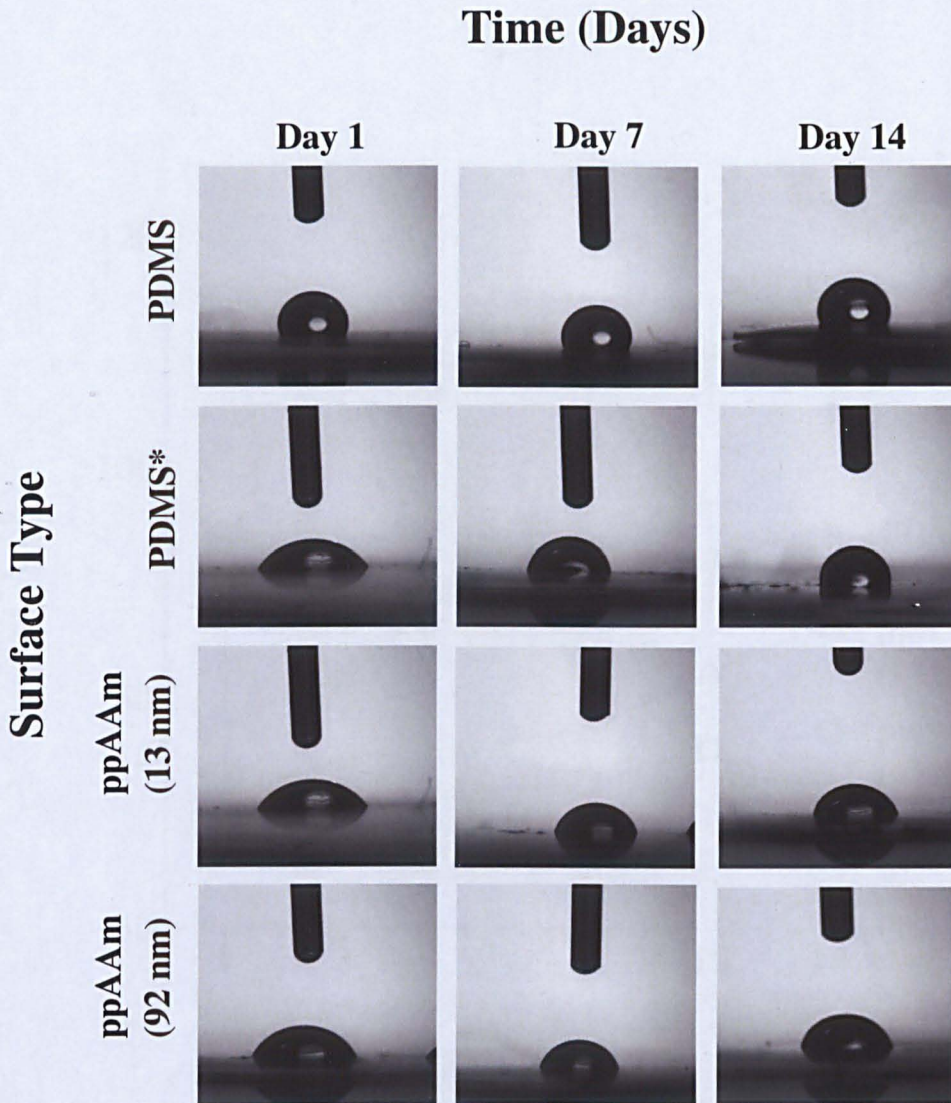


Figure 4.2 Images showing the interaction of a water droplet with the untreated PDMS (PDMS), oxygen etched PDMS (PDMS*), ppAAm (13 nm) and ppAAm (92 nm) surface during 14 days. Images were taken using the CAM 200 Optical Angle Meter equipped with a Basler A602f camera (KSV Instruments Ltd., Helsinki, Finland).

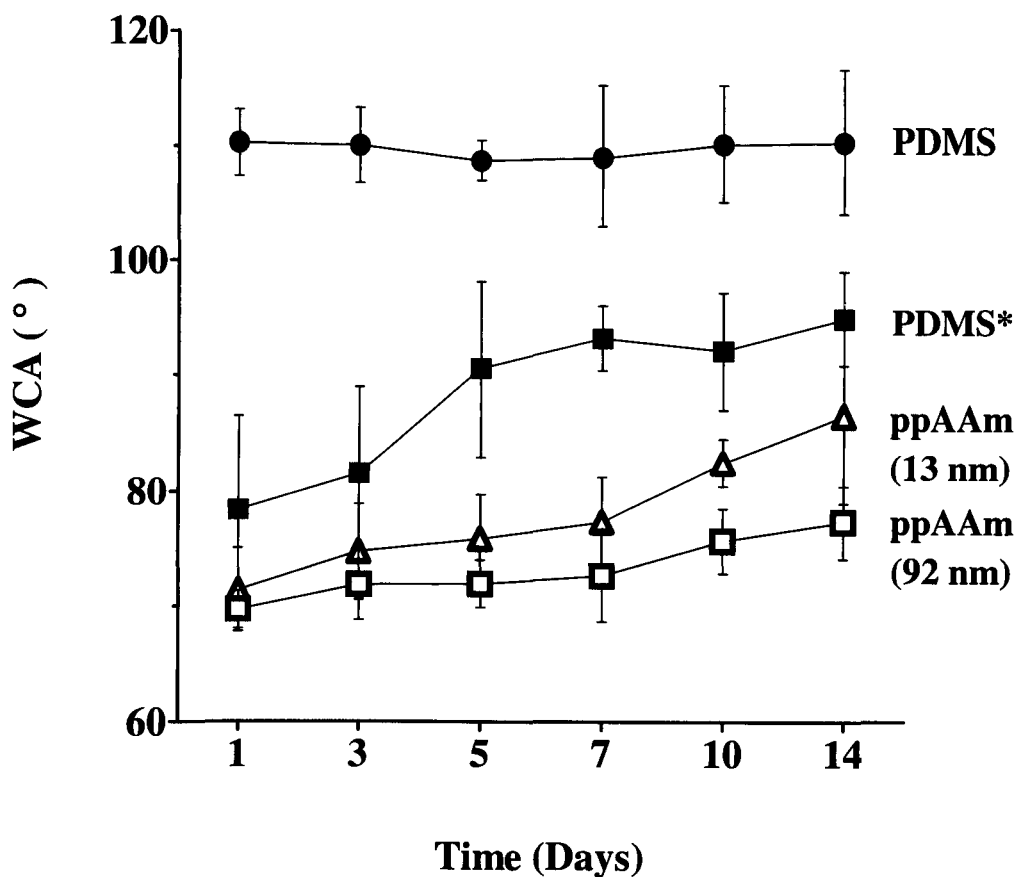


Figure 4.3 Hydrophobicity analyses of ppAAm deposited PDMS. A) Average WCA values for PDMS, PDMS*, ppAAm (13 nm) and ppAAm (92 nm) treated surfaces during 14 days. Surface hydrophobicity was measured using a CAM 200 Optical Contact Angle Meter (KSV Instruments Ltd., Helsinki, Finland) and associated software. Data points represent means \pm SD of nine independent measurements.

impeding the diffusion of LMW chains to the surface by virtue of the increased deposition thickness.

4.3.3 XPS

To further understand the loss of hydrophilic properties after plasma deposition, XPS was used to determine the topographical atomic percentage of nitrogen (N), oxygen (O) and silicon (Si). The results are shown in Figure 4.4. The presence of ppAAm would provide N atoms and mask O and Si atoms contained within the underlying PDMS sheet. XPS shows that the untreated PDMS surface is composed of >20% of Si and O, and <1% of N at days 1, 7 and 14 (Figure 4.4). Comparatively, Figure 4.4 also shows that ppAAm surfaces have a greater atomic % of N at all time-points compared to Si and O demonstrating the presence of the N-rich ppAAm coating. In agreement with WCA data there is an incremental rise in the atomic percentage of O during 14 days for ppAAm (13 nm) and (92 nm) surfaces demonstrating hydrophobic recovery of the surface. Furthermore, the atomic % of Si and O increases by threefold for ppAAm (92 nm) over 14 days. It can be assumed that this is a direct result of Si and O species migrating to the surface from the bulk PDMS. PpAAm (92 nm) surfaces are most stable due to their denser deposition layer (Figures 4.3 and 4.4) and remain hydrophilic for beyond two weeks (data not shown). It can be hypothesised that this is due to reduced surface molecular movement as previously reported¹¹⁵. This approach therefore created a stable hydrophilic surface on elastomeric PDMS which impeded hydrophobic recovery compared to the surface subjected to oxygen

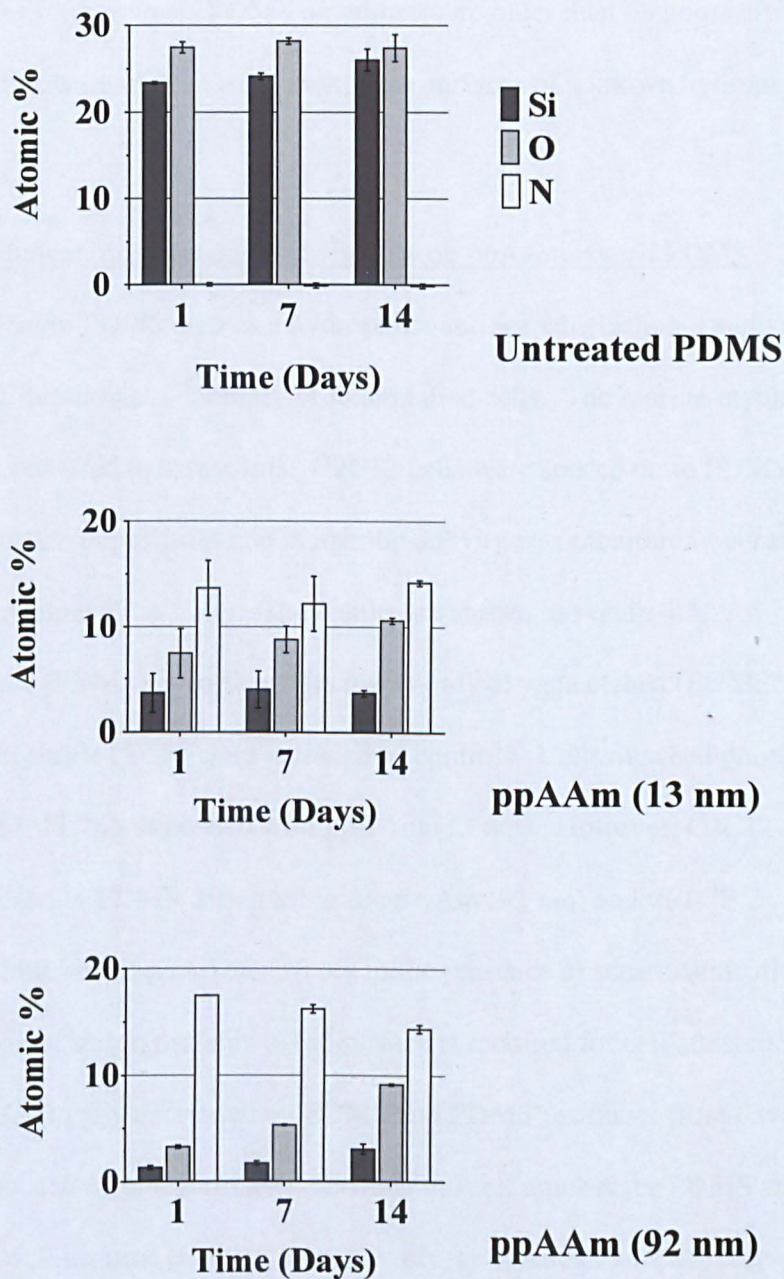


Figure 4.4 Atomic analyses of ppAAm-coated PDMS to assess surface coverage of deposited ppAAm over a 14 day period. XPS was used to determine the atomic percentage of silicone (Si), oxygen (O) and nitrogen (N) on A) PDMS, B) ppAAm (13 nm) and C) ppAAm (92 nm) surfaces during 14 days. Data points represent means and SD of six independent measurements.

etching alone. For further work, PDMS membranes no older than 48 hours after ppAAm depositions were used to consistently use surfaces of a known hydrophilic nature.

4.3.4 Cell attachment, proliferation and viability on ppAAm coated PDMS

PpAAm deposition on PDMS creates a hydrophilic surface which should support the adhesion, proliferation and viability of mammalian cells. The murine myoblast cell line, C2C12 was used to assess this. C2C12 cells were seeded on to PDMS with different ppAAm depositions and metabolic activity was monitored over two weeks using the Alamar Blue assay. The results are shown in Figure 4.5. An unmodified surface (PDMS), a surface which was only oxygen etched (PDMS*) and tissue-culture plastic (TCP) were included as controls. Cells attached poorly to PDMS, PDMS*, PDMS deposited with ppAAm (13 nm). However, C2C12 cells readily attached to PDMS deposited with ppAAm (92 nm) and to TCP. These cells only attached to ppAAm surfaces in the presence of serum, indicating that pre-absorption of serum proteins to the surface is required for cell attachment. Cell number consecutively decreased on PDMS and PDMS* surfaces from day 1 to 14. There is no statistical significance between the cell number for PDMS and PDMS* surfaces at each time point. Comparatively, cell number successively increased for ppAAm (13nm), ppAAm (92nm) and TCP surfaces. Cell number on ppAAm (92 nm) is significantly higher ($p < 0.001$) compared to PDMS and PDMS* surfaces at each time point. As the ppAAm (92 nm) surface is both heavily

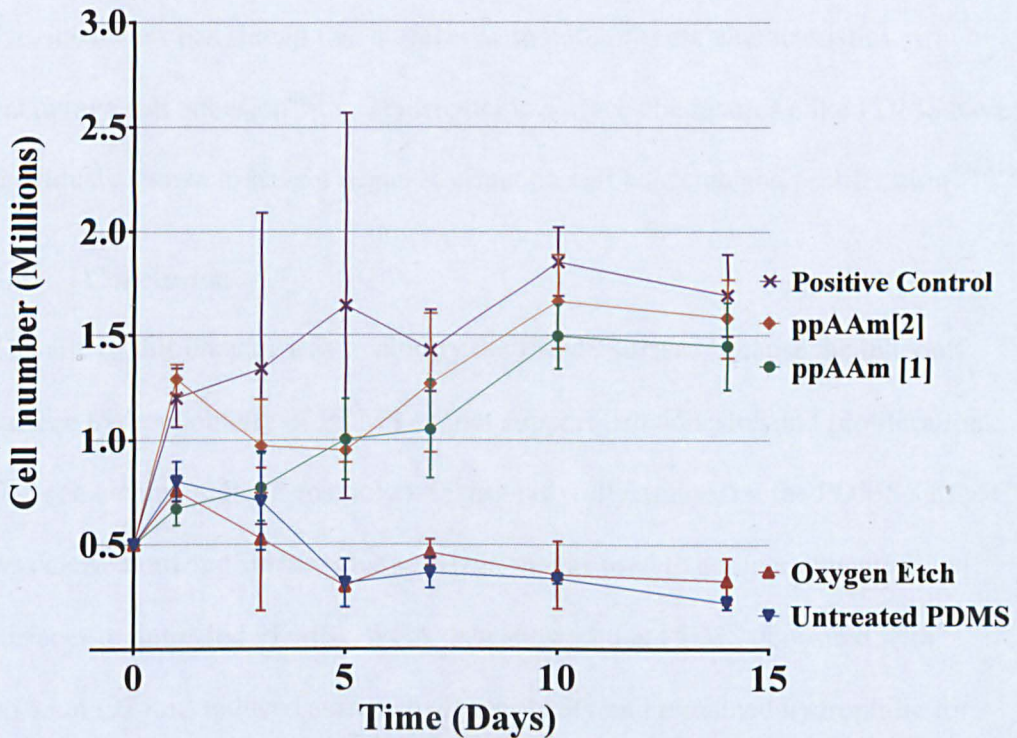


Figure 4.5 Proliferation of cells on ppAAm-coated PDMS. Metabolic activity of C2C12 myoblasts on PDMS, PDMS*, ppAAm (13 nm), ppAAm (92 nm) and TCP surfaces during 14 days. Data points represent means and SD of six independent measurements.

enriched with N and confers hydrophilic behaviour in comparison to PDMS and PDMS* it is hypothesised that this surface will be most suited for cultivating cells.

Previous work has shown that surfaces with both of these characteristics encourage cell adhesion^{86,115}. Hydrophobic surface chemistries alike PDMS have previously shown to have a negative effect on cell adhesion and proliferation^{102,116}.

4.4 Conclusion

The aim of this chapter was to modify the PDMS surface because the inherent surface hydrophobicity of PDMS cannot support cell adhesion and proliferation. Oxygen etching and plasma polymerizing poly(allylamine) on the PDMS surface was carried out and surface characterization was used to compare the modified surfaces to untreated PDMS. WCA data showed that PDMS deposited with ppAAm (92 nm) reduced surface hydrophobicity and remained hydrophilic for greater than two weeks. Comparatively, oxygen etched PDMS and ppAAm (13 nm) surfaces were unstable, regaining surface hydrophobicity within two weeks. WCA and XPS data suggest that PDMS deposited with ppAAm (92 nm) is most effective at reducing surface hydrophobicity because it is both, a thick and dense (nitrogen enriched) layer compared to oxygen etched and ppAAm (13nm) deposited PDMS, which presumably impedes oligomers rising to the surface.

The data from cell culture studies on PDMS modified surfaces show that cells readily attached to ppAAm (92 nm) deposited PDMS and cell proliferation was relative to TCP (positive control) during 14 days. Comparatively, cells poorly

attached and proliferated to untreated PDMS, oxygen etched PDMS and ppAAm (13 nm) surfaces. Therefore, for future work the PDMS deposited with ppAAm (92 nm) surface will be used to encourage cell adhesion and proliferation.

5

Surface micropatterning of PDMS to create spatially ordered cell monolayers

5.1 Introduction

Adult tissue function relies on the highly ordered positioning of specialized cells within the tissue's architecture. Myocardial tissue consists of aligned cardiomyocytes such that the contraction of individual cells produces an organized population contraction, generating both directional and greater force. Thus, failure to orient and position cells correctly during *in vitro* development of engineered myocardium leads to dysfunction and adult disease phenotypes, for example, myocardium affected by hypertrophic cardiomyopathy¹. Surface micropatterning has been used previously to modulate cell-cell and cell-surface interactions with the aim to achieve such organisation *in vitro*². This is achieved by creating surface features at the cellular/ sub cellular level that provide either physical or chemical cues to achieve a cellular response. These cues influence cell behaviour from initial attachment to the surface and migration, production of extracellular matrix proteins (ECM), to changing phenotype and resembling functional engineered

tissue³. In turn, the patterning of cells provides insight into complex cellular signalling pathways and cell-cell communication. This is particularly important as many tissue engineering attempts fail to achieve fully functioning tissue as cell position and organisation of cells within tissues have been overlooked⁴⁻⁶.

Predominant micropatterning methodologies are lithography based including photo and soft lithography⁷⁻¹¹. Techniques such as micro-contact printing, micro-fluidics and sub-micron spot printing include patterning ECM proteins to mediate cell adhesion via chemical interaction with cell membrane proteins^{6,12-14}. Cell adhesion has also been controlled through changes in surface chemistry. This includes spatially selective plasma deposition to change the hydrophobicity characteristics and create cell repellent regions on a surface¹⁵. Frimat et al. (2009) introduced plasma stencilling, selectively transforming surface areas to a hydrophilic state to create small scale micropatterns that remained confined for several days of culture¹⁶. This system used a micro-fluidic cell to direct oxygen etching at ambient pressure. Micropatterning of single cell types has been refined to create co-culture systems. These systems have been employed in adhering heterotypic cell lines adjacent to each other to better mimic the organization and complexity of physiological tissue^{2,8}.

The work in the previous chapter demonstrated that PDMS surfaces deposited with ppAAm (92 nm) were hydrophilic, maintaining surface stability for >2 weeks. These surfaces encouraged cell adhesion and proliferation, thus this method could

be exploited to encourage cell adhesion to specific regions on the hydrophobic PDMS surface. In this chapter, a novel micropatterning technique is explored to create both singular and co-culture patterns. The method incorporates selective ppAAm (92 nm) deposition and aerosol deposition (airbrushing) of ECM proteins through a microstencil to create cell adhesive, hydrophilic regions on the cell repellent PDMS surface. ECM deposition is included to create a method where cell attachment does not rely on pre-absorption of serum or media proteins to the culture surface. This would allow cell types requiring specifically coated surfaces to be patterned on a continuous interface.

5.2 Materials and Methods

5.2.1 Membrane fabrication

Elastomeric membranes of 50 μm thickness were formed by spin coating PDMS on to stainless steel sheets as described in 2.2.3.

5.2.2 Surface micropatterning

Microstencils were manufactured and used to selectively deposit ppAAm (92 nm) as described in 2.2.6 and 2.2.8. ECM deposition was achieved using an airbrushing technique. Liquid fibronectin (Fn) was fluorescently labelled and airbrushed onto the PDMS surface as described in 2.2.8.

5.2.3 Surface characterisation

ToF-SIMS was used to visualise the selective deposition of ppAAm on the PDMS surface, the method is described in 2.2.7.4.

5.2.4 Cell culture

C2C12 myoblasts, NIH-3T3 and BJ6 fibroblasts, HL1 cardiomyocytes and the HUES7 HESC line were maintained as described in 2.2.4. All cell lines were genetically labelled as described in 2.2.4.2. Cell suspensions of 1×10^6 cells (in 4 ml/ well) were used for seeding micropatterned PDMS membranes in media A (see appendix 1.1) lacking calcium (Ca^{2+}). For samples used for co-culture patterns, media A was replaced with media A containing 0.1 % porcine skin gelatine for 1 hour following 24 hours attachment of the first cell line. Media was then replaced and a cell suspension of 2×10^6 cells was used to seed the second cell line.

5.2.5 Imaging

Bright field and fluorescent images were taken using a Nikon TS100 microscope. Low magnification images of entire surface micropatterns and tubes micropatterned with ppAAm/ Fn were taken using a Nikon SMZ1500 microscope with a SPOT insight camera (Diagnostic instruments, UK). To image cell micropatterned tubes a TCS LSI Super zoom confocal was used (Leica, UK).

5.3 Results and Discussion

5.3.1 Plasma-stencilling of ppAAm (92 nm) on PDMS

Microstenciling was used to selectively control cell position over the PDMS membrane surface area. Microstencils were used as a mask to selectively deposit ppAAm (92 nm) on to the PDMS surface. After 48 hours, ppAAm micropatterned membranes were characterised using ToF-SIMS. The mass spectra of PDMS and ppAAm (92 nm) coated PDMS in Figure 5.1.A were used to characterise ions specific to both chemistries. There is a clearly distinguishable CN^- peak for ppAAm (92 nm). In comparison, the CN^- peak for PDMS is negligible. PpAAm (92 nm) surfaces show a reduced Si^- peak intensity in comparison to PDMS. Additional secondary ions were identified in the positive ion spectra that reinforced the identification of ppAAm, these include $\text{C}_2\text{H}_4\text{N}^+$, $\text{C}_3\text{H}_6\text{N}^+$, CH_4N^+ and $\text{C}_3\text{H}_8\text{N}^+$. The CN^- and Si^- peaks (highlighted in figure 5.1.A) were solely used to retrospectively reconstruct secondary ion images of the patterned PDMS surface shown in figure 5.1.B. The spatial distribution of ppAAm (92 nm) (CN^-), and PDMS (Si^-) confirm that plasma stencilling produces a faithful pattern. However, there is still a Si^- ion signal present in the ppAAm (92 nm) regions. This is most likely attributed to PDMS-oligomers migrating over the ppAAm (92 nm) pattern from the surrounding PDMS regions that have not been deposited with ppAAm (92 nm). Figure 5.1.C is a corresponding CN^- ion intensity line scan of the micropatterned PDMS surface area across a 500 μm distance. The full width at half maximum (FWHM) calculation was used to measure the size of the surface

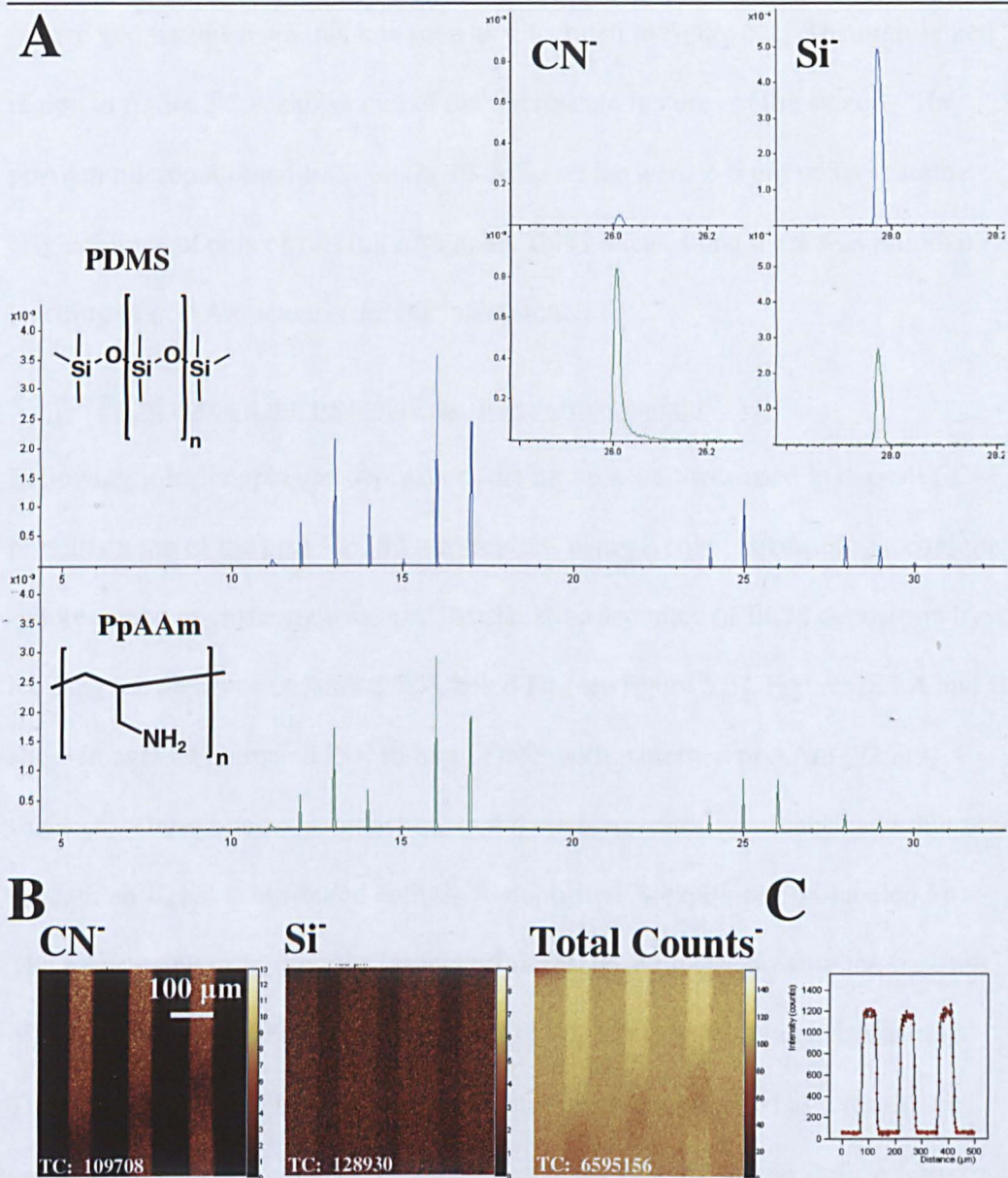


Figure 5.1 ToF SIMS analysis of ppAAm-coated PDMS. **A**) Mass spectra of untreated PDMS (top) and PDMS with ppAAm (92 nm) deposition (bottom). Corresponding chemical structures are inset. **CN⁻** and **Si⁻** ion peaks are enlarged. **B**) Images of ppAAm (92 nm) deposited pattern on the PDMS surface, compiled using signals from **CN⁻**, **Si⁻** and total counts⁻. **C**) Corresponding line scan of **CN⁻** ion intensity (scan line is centrally positioned).

pattern geometries from this line scan as illustrated in figure 5.2. The highlighted region in figure 5.2.A shows one of the microscale features of the stencil. The ppAAm micropatterned lines on the PDMS surface were 2-6 μm wider than the original line cut outs of this microstencil. This indicates that there was minimal leaching of ppAAm underneath the microstencil.

5.3.2 ECM aerosol microstencilling of ppAAm coated PDMS

Following selective plasma deposition, the microstencil was used to deposit ECM protein on top of the ppAAm (92 nm) regions using a novel airbrushing technique. Fluorescence microscopy was used to assess the accuracy of ECM deposition by locating the presence of Alexa568-labeled Fn (see figure 5.3). Figures 5.3.A and B show images of untreated PDMS and PDMS with patterned ppAAm (92 nm) surfaces. These images demonstrate that there is no autofluorescence and thus any rhodamine signal is attributed entirely to deposited AlexaFluor 568-labeled Fn. The micrograph in figure 5.3.C is an epifluorescence image showing the location of rhodamine labelled Fn on an untreated PDMS surface following airbrushing. The Fn repelled the hydrophobic PDMS surface and aggregated as a result. Fn aggregation was prevented by depositing ppAAm (92 nm) on the surface prior to airbrushing. The hydrophilic characteristic of ppAAm resulted in homogenous coverage of Fn (see Figure 5.3.D). Cell culture was incorporated to show the control of cell positioning on the PDMS membranes as a result of surface micropatterning.

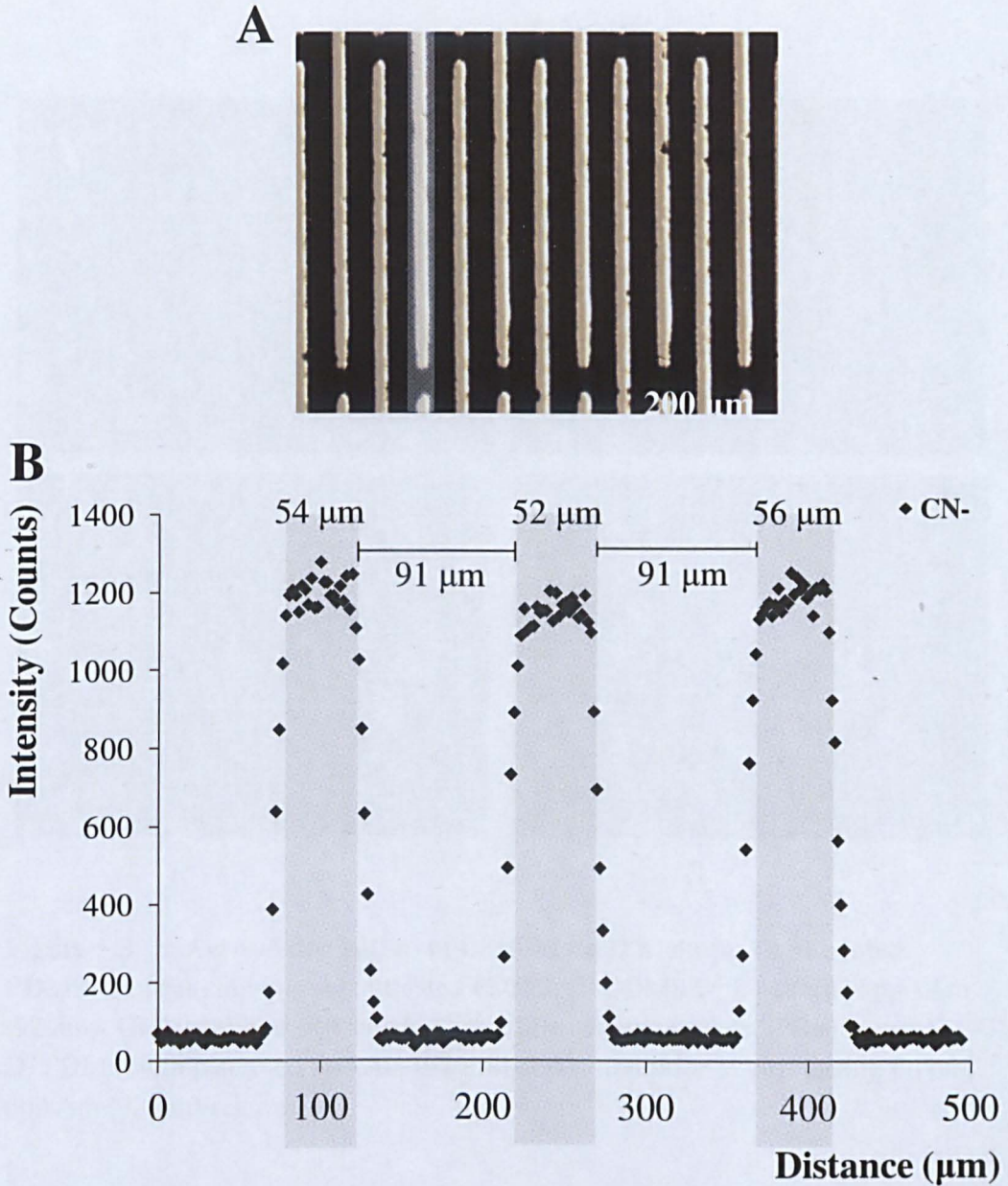


Figure 5.2 Accuracy of ppAAM deposition through Microstencils. A) Image showing original micro-stencil. The highlighted region shows the line cut outs with a width of $50\mu\text{m}$. Gaps in between lines were $90\mu\text{m}$ in width. **B)** Line scan showing CN^- ion intensity of ppAAM (92 nm) pattern on PDMS surface using TOF-SIMS. Highlighted regions show the width of the ppAAM (92 nm) geometries. Values were calculated using the FWHM calculation.

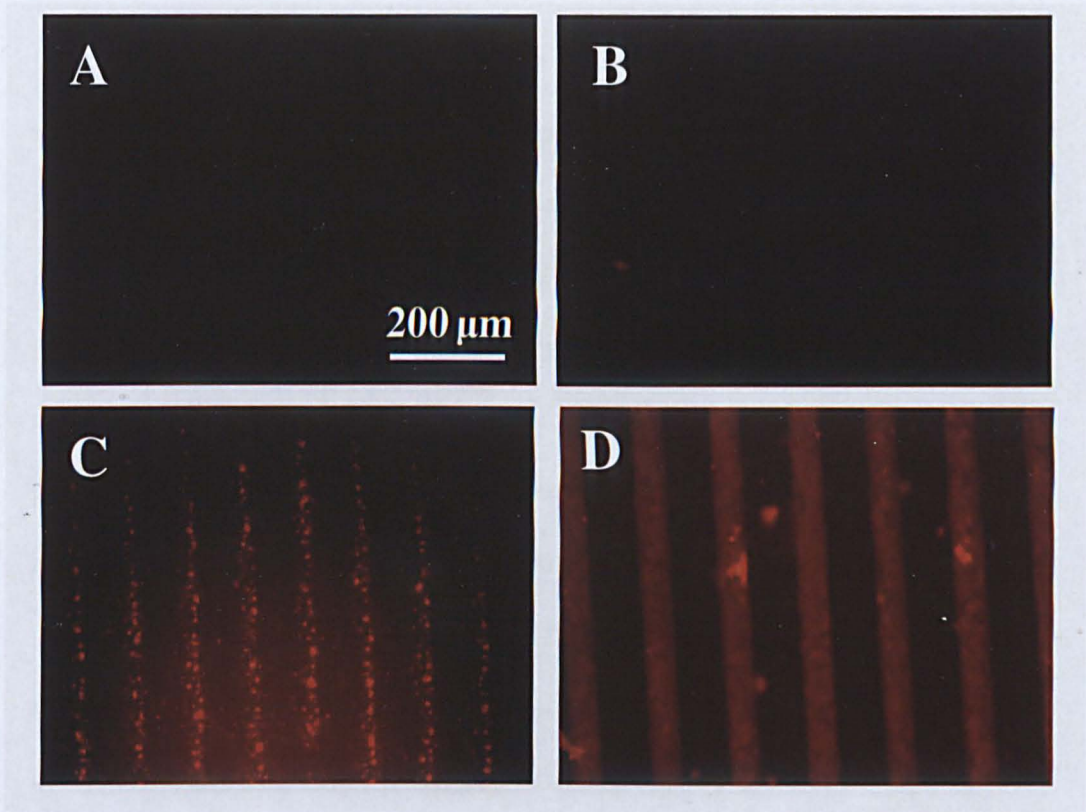


Figure 5.3 Aerosol deposition of fibronectin (Fn) on ppAAm-coated PDMS. Images showing **A**) untreated PDMS, **B**) PDMS with patterned ppAAm (92 nm), **C**) AlexaFluor-568 labeled Fn airbrushed on untreated PDMS surface. **D**) PDMS with patterned ppAAm (92 nm) deposition prior to airbrushing Fn on ppAAm (92 nm) regions.

5.3.3 Micropatterned cell culture

NIH-3T3 fibroblasts were seeded on ppAAm (92 nm)/ Fn micropatterned PDMS membranes. These cultures were used to investigate the cell culture parameters required to maintain a faithful cell micropattern. Previous plasma stencilling work has demonstrated that cell adherence is dependent on serum proteins. In this work, removal of serum during cell seeding had no effect on the ability of cells to attach to coated surfaces as demonstrated in Figure 5.4. This confirmed that this micropatterning method facilitated cell binding to patterned surfaces without the pre-absorption of media proteins to the culture surface. High cell densities were required to fully populate the patterned surface area. Since the patterned/ non-patterned surface area ratio is low then it may be expected that many cells will remain unattached. Certain cell lines, (including HESCs), aggregate at high densities when unattached. It was hypothesised that if extensive cell aggregation occurred prior to surface attachment, this could affect the quality of the cell micropatterns. Previous work has also shown that the presence of Ca^{2+} in media leads to cell aggregation¹⁷. Thus the effect of Ca^{2+} removal from media on cell attachment was assessed (figure 5.4). Media supplemented with Ca^{2+} caused aggregation of non-adhered NIH-3T3 cells at high densities. Media absent of Ca^{2+} prevented aggregation and was used for subsequent cell patterning work. Cell lines were genetically labelled with green fluorescent protein (eGFP) or monomeric red fluorescent protein (mRFP), thus fluorescence microscopy could be used to assess whether the cell micropatterns remained faithful¹⁸. The images

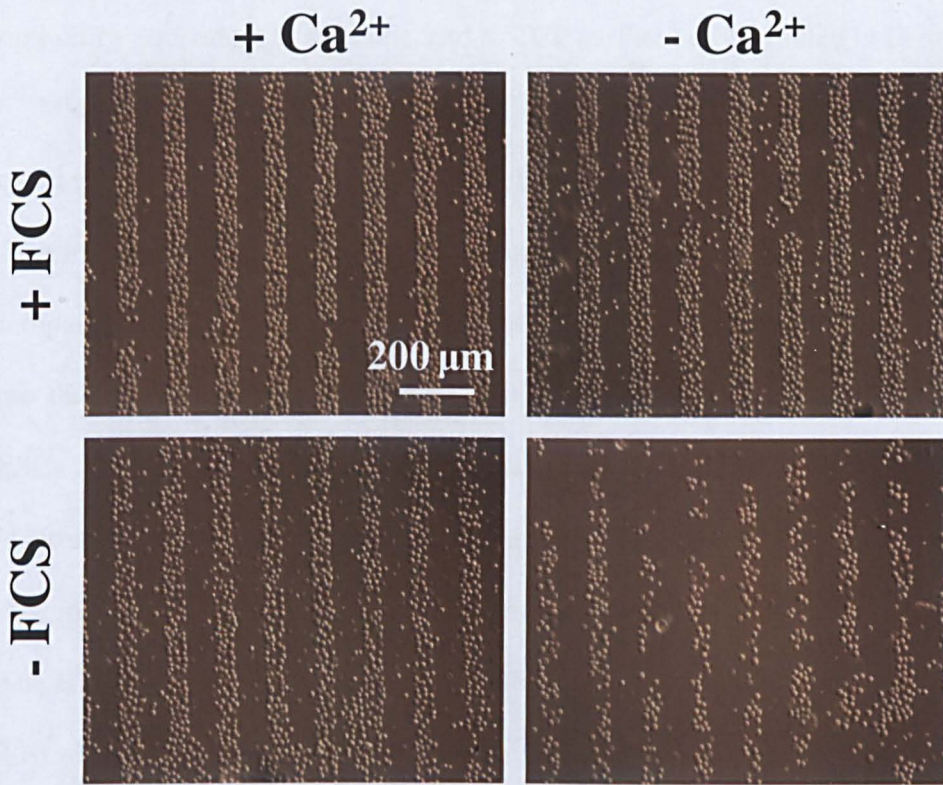


Figure 5.4 Testing media conditions for micropatterned PDMS membranes. eGFP labeled NIH-3T3 cell micropatterns on PDMS membranes cultured in media either in the presence or absence of FCS and Ca²⁺. Images were taken 20 minutes post-patterning.

in figure 5.5 show faithful cell micropatterns using NIH-3T3, C2C12, HL1 and BJ6 cell lines in these defined media conditions. Cells required 15-20 minutes to fully adhere to the micropattern and required several hours to assume a typical morphology equivalent to cells attached to TCP surfaces as illustrated in Figure 5.6. Micropatterned cultures with HUES7 HESCs in serum free media were created using aerosol deposition of Matrigel™ rather than Fn to prevent differentiation (see figure 5.7). The cell morphology of HUESCs on micropatterned PDMS membranes 24 hours post seeding (figure 5.7.D) is equivalent to HESC during conventional culture on Matrigel™ (figure 5.7.A). HESCs take longer to adhere to the micropatterned PDMS surface (45-60 minutes) and airbrushing Fn to the surface resulted in cell micropattern cultures that could not be maintained beyond 24 hours (see figure 5.8). Thus Matrigel™ was used to create HESC cultures that maintained a faithful pattern for several days (see figure 5.7.E). The cell micropatterns included above demonstrate the versatility of this micropatterning technique to create patterns with various cell lines. This is achieved by depositing specific ECM proteins on the PDMS surface. Furthermore, this technique does not depend on external factors to include the presence or absorption of serum proteins to aid cell attachment.

5.3.4 Patterning complex geometries

Figure 5.9.A shows magnified images of stencils with different microscale features, these were used to create complex cell patterns on PDMS membranes. The images in Figure 5.9.B show the corresponding surface micropatterns using

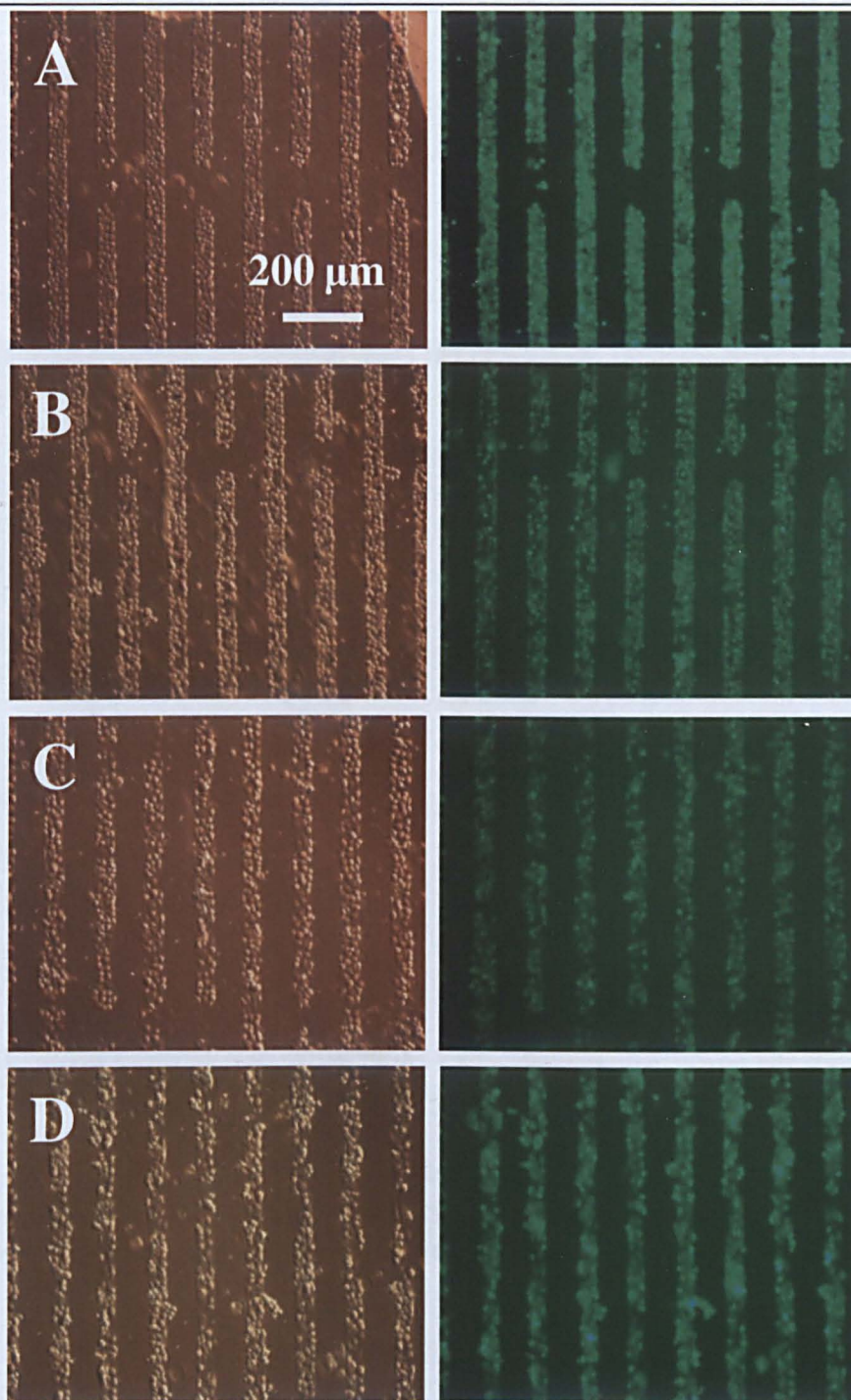


Figure 5.5 Micropatterning of cell lines. Bright field and fluorescent images of eGFP labeled cell micropatterns on PDMS membranes using A) NIH-3T3, B) C2C12, C) HL1 and D) BJ6 cell lines. Images were taken 1 hour post patterning.

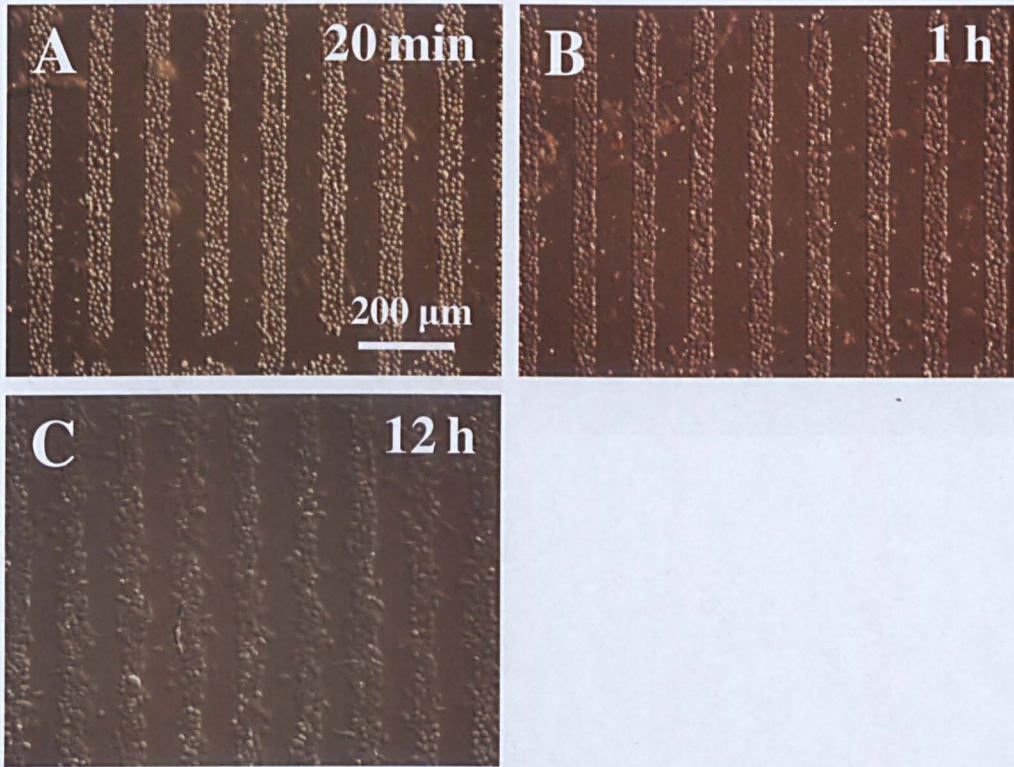


Figure 5.6 Morphology of NIH-3T3 cells during micropatterning. Bright field images of NIH-3T3 cells on PDMS surfaces patterned with ppAAm/Fn cultured for A) 20 minutes, B) 1 hour and C) 12 hours.

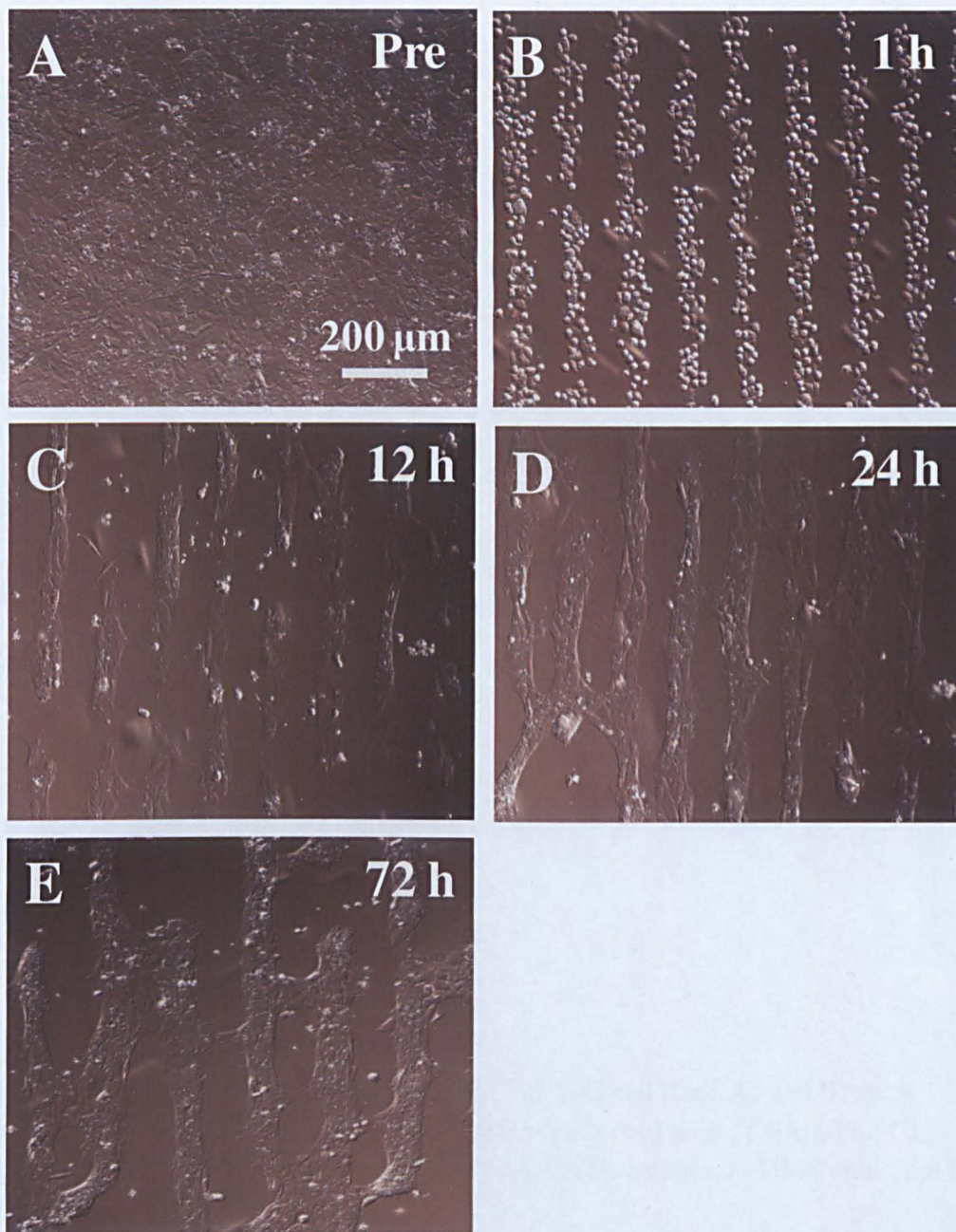


Figure 5.7 Micropatterning of HUES7 HESC line. Bright field images of: A) HUES7 HESCs during conventional culture on MatrigelTM. HUES7 HESCs cultured on PDMS surfaces patterned with ppAAm (92 nm)/ MatrigelTM for B) 1, C) 12, D) 24 and E) 72 hours.

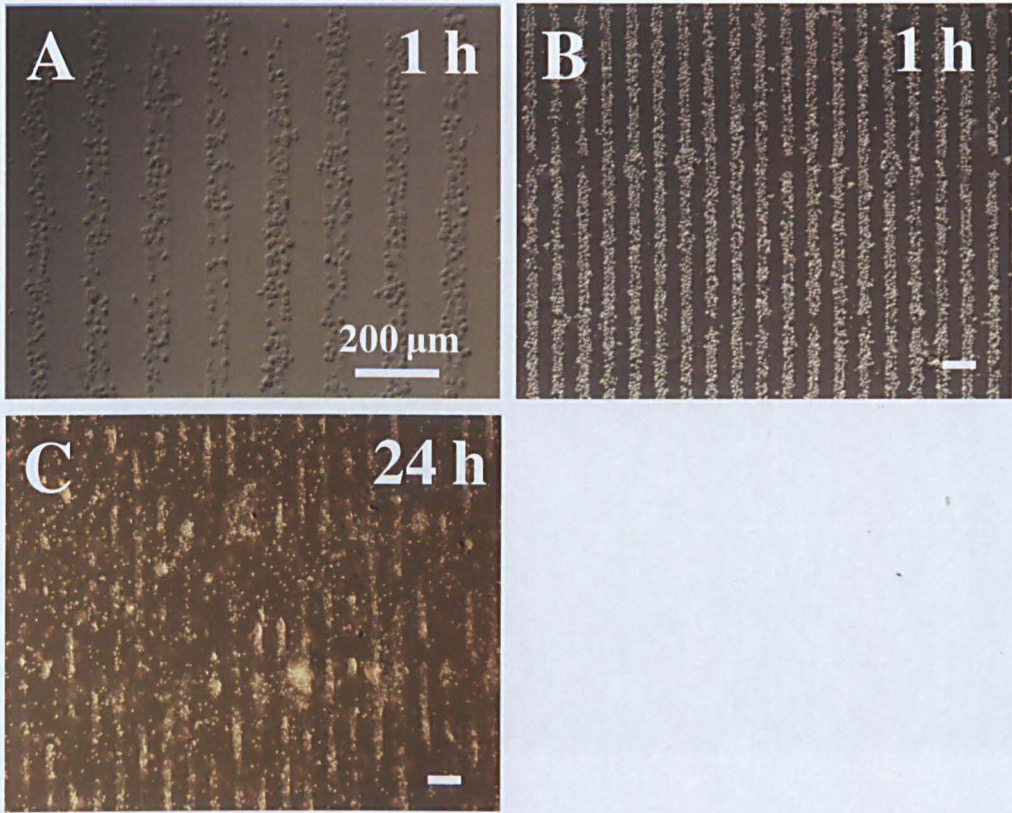


Figure 5.8 Micropatterning of HUES7 HESC cell line. A) and B) show attachment of HUES7 cells on PDMS surfaces patterned with ppAam/Fn. C) shows that HUES7 cell micropatterns on ppAam/Fn patterned PDMS could not be maintained beyond 24 hours.

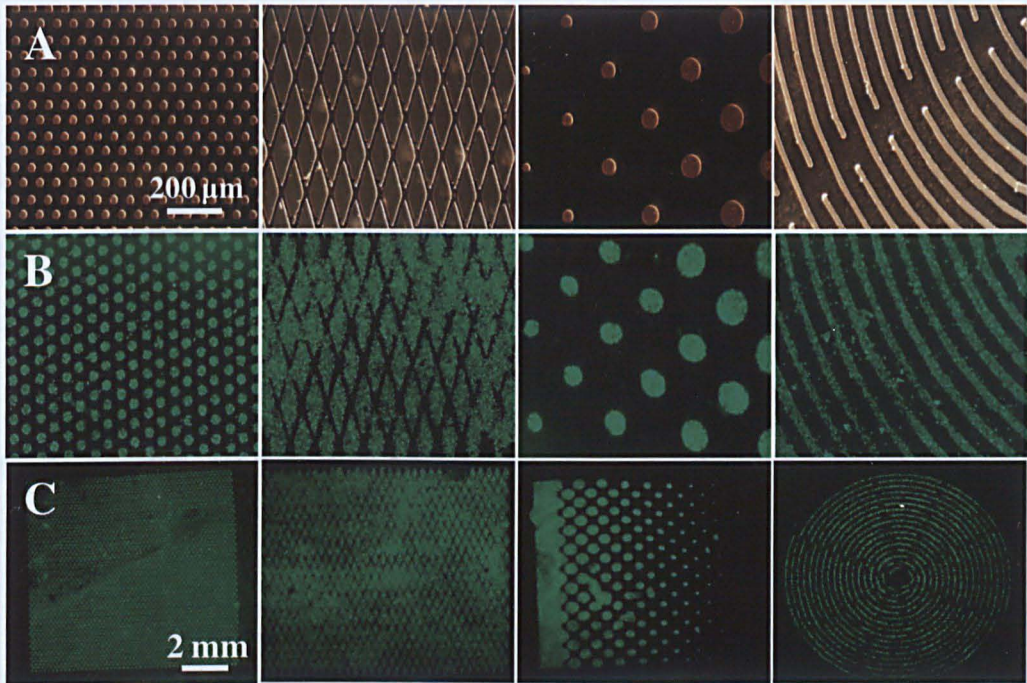


Figure 5.9 Micropatterning of Complex Designs. Micrographs showing **A)** micro-stencils with complex pattern features. **B)** The corresponding eGFP labeled NIH-3T3 cell micropatterns on PDMS membranes. **C)** The entire surface cell micropattern. Images were taken 1 hour post-patterning.

eGFP labelled NIH-3T3 cells. These cells remained confined to the ppAAm (92 nm)/ Fn regions creating a micropattern that remained faithful over a centimetre-scale area (see figure 5.9.C). Previous micropatterning techniques have employed oxygen etching to create cell patterns on the PDMS surface^{16,19}. These studies using oxygen plasma etching alone relied upon the formation of a surface silica layer that increases surface compliance. In contrast, ppAAm (92 nm) deposition is likely to be more stable under flexing than a brittle silica layer, without compromising the local mechanical properties of PDMS. To demonstrate this, micropatterned PDMS membranes were manipulated to form three-dimensional structures after cell seeding. PDMS sheets patterned with ppAAm (92 nm)/ Fn were rolled to create radial patterned tubes as illustrated in figure 5.10.A. These patterned tubes were able to hold and support the flow of liquid demonstrating the rigidity of these three-dimensional structures. Following seeding of eGFP labelled NIH-3T3 cells, cell micropatterned PDMS sheets were also rolled (figure 5.10.B) and imaged using confocal microscopy (figure 5.10.C).

5.3.5 Patterning of cell co-cultures

Co-culture patterns were generated on PDMS membranes with minor modification to the surface micropatterning method used for adhering single cell lines. The images in figure 5.11.A and B show single cell patterns after 24 hours of culture of eGFP labelled HL1 and NIH-3T3 fibroblasts, respectively. PDMS membranes were immersed in gelatine prior to seeding the second cell line. The mRFP labelled NIH-3T3 and C2C12 cells adhered to the unpatterned regions as seen in

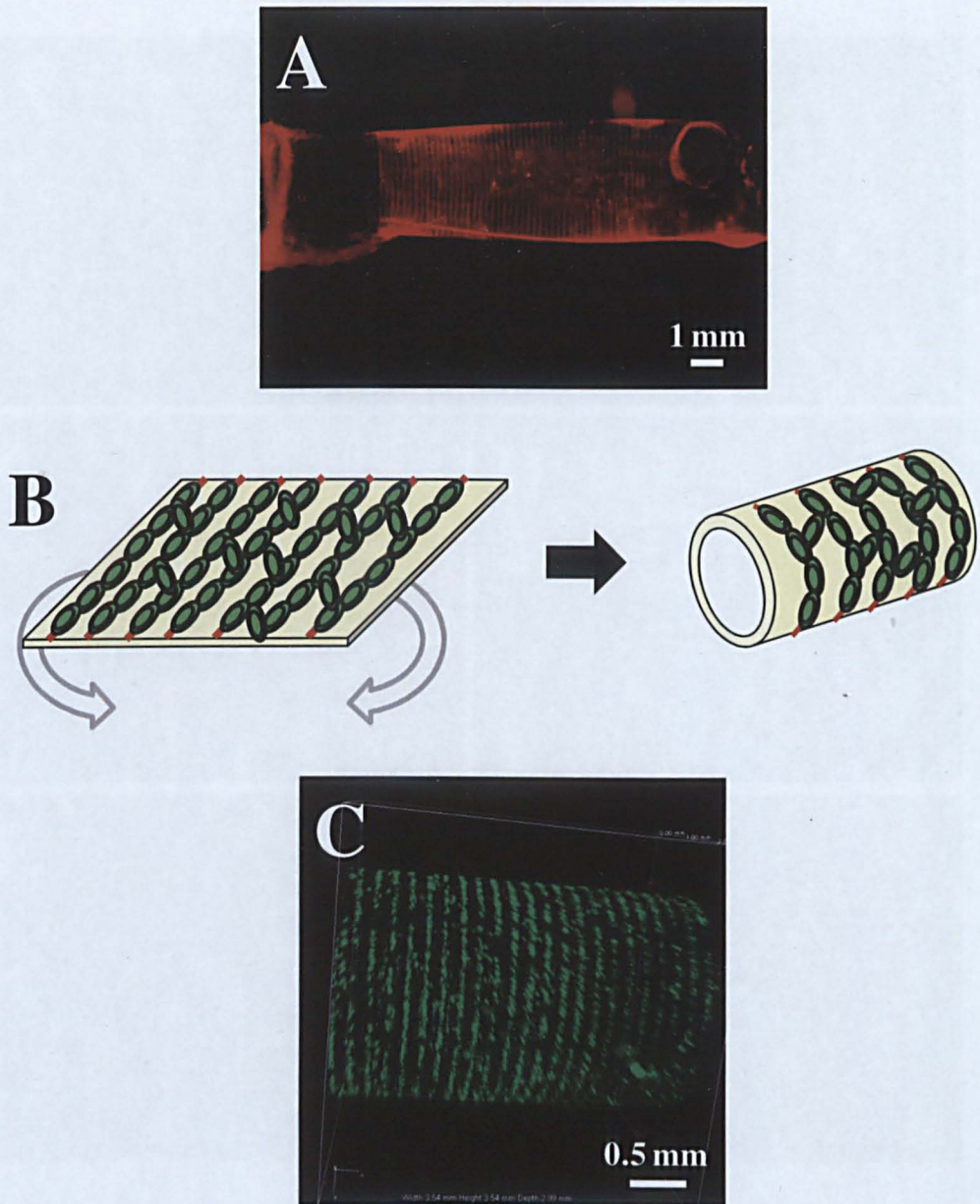


Figure 5.10 Three-dimensional structures of micropatterned PDMS sheets. PDMS sheets can be manually rolled to form tubes. **A)** ppAAm (92 nm)/ Fn patterned PDMS sheet manually rolled to form radially patterned tube holding fluid. **B)** Representation of PDMS sheets rolled in to tubes post cell attachment, of eGFP labelled NIH-3T3 fibroblasts. **C)** Confocal image of tube taken 2 hours post patterning with eGFP labelled NIH-3T3 fibroblasts and 2 hours post-rolling.

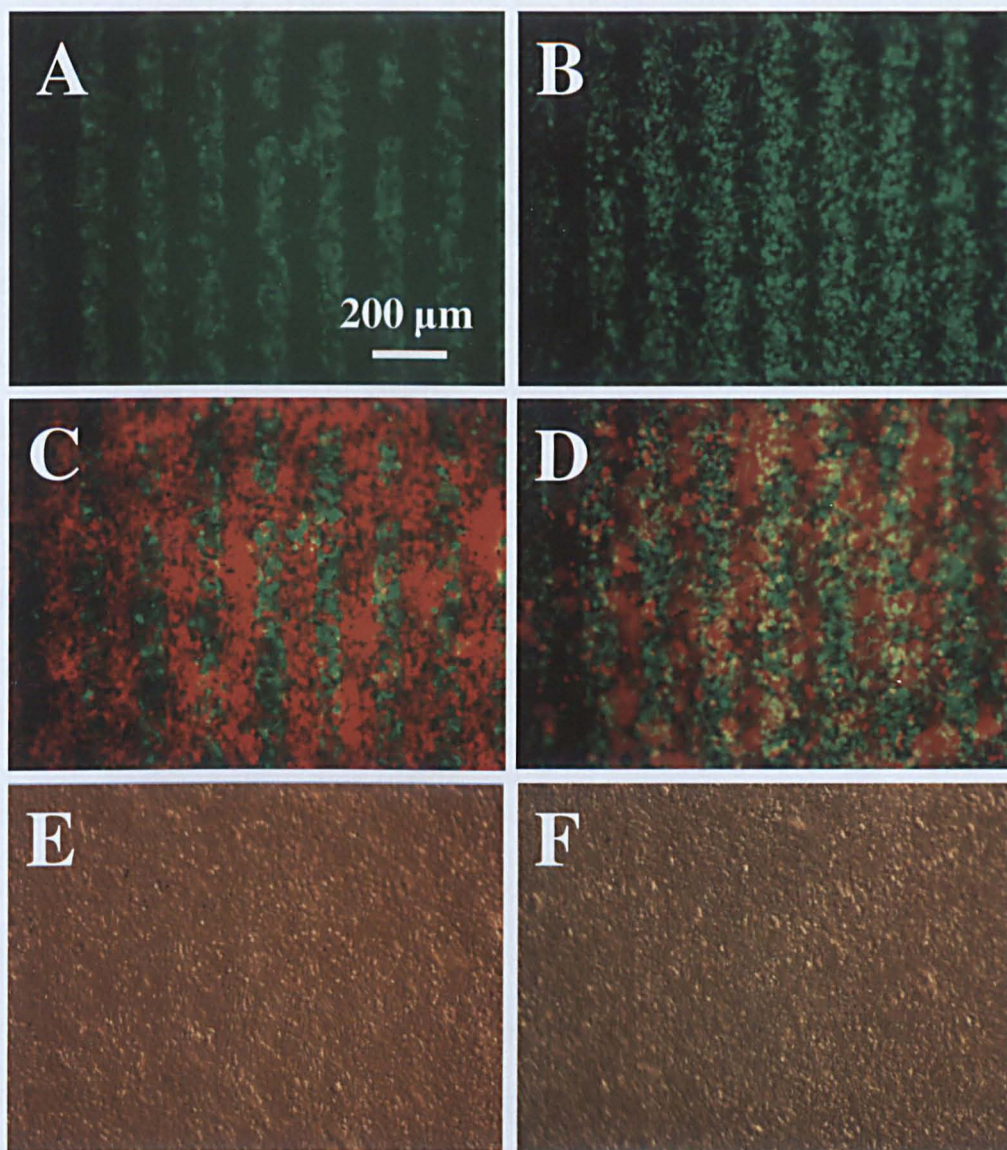


Figure 5.11 Co-culture Micropatterning. Cell micropattern of eGFP labeled A) HL1 and B) NIH-3T3 cells on the PDMS surface after 24 hours. Co-culture patterns created using C) eGFP labeled HL1 and mRFP labeled NIH-3T3 cells, D) eGFP labeled NIH-3T3 and mRFP labeled C2C12 cells. E-F) Bright field images of corresponding cell monolayers. Co-culture images were taken 26 hours post-patterning and 2 hours post-plating the second cell line.

figures 5.11.C and D, respectively. Dual cell lines integrated to form a confluent cell monolayer (figures 5.11.E and F) without negative ramifications to the initial single cell micropattern. This method is similar to Bhatia et al. who used collagen patterned PDMS to create a NIH-3T3/ hepatocyte co-culture². This versatile co culture patterning technique will be useful for future work to study the communication between different cell lines. Particularly environments integrating HESCs with differentiated cells, the effect of cell spatial organization could be used to regulate stem cell fate.

5.4 Conclusion

This chapter shows how plasma surface deposition introduced in chapter 4 can be exploited to selectively create hydrophilic regions on the PDMS surface by depositing ppAAm (92 nm) through a micro-stencil. PpAAm (92 nm) deposition is required to aid the uniform adherence of ECM on to the PDMS surface whilst the hydrophobic surface chemistry controls cell spreading. ECM is deposited on to ppAAm (92 nm) patterned regions as a novel airbrushing technique. Pre-deposition of specific ECM proteins controls cell attachment and does not rely on the presence or absorption of serum proteins. This demonstrates the versatility of the micropatterning technique to attach different cell lines to the patterned PDMS surface. These micropatterns remain faithful over several days and can be complex as well as discontinuous. Importantly, these micropatterns have micron resolution over a macro scale. This will be useful for engineering functional tissue because cell positioning can be controlled over a large area. Furthermore, the

inherent elasticity of PDMS can be exploited to form three dimensional structures without compromising the cell micropattern. The entire fabrication procedure is complete within three days and this technique is capable of mass production if necessary. In conclusion this is a high-throughput, versatile micropatterning technique capable of producing faithful single and co-culture micropatterns at a macroscopic scale.

6

Effect of substrate strain and geometric constraints on cell alignment and cytoskeletal organisation

6.1 Introduction

The application of external mechanical force to a population of cells plays a critical role in determining cell functionality. Previous research has shown that the micro-mechanical environment is becoming increasingly linked to gene expression and cell protein organisation⁷⁵. Methods for investigating the response of a cell population to external mechanical stimuli include the application of substrate strain or shear flow^{133,134}. Previous work has also shown how independent control of substrate elasticity can modulate the differentiation of stem cells. Engler et al. demonstrated that mesenchymal stem cells (MSCs) plated on polyacrylamide gels committed to a specific lineage depending on substrate stiffness¹⁸. MSCs have also been transplanted in to the heart and have differentiated in to smooth muscle cells in response to cyclic loading *in vivo*¹³⁵. This is due to the extreme sensitivity

of anchorage dependent cells such as MSCs to tissue-level elasticity and the extracellular mechanical environment.

The effect of substrate strain on cell functionality has been investigated *in vitro* by Ahmed et al., applying cyclic mechanical strain (CMS) to a substrate following cell attachment, mimicking cyclic loading *in vivo*¹³³. This study showed that both cell biological and morphological responses are dependent on the strain direction relative to cell orientation. Ahmed et al. used micropatterned PDMS substrates to orient cells 0°, 45° and 90° relative to the direction of applied CMS. Cells were subsequently subjected to 7% CMS at 0.5 Hz for 4 days. Results showed that actin fiber organization was dominantly controlled by CMS. Conversely, nuclei shape was dominantly affected by geometric constraints, created by micropatterning 30µm wide parallel lines on PDMS using micro-contact printing. Park et al. investigated the differential effects of cyclic equiaxial and uniaxial strain on confluent monolayers of MSCs¹³⁶. MSCs subjected to cyclic uniaxial strain exhibited increased expression of smooth muscle markers. Application of cyclic equiaxial strain resulted in down regulation of the same markers. Although subjecting MSCs to cyclic uniaxial strain promoted gene expression of smooth muscle contractile markers, these changes were transient. This may have been because MSCs were not specifically orientated on the substrate. As a result, cells repositioned themselves in response to substrate strain in order to withstand external forces on the cell body.

Physiologically, cells are specifically orientated to control cell shape and alignment since both factors modulate cell response to external forces¹³⁷. Similarly, using micropatterning techniques to introduce geometric constraints on the substrate surface can be used to influence cell orientation *in vitro*. Kurpinski et al. seeded MSCs to elastomeric membranes with parallel microgrooves created using soft lithography¹³⁵. Cells were subsequently subjected to 5% CMS at 1 Hz for 2 to 4 days and orientated either parallel or perpendicular to the strain direction. Following 2 days, MSCs orientated parallel to the strain axis exhibited an increase in the smooth muscle marker calponin I and increased cell proliferation. Furthermore, MSCs exhibited alignment and morphology mimicking smooth muscle cells *in vivo*. Comparatively, CMS applied in the transverse direction to cell orientation resulted in the down regulation of smooth muscle markers and no change in cell number. The increase of contractile markers and decrease in cartilage markers of MSCs suggest that tension-bearing tissue phenotype is promoted as a result of applying uniaxial CMS in the parallel direction to MSCs. Importantly, this study showed that incorporating micropatterning techniques with mechanical loading can be used to better mimic physiological conditions *in vitro* compared to applying substrate strain to cells in monolayers, exhibiting no specific orientation.

The literature discussed above focuses on the effect of substrate strain applied post cell attachment. There is limited literature investigating the effect of cell response to surfaces subjected to strain prior to cell attachment and whether such *in vitro*

models would be useful for guiding cell alignment and functionality. Gopalan et al. used an elliptical stretcher to subject PDMS membranes to anisotropic strain¹³⁷. Membranes were subsequently micropatterned using microfluidics and used as surface geometrical constraints to orient ventricular myocytes in the parallel or perpendicular direction to the axis of greater strain (10%). 10% strain applied in the transverse direction resulted in an increased number of cell-cell junctions, hypertrophic cells and the presence of sarcomere organisation compared to cells subjected to strain in the parallel direction. This study showed that ventricular myocytes responded to substrate strain applied prior to cell attachment. Yet, the response of naive stem cell lines such as MSCs to pre-strained substrate surfaces remains unknown. Additionally, there is no research investigating the effect of substrate strain on the surface chemistry of micropatterned elastic substrates such as PDMS, which could consequently affect cell attachment and behaviour.

There are two distinct objectives of the work carried out in this chapter. Firstly, to characterise the surface of ppAAm (92 nm)/ Fn micropatterned PDMS subjected to uniaxial strain. Secondly, cell micropatterns on unstrained and strained PDMS will be used to investigate the effect of geometric constraints and uniaxial strain direction applied prior to cell attachment, on cell alignment and cytoskeletal organisation.

6.2 Materials and Methods

6.2.1 Membrane fabrication

Elastomeric membranes of 50 μm thickness were formed by spin coating PDMS on to stainless steel sheets as described in 2.2.3.

6.2.2 Surface micropatterning

Microstencils were manufactured and used to selectively deposit ppAAm (92 nm) as described in 2.2.6 and 2.8. Fn deposition on ppAAm regions was achieved using an airbrushing technique as described in 2.2.8.

6.2.3 Subjecting micropatterned PDMS membranes to uniaxial strain

PDMS membranes were mounted on strain rigs 48 hours after surface micropatterning as illustrated in figure 6.1. Once secured, a screw was used to apply uniaxial tensile strain (abbreviated to TS) to the PDMS membrane. PDMS membrane strain was controlled using a camera extensometer as described in 3.2.5. Membranes were orientated to apply uniaxial strain in either the parallel (0°) or perpendicular (90°) direction to the micropatterned ppAAm/ Fn lines. Unstrained samples were also mounted on tensile rigs and used as a control. Three membranes of each surface condition were investigated.

6.2.4 Surface characterisation

ToF-SIMS was used to visualise the selective deposition of ppAAm on strained and unstrained PDMS surfaces, the method is described in 2.2.7.4.

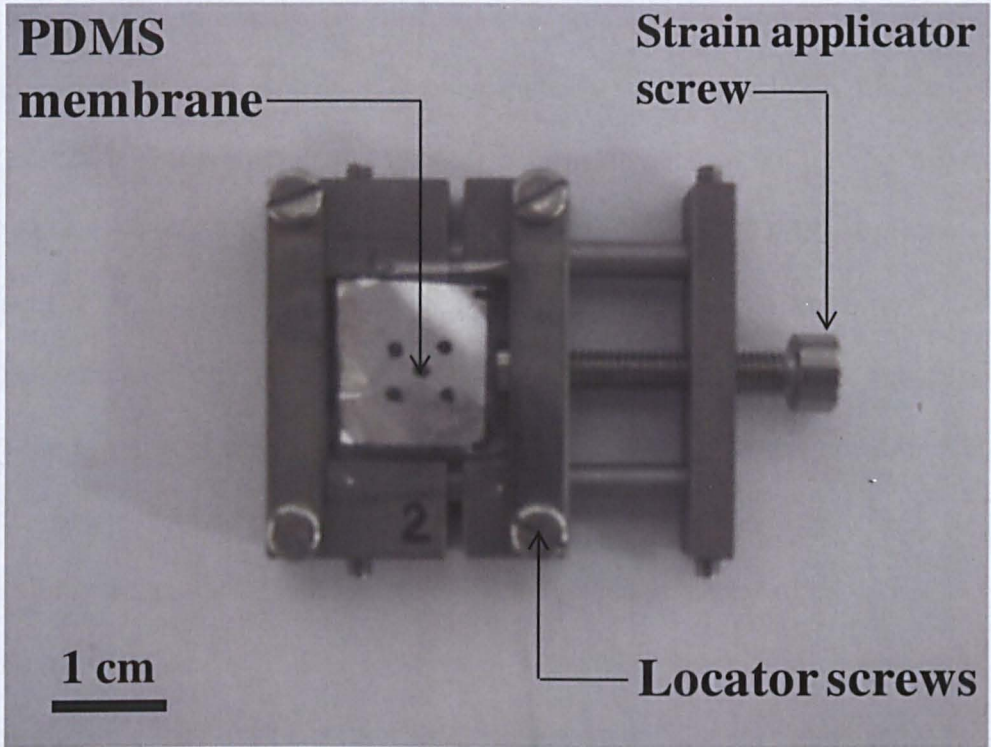


Figure 6.1 Image of PDMS membrane mounted on strain rig. PDMS membranes were held in place using locator screws. Once located, PDMS membranes were held under constant tension by rotating the strain applicator screw anticlockwise.

6.2.5 Cell culture and immunofluorescent staining

Immortalised human mesenchymal stem cells (iHMSCs) were kindly provided by Dr. J E Dixon and genetically labelled to express enhanced green fluorescent protein (eGFP) as described in 2.2.4.2. Cells were not used beyond passage 15 and were maintained in media A (see appendix 1.1) as previously described in 2.2.4. To inhibit proliferation, cells were exposed to mitomycin C (10 µg/ ml) for 2 hours and washed three times with media prior to plating. PDMS substrates were UV sterilised for 45 minutes prior to cell seeding. Cell suspensions of 5×10^5 cells/ 500 µl were plated on micropatterned PDMS membranes subjected to 0% strain, uniaxial strain applied to 0° and 90° orientated micropatterned lines and homogeneously functionalised surfaces (TCP). Triplicates of each surface condition were used for cell studies. Cell samples were incubated for 45 minutes before non-adhered cells were removed by gently washing cells twice with PBS and replacing with fresh growth media. Cells were cultured for 2 days and then fixed in 10% formalin for 10 minutes at room temperature. Cells were permeabilized with 0.3% TritonX100 for 5 minutes and incubated in AlexaFluor-532 conjugated phalloidin (Invitrogen) for 20 minutes at room temperature. Two drops of NucBlue™ (Invitrogen) per sample were used to stain cell nuclei. Cells were washed twice with PBS between each step and incubated in PBS for imaging.

6.2.6 Imaging

Bright field and fluorescent images were taken using a Nikon TS100 microscope. Images of Alexa532-labeled phalloidin/ DAPI stained cells were acquired with a

TCS LSI Superzoom confocal (Leica, UK). Image j was used for all image analysis. Actin orientation was determined manually, tracing fibers and measuring the angle relative to the patterned line direction. Each nucleus was treated as a single particle and an ellipse was fit to determine the nuclei aspect ratio and orientation angle. Orientation angles of cell nuclei and actin stress fibers are reported as symmetric about the axis of the line pattern, ($n=100$ cells for each surface condition).

6.3 Results and Discussion

Chapter 5 demonstrated that a novel micropatterning technique could be used to influence cell positioning on PDMS membranes. In this chapter, micropatterned PDMS membranes were subjected to uniaxial TS to investigate the independent effect of both geometrical constraints and external mechanical stimuli on cell alignment and cytoskeletal organisation.

6.3.1 Surface characterisation of ppAAm micropatterned PDMS subjected to strain

Initially, surface characterisation studies were used to assess the effect of mechanical stretch on the deposition of ppAAm (92nm) and Fn patterned regions on PDMS. Surface characterisation of PDMS membranes subjected to 0% and 95% TS was carried out. It was reasoned that any distinct variance in surface chemistry occurring at such a high level of strain would be an exaggeration of micropatterned PDMS membranes subjected to smaller levels of strain. ToF-

SIMS analysis of unstrained and strained micropatterned PDMS membranes was used to assess the spatial deposition of ppAAm (92 nm). Previous ToF-SIMS work shown in Chapter 5 established ions that were specific to both PDMS and ppAAm chemistries and have been used to characterise the micropatterned PDMS surfaces here. CN^- and Si^- ion peaks were used to reconstruct secondary ion images of the patterned areas. Figure 6.2.A shows an unstrained micropatterned PDMS surface. Figure 6.2.B shows the same membrane subjected to 95% tensile strain parallel to the ppAAm (92 nm) line direction, (abbreviated to 95 % TS (0°)). Mass spectrum analysis was carried out 48 hours after TS was applied. Similarly, the unstrained micropatterned PDMS surface was analysed prior to applying 95% TS in the perpendicular direction to the ppAAm (92 nm) line direction (abbreviated to 95% TS (90°)), (see figures 6.3.A and B, respectively). Since PDMS membranes were suspended on the strain rigs, there was an accumulation of charge on the PDMS membranes during ToF-SIMS analysis. This affected the image visibility of ppAAm (92 nm) micropatterned areas on the PDMS surface. To reduce this affect, images compiled using CN^- and Si^- signals were normalised to the total number of counts. The spatial distribution of ppAAm (92 nm) (CN^-) and PDMS (Si^-) confirm that plasma stencilling produced a faithful pattern on unstrained surfaces. There is still a distinct line pattern present on strained PDMS surfaces but the width of the ppAAm (92 nm) lines have decreased and increased as a result of applying 95% TS in the parallel and perpendicular direction to the pattern, respectively (figures 6.2 and 6.3). To investigate further, line scanning of

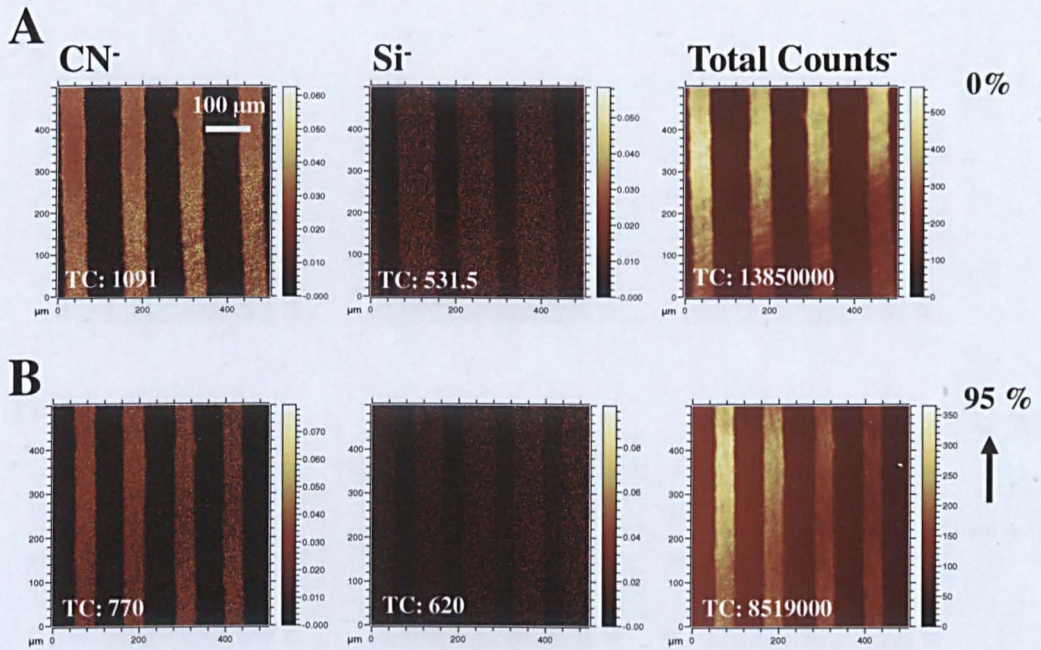


Figure 6.2 ToF SIMS analyses of ppAAm-coated PDMS. Images of ppAAm (92 nm) deposited pattern on the A) unstrained PDMS surface and B) PDMS surfaces subjected to 95% strain parallel to the line direction. Images compiled using signals from CN⁻, Si⁻ and total counts. CN⁻ and Si⁻ signals are normalized to the total number of counts. The arrow identifies the direction in which tensile strain was applied to the membrane.

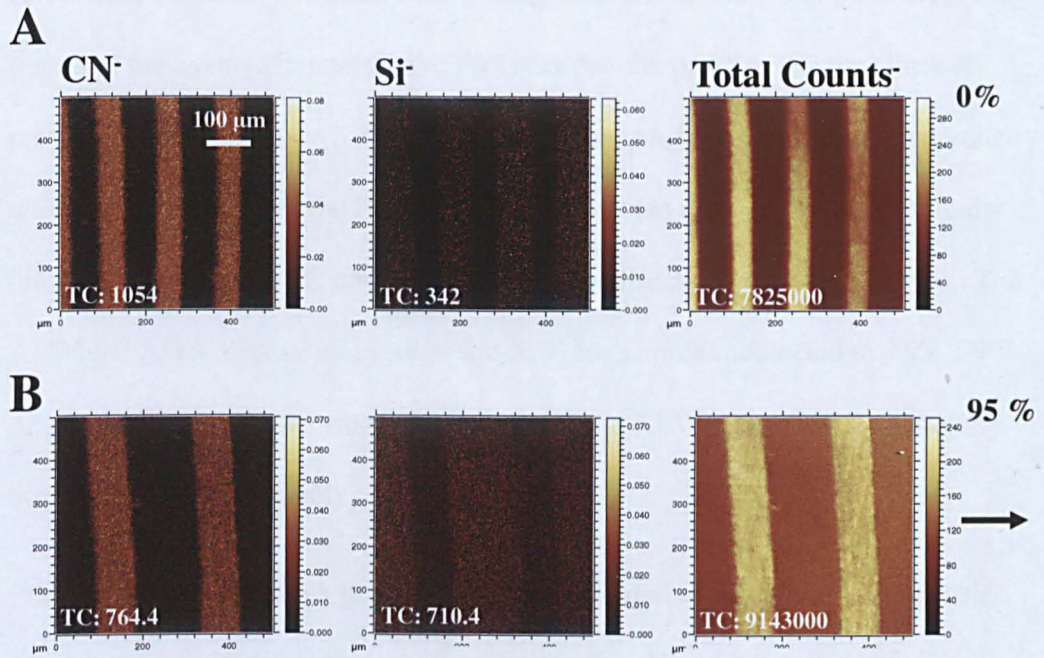


Figure 6.3 ToF SIMS analyses of ppAAm-coated PDMS. Images of ppAAm (92 nm) deposited pattern on the **A**) unstrained PDMS surface and **B**) PDMS surfaces subjected to 95% strain perpendicular to the line direction. Images compiled using signals from CN⁻, Si⁻ and total counts. CN⁻ and Si⁻ signals are normalized to the total number of counts. The arrow identifies the direction in which tensile strain was applied to the membrane.

the corresponding CN^- ion intensity was used to compare the geometry of micropatterned ppAAm (92 nm) on the unstrained and strained PDMS surface across a $500 \mu\text{m}^2$ area (see figure 6.4). The full width half maximum (FWHM) calculation was used to measure the average line width (ALW) of ppAAm (92 nm) lines and the average gap width (AGW) between the ppAAm (92 nm) lines as previously described (see 5.3.1). The change in ppAAm (92 nm) pattern geometry was significantly larger for PDMS surfaces subjected to TS in the perpendicular direction compared to TS applied in the parallel direction to the line pattern. The ALW and AGW decreased by 15% and 22% for samples subjected to 95% TS (0°), respectively. In the transverse direction, the ALW and AGW increased by 50% and 95%, respectively.

Principal component analysis (PCA) was used to derive quantitative information from qualitative ToF-SIMS data to verify whether there was any variance of surface molecular ions between unstrained and strained micropatterned PDMS. PCA confirmed that there is a distinct difference in the intensity of surface molecular ions for PDMS membranes subjected to 0% and 95% strain. Figure 6.5.A and B shows the normalised ion intensity of PDMS related ions on strained and unstrained surfaces. The intensity of PDMS related ions from the negative and positive spectra were analysed, respectively. PDMS membranes subjected to 95% TS exhibited a higher intensity of PDMS-related ions compared to unstrained samples. Figure 6.5.C and D show the normalised intensity of ppAAm related ions on PDMS subjected to 0% and 95% strain. The intensity of ppAAm related

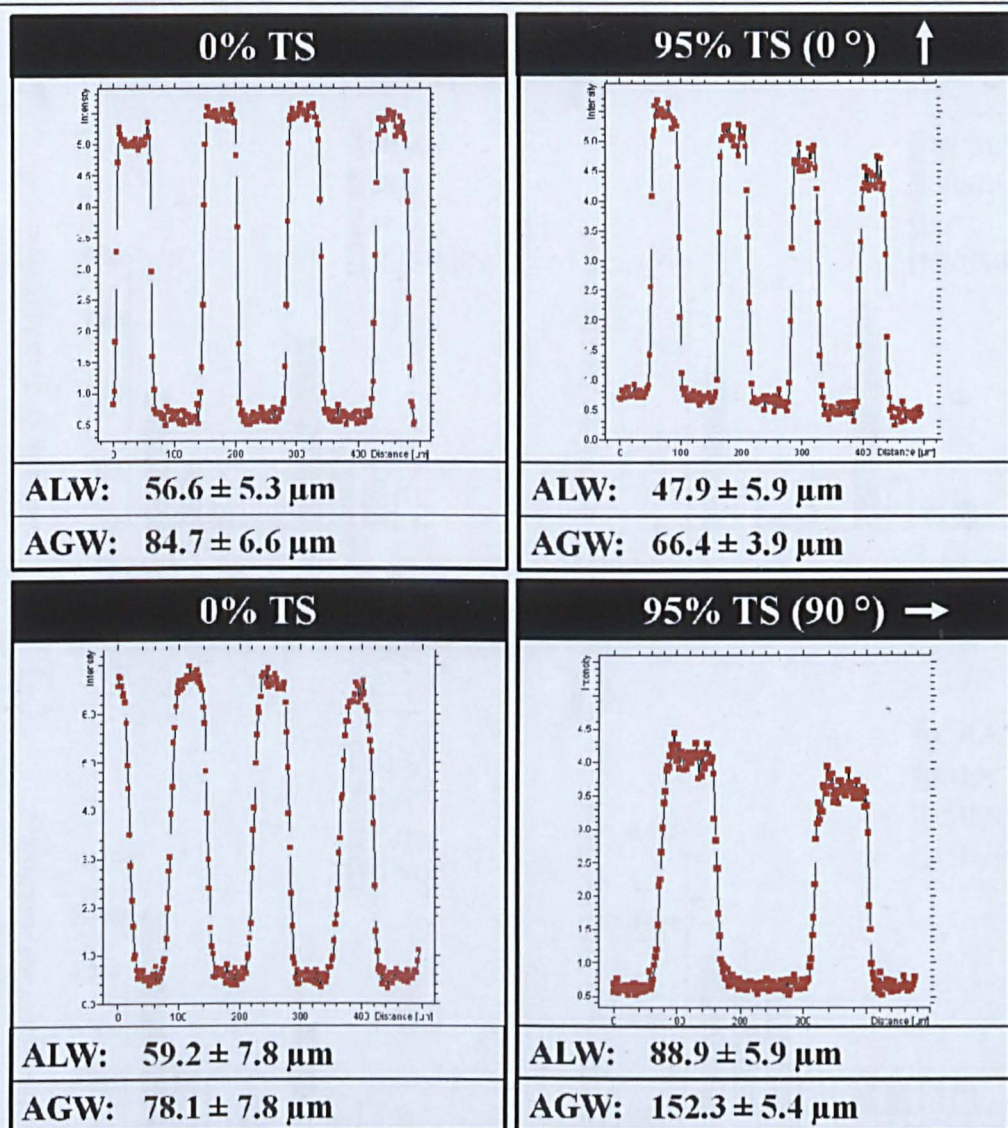


Figure 6.4 Line scan of CN^- ion intensity across $500 \mu\text{m}^2$ area of ppAAm micropatterned PDMS subjected to 0% and 95% tensile strain (TS). Normalized CN^- ion intensity was used to determine geometrical changes of the ppAAm (92 nm) micropattern from PDMS membranes subjected to: 0% tensile strain (0% TS) and 95% TS applied in the parallel and perpendicular direction, abbreviated to 95% TS (0°) and 95% TS (90°), respectively. The full width half maximum (FWHM) calculation was used to calculate the average ppAAm (92 nm) line width (ALW) and the average gap width (AGW) between the ppAAm (92 nm) lines. The arrow identifies the direction in which tensile strain was applied to the membrane

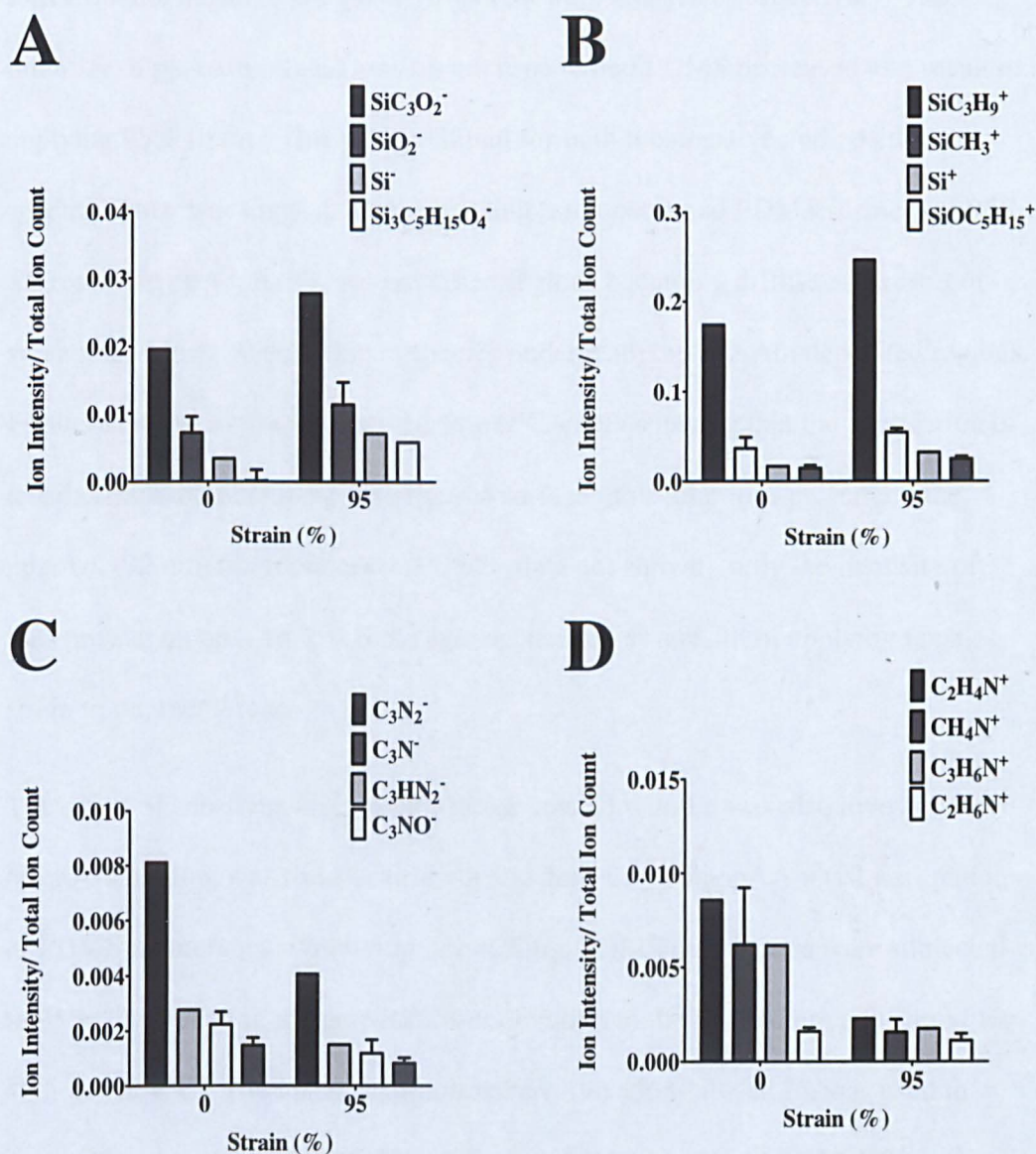


Figure 6.5 Intensity of molecular ions from ppAAm (92 nm) micropatterned PDMS surfaces subjected to 0% and 95% TS. These secondary ions were found to be of significance through principal component analysis (PCA) of ToF-SIMS data. Normalized intensity of ions specific to PDMS identified in the **A**) negative and **B**) positive spectra. Normalized intensity of ions specific to ppAAm (92 nm) identified in the **C**) negative and **D**) positive spectra.

ions from the negative and positive spectra were analysed, respectively. The intensity of ppAAm related ions on micropatterned PDMS decreased as a result of applying 95% strain. This was exhibited for both the negative and positive spectra. This data suggests that subjecting micropatterned PDMS surfaces to 95% TS results in ppAAm (92 nm) patterned regions becoming diffuse as a result of spreading, which reveals silicon species underneath the ppAAm deposited regions. Further confirmation was received from PCA data showing that the application of tensile strain did not change the type of surface molecular ions present on the ppAAm (92 nm) micropatterned PDMS (data not shown), only the intensity of ions present on ppAAm (92 nm) regions changed as a result of applying tensile strain to the membrane.

The effect of substrate strain on PDMS deposited with Fn was also investigated. Micro-stencilling was used to airbrush and deposit Fn on ppAAm (92 nm) regions of PDMS membranes. Following airbrushing, PDMS membranes were subjected to 95% TS applied in the perpendicular direction to the line pattern and stored for 48 hours at 4°C. The location of airbrushed Alexa568-labeled Fn was used to assess the micropattern on PDMS surfaces subjected to 0% and 95% TS using fluorescence microscopy. The images in figures 6.6.A and B reveal that the Fn patterned regions on PDMS respond to substrate strain in a similar manner to ppAAm (92 nm) patterned regions. The width of the Fn lines and the gap width between the Fn lines increase in response to substrate strain applied in the

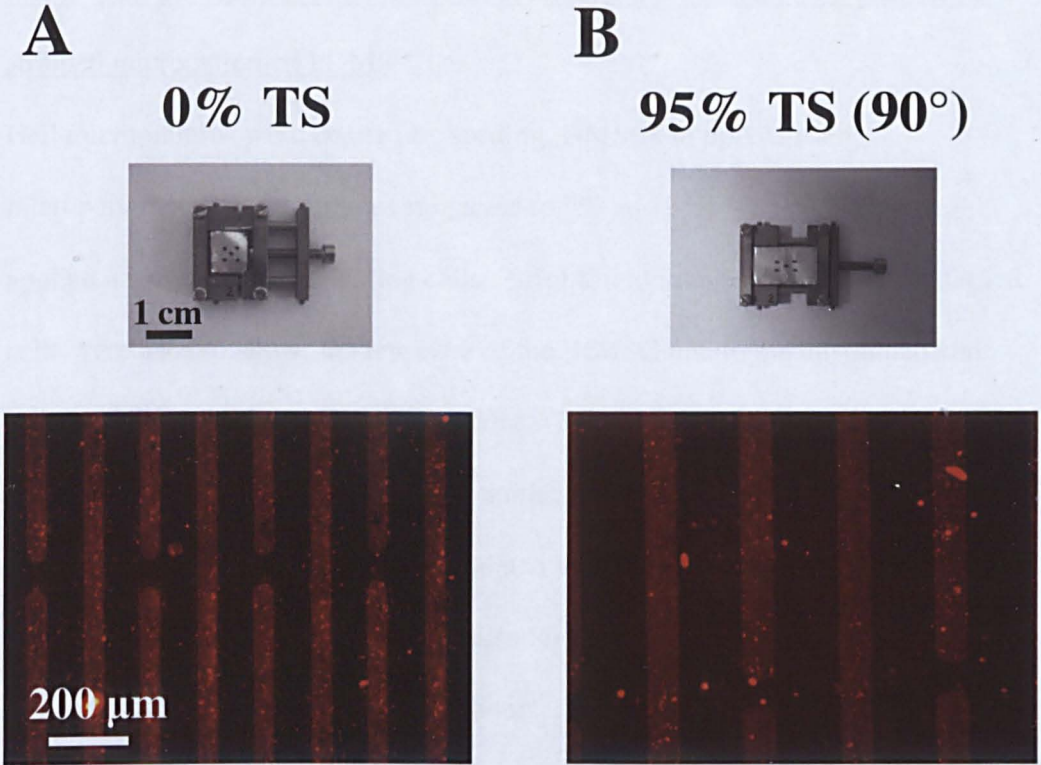


Figure 6.6 Aerosol deposition of Fn on ppAAm deposited PDMS. Images showing **A**) unstrained PDMS membrane (0% strain) mounted on strain rig. The corresponding image below shows the PDMS surface patterned with ppAAm (92nm) and Alexafluor-568 labeled Fn airbrushed on ppAAm deposited regions. **B**) Image showing PDMS membrane subjected to 95% TS (90°) in strain rig. The corresponding image below is the PDMS membrane with ppAAm (92 nm)/ Fn micropattern.

perpendicular direction to the line pattern. Next, the response of cells to unstrained and strained micropatterned PDMS was investigated.

6.3.2 Cell attachment, alignment and cytoskeletal organisation on unstrained/strained micropatterned PDMS

Cell micropatterns were created by seeding iHMSCs to ppAAm/ Fn micropatterned PDMS surfaces subjected to 0% and 95% TS (90°). TS was applied 48 hours prior to seeding cells. Bright field images of the micropatterned cells were used to assess the response of the iHMSC line to the unstrained and strained PDMS surface (figure 6.7). iHMSCs took approximately 45 minutes to fully adhere to micropatterned PDMS subjected to 0% and 95% TS. Patterned regions on both surfaces are well populated with cells 1 hour post seeding, demonstrating that surface changes caused by applying substrate strain did not affect cell attachment. Following 12 hours, iHMSCs exhibited a more elongated morphology on both the unstrained and strained PDMS surface. However, within 24 hours of seeding, most of the cells adhered to the 95% TS (90°) PDMS unattached from the surface. Cells that remained attached to the strained surface looked significantly elongated in comparison to cells adhered to the unstrained PDMS surface. This morphology change is most likely due to attached cells becoming senescent in response to external stresses acting on the cell¹³⁸. Attempts to use higher cell densities as well as adhering PDMS surfaces subjected to 70% and 50% TS (90°) also resulted in cell detachment following 24 hours (data not shown). Cell senescence and detachment from the PDMS surface within 24 hours

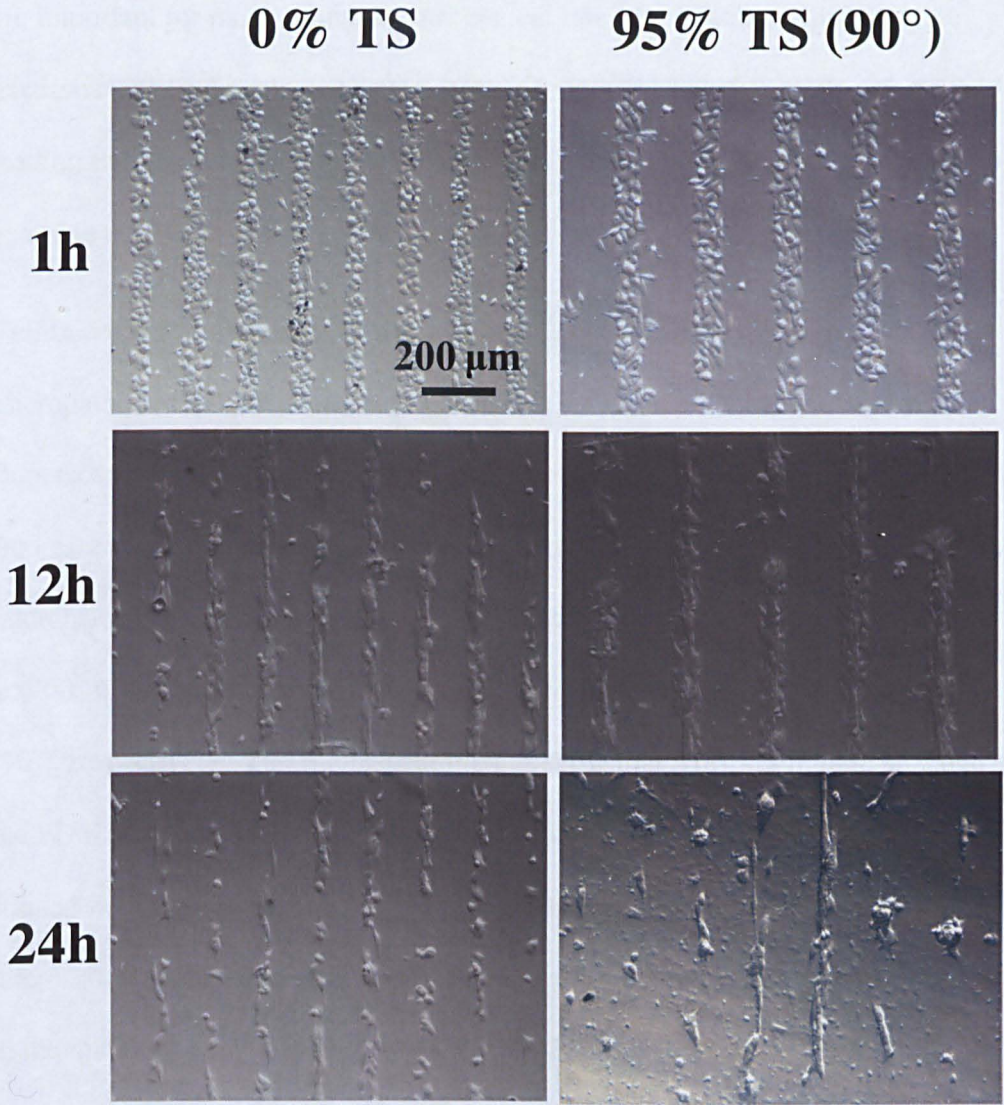


Figure 6.7 Micropatterning of cell lines. Bright field images of iHMSCs on micropatterned PDMS membranes subjected to 0% TS and 95% TS (90°) strain at 1, 12 and 24 hours post seeding.

of attachment could be attributed to damage of the intermediate filament network of the iHMSC line. Previous studies have illustrated that intermediate filaments are important for maintaining the mechanical integrity of cells. Applying excessive external strain can cause damage to intermediate filaments consequently leading to loss of cell adhesion¹³⁹. However, further studies would be required to examine this mechanism.

Cell micropatterns were maintained beyond 24 hours when seeded to micropatterned PDMS subjected to 20% TS (90°). To aid visualisation by fluorescence microscopy the iHMSC cell line was genetically labelled with green fluorescent protein (eGFP). Figure 6.8 shows eGFP-iHMSCs seeded on micropatterned PDMS subjected to 0% (Control(lines)) and 20% TS applied to 0° and 90° orientated micropatterned lines, abbreviated to 20% TS (0°) and 20% TS (90°), respectively. The fluorescent images show that iHMSCs remain attached to the PDMS surface for 2 days. Following 48 hours, attached cells were fixed and stained with DAPI and Alexa532-labeled phalloidin (see figure 6.9). Confocal microscopy was used to image actin stress fiber and nuclei orientation with respect to the micropatterned lines subjected to 0%, 20% TS (0°) and 20% TS (90°). Green and magenta pseudo colour was used to determine the location of actin stress fibers and nuclei in the merged images. iHMSCs cultured on TCP for 48 hours were also fixed and stained alongside PDMS membranes. Separated gray scale images of actin stress fibers and nuclei were used to analyse the response of iHMSCs to geometrical constraints and uniaxial strain direction. Figures 6.10.A-D

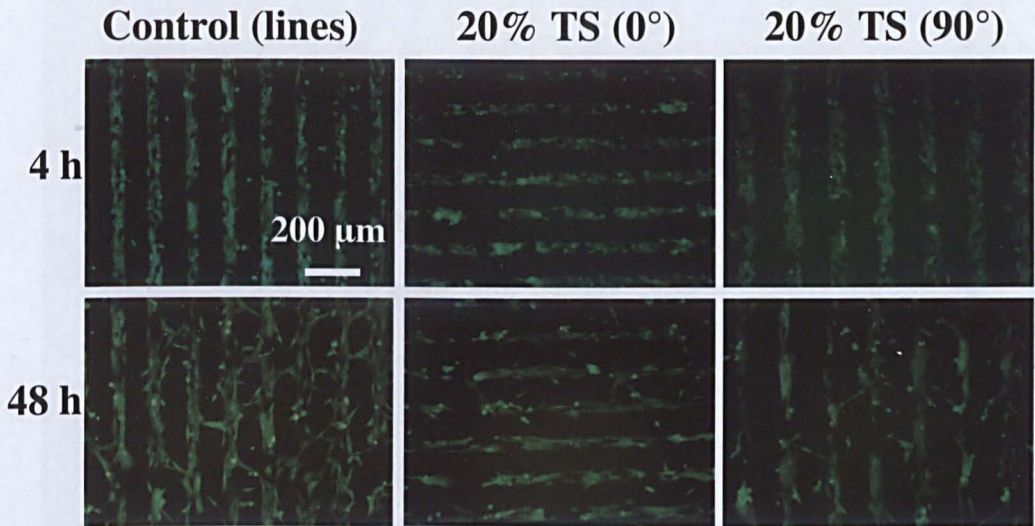


Figure 6.8 Fluorescent images of eGFP labeled iHMSC micropatterns on PDMS membranes. Images showing iHMSCs seeded on PDMS subjected to 0% TS (Control (lines)), 20% TS applied to 0° (20% TS (0°)) and 90° (20% TS (90°)) relative to micropatterned lines. Images were taken 4 and 24 hours post seeding.

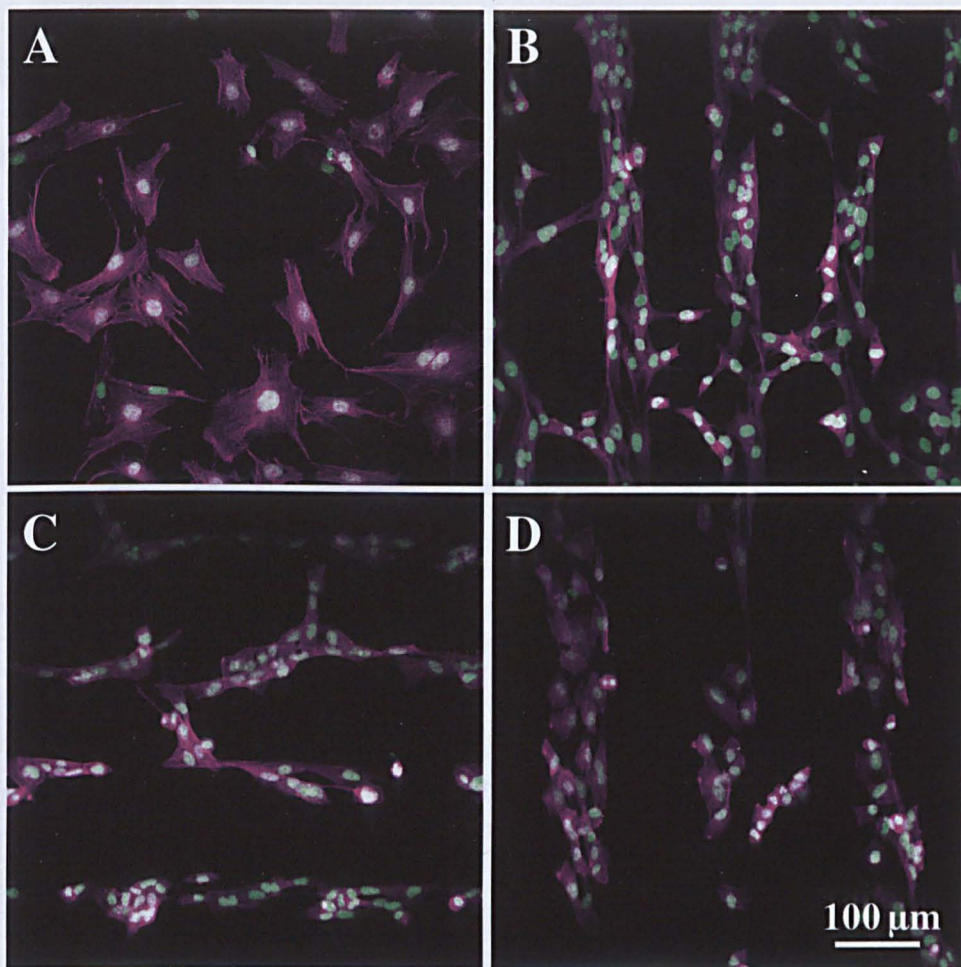


Figure 6.9 Images showing actin stress fiber and nuclei orientation of iHMSCs 48 hours post seeding. Confocal images show Alexa532-labelled phalloidin stained actin stress fibers and DAPI stained nuclei of iHMSCs cultured on: **A**) TCP, **B**) Control (lines), **C**) 20% TS (0°) and **D**) 20% TS (90°) surfaces.

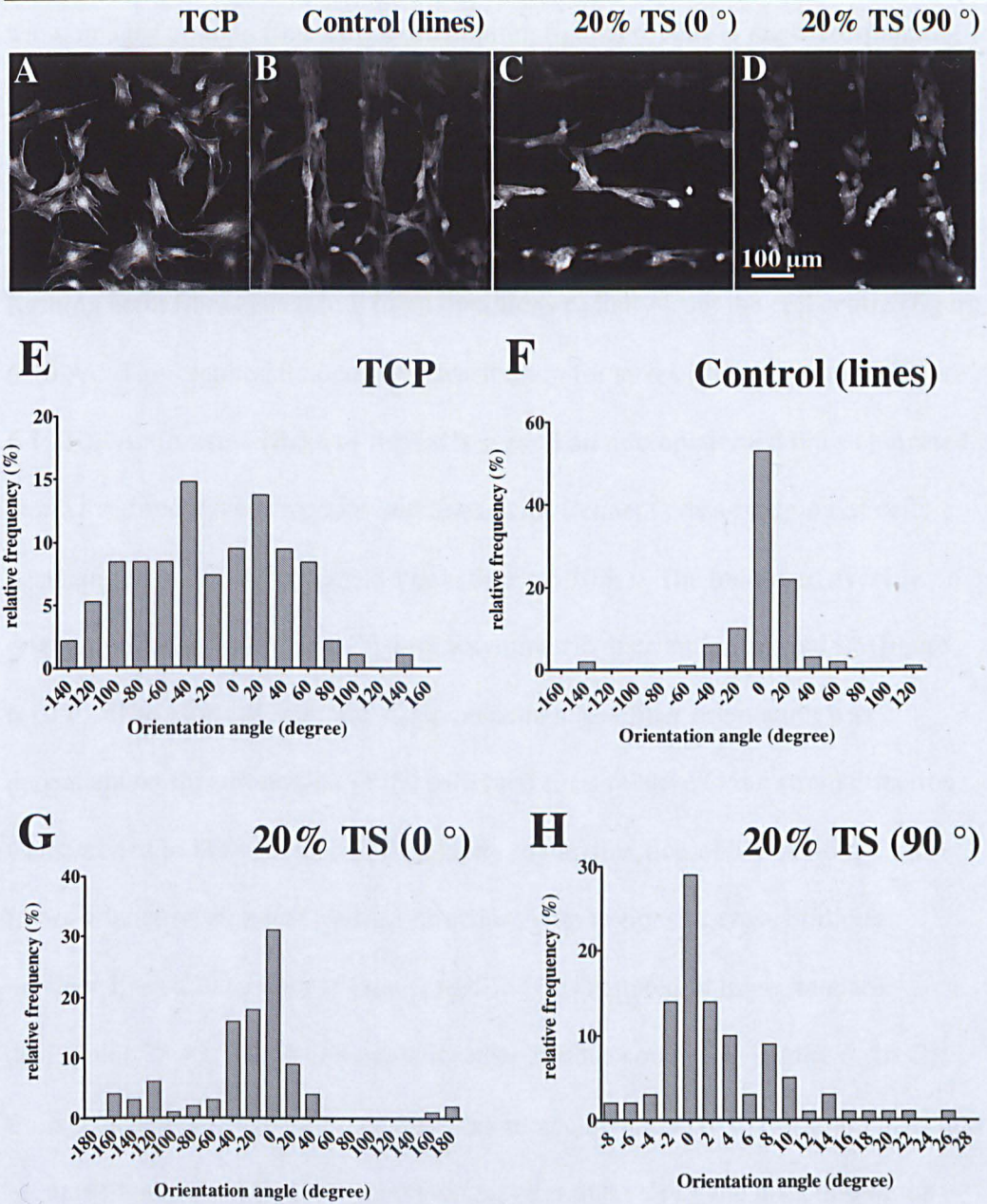


Figure 6.10 Actin stress fiber orientation of iHMSCs. Images of iHMSCs cultured on **A**) TCP, **B**) Control (lines), **C**) 20% TS (0°) and **D**) 20% TS (90°) surfaces. Corresponding histograms of actin stress fiber orientation are shown below: (**E-H**), ($n=100$ cells for each surface condition)).

show images of actin fiber stress orientation, figures 6.10.E-H are corresponding histograms showing the orientation angle of the actin stress fibers relative to the direction of the micropatterned lines. In the absence of constant strain and micropatterning, iHMSCs cultured on TCP exhibited no specific orientation, forming actin fibers extending in all directions radially from the cell centre (figure 6.10.A). This resulted in a random distribution for stress fiber orientation (figure 6.10.E). Actin stress fibers of iHMSCs seeded on micropatterned lines elongated along the direction of the patterned lines, with frequent cross-bridging of cells occurring between the patterned lines (figure 6.10.B). The measured average orientation angle is $0.8^\circ (\pm 31^\circ)$ with a symmetric distribution around 0° (figure 6.10.F). The effect of constant strain on actin stress fiber orientation was dependant on the orientation of the patterned lines relative to the strain direction. Cells seeded to lines orientated 0° relative to the direction of TS exhibited actin fibers orientated along an oblique direction, with regions of cross bridging between lines still evident (figure 6.10.C). This resulted in large standard deviation ($-23.4 \pm 60.2^\circ$) compared to other surface conditions (figure 6. 10.G). Cells attached to micropatterned lines orientated 90° relative to the strain direction became highly elongated with preferential alignment along the direction of the micropatterned lines. Less cross bridging between the micropatterned lines was observed (figure 6.10.D). This resulted in a significantly lower standard deviation compared to the other three surface conditions ($1.8 \pm 6^\circ$) and preferential orientation of 0° relative to patterned lines (figure 6.10.H).

The effect of geometric constraints and strain direction on nuclei orientation and shape was also investigated. Greyscale images of DAPI stained nuclei and the corresponding histograms to show the nuclei orientation angle relative to the direction of the micropatterned lines is shown in figure 6.11. On TCP, nuclei were randomly orientated with no preferential orientation (figures 6.11.A and E).

Comparatively, a greater number of cells orientated 0° relative to the patterned lines on the control (lines) surface (figure 6.11B and F). For 20% TS (0°) surfaces, nuclei preferentially orientated along the patterned lines (figure 6.11.C and G). Applying 20% TS in the perpendicular direction to the line pattern resulted in the highest number of nuclei orientated in the 0° direction compared to other surface conditions (figure 6.11.D and H). The effect of geometric constraints and TS on nuclei shape was analysed by measuring the nuclei aspect ratio, the results are shown in figure 6.12. On homogeneously functionalised surfaces, cell nuclei were roundly shaped (see figure 6.11.A) with an average aspect ratio of 1.35. Nuclei shape was more varied for cells seeded on the control (lines) surface, resulting in large standard deviation. Additionally, cells seeded on micropatterned lines exhibited a statistically significant increase (30 %) of the average nuclei aspect ratio compared to nuclei of cells seeded on TCP. Nuclei elongation was the same for cells seeded on both line orientations relative to the strain direction.

Analysis of cell actin stress fibers and nuclei demonstrate that both geometric constraints and uniaxial strain affect iHMSC alignment. Micropatterned lines on the PDMS surface acted as geometric constraints and influenced iHMSCs to

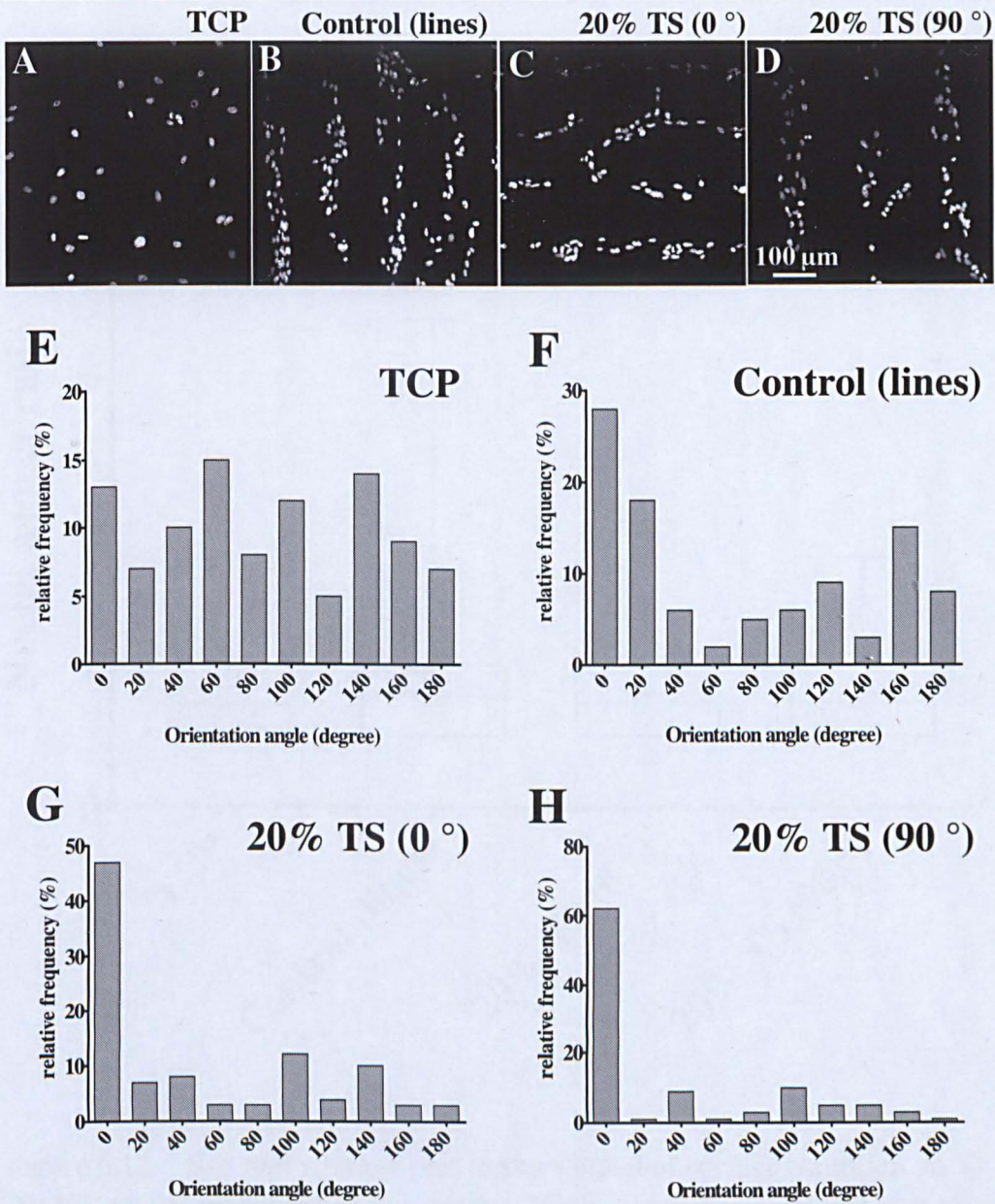


Figure 6.11 Nuclei orientation of iHMSCs. Images of iHMSCs cultured on: A) TCP, B) Control (Lines), C) 20% TS (0°) and D) 20% TS (90°) micropatterned PDMS surfaces. Corresponding histograms of nuclei orientation are shown below: (E-H), ($n=100$ cells for each surface condition).

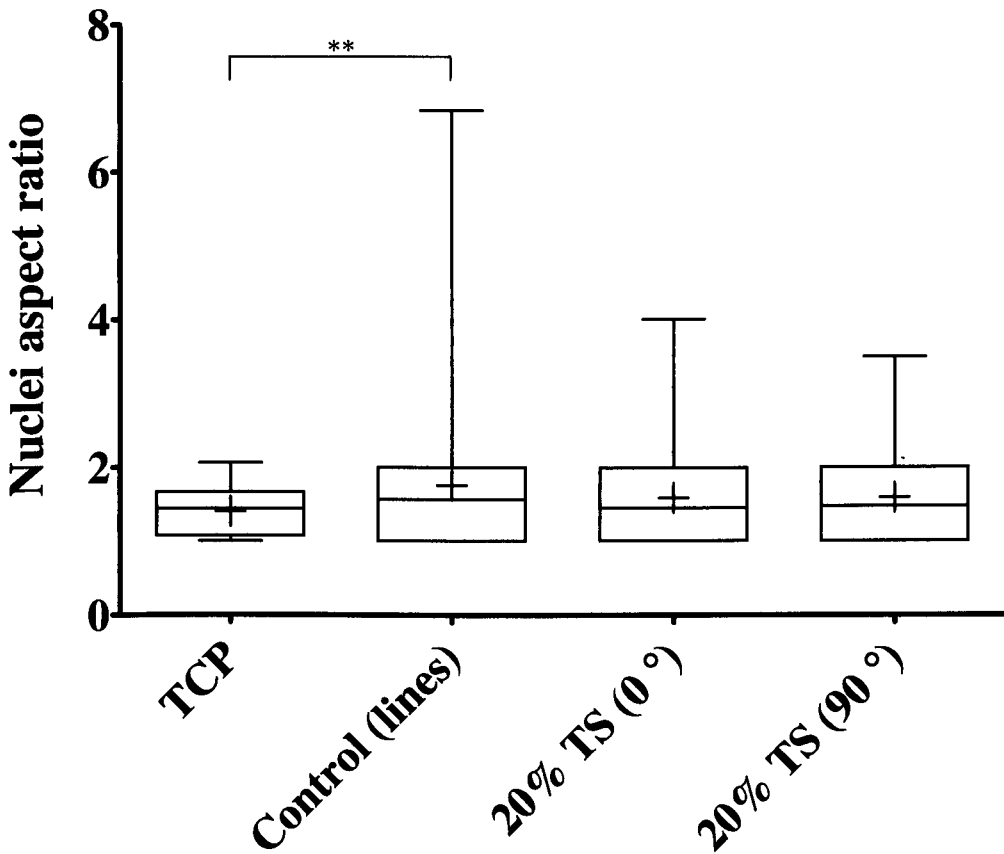


Figure 6.12 Box and whisker plot to show effect of surface condition on iHMSC nuclei aspect ratio (elongation). Nuclei elongation of iHMSCs cultured on: TCP, Control (lines), 20% TS (0°) and 20% TS (90°) surfaces, ($n=100$ cells for each surface condition). The cross in the centre of the box represents the mean nuclei aspect ratio. The horizontal line through the box indicates the median nuclei aspect ratio and the lower and upper edges represent the 25th and 75th percentile, respectively. The whiskers extending from the box represent the standard deviation. Asterisks represent the level of significance ($p < 0.05$).

preferentially align along the direction of the line orientation, similar to previous work¹³⁵. The application of TS to the micropatterned PDMS surface reorganised actin stress fibers whilst remaining geometrically constrained to the line pattern.

Actin stress fiber orientation was dependant on the direction of applied strain relative to the patterned line direction. Actin stress fibers orientated preferentially aligned in the 0° direction relative to the line pattern in the absence of TS.

Conversely, cells preferentially aligned in the perpendicular direction relative to the uniaxial strain direction, similar to previous work by Park et al.¹³⁶. Aligning in the perpendicular direction to strain could be an adaptation process of MSCs to minimize the force applied on the cell body. Both pattern geometry and uniaxial strain are competing forms of external stimuli influencing actin stress fiber orientation. This explains why iHMSCs orientated along an oblique direction and greater cross-bridging of cells between lines was observed when TS was applied in the parallel direction to micropatterned lines. This phenomenon also explains why applying uniaxial strain in the transverse direction to the line pattern influenced cells to preferentially orientate along the line pattern. Application of TS is the dominant factor for determining nucleus orientation, although the direction of applied strain relative to the micropattern made no difference to nuclei orientation. Additionally, there was minimal difference in nuclei shape for strained and unstrained micropatterned PDMS. This suggests that there was no competition between both stimuli to orient cell nuclei and influence nuclei shape. Furthermore, these results show that nuclei orientation does not follow actin stress fiber

orientation under the influence of either geometric constraints or application of TS.

Similar results were found by Ahmed et al. investigating the response of C2C12 myoblasts to CMS direction on micropatterned PDMS surfaces¹³³. Unlike actin stress fibers which are directly anchored to the substrate via focal adhesion complexes, the nucleus is not directly anchored to the substrate surface. This could explain why the influence of TS on nuclei orientation does not follow actin stress fiber orientation. However, previous work has demonstrated that the actin cytoskeleton of animal cells plays an important role in nucleus positioning since the nucleus envelope is tethered to the actin cytoskeleton¹⁴⁰. Thus, further work would be required to understand the mechanism influencing nucleus orientation.

6.4 Conclusion

This study provides an understanding of how the surface chemistry of ppAAm/ Fn micropatterned PDMS responds to uniaxial strain. Surface characterisation revealed that ppAAm (92 nm)/ Fn patterned lines underwent geometrical changes depending on the direction of TS relative to the line pattern. Substrate strain causes the deposition of ppAAm (92 nm) to spread revealing silicone species underneath. Cell micropatterns on unstrained and strained surfaces showed that iHMSCs respond to strain applied to micropatterned PDMS prior to cell attachment. Applying uniaxial substrate strain $\geq 50\%$ resulted in cell detachment within 24 hours of cell seeding. Thus, for future work micropatterned PDMS membranes should be subjected to $\leq 20\%$ TS only. Micropatterned PDMS surfaces subjected to 20 % TS demonstrated that geometric constraints and strain direction

act as independent controls to influence cell alignment and cytoskeletal organisation. There was a profound effect on cell alignment for iHMSCs adhered to micropatterned PDMS subjected to 20% TS in the perpendicular direction to the line pattern. Importantly, this study demonstrates that micropatterned PDMS membranes held at constant strain could be used in the future to influence cell positioning for the purpose of engineering tissue capable of physiological function.

7

General discussion, conclusions and future development

The work presented in this thesis focused on developing an *in vitro* pump to mimic the physiological function of the heart. This will be the first component of a long-term strategy to build internal circulatory systems for *in vitro* engineered tissue. The research addressed two aims, both concerning engineering of the structural constituent of the 3-D pump. The first aim was to manufacture a scaffold with finely tuned mechanical properties such that the strength of contraction of cardiomyocytes adhered to the substrate surface can drive fluid movement (covered in chapter 3). The biocompatibility of the scaffold was also investigated by assessing cell attachment and proliferation (covered in chapter 4). The second aim was to establish a method that controls cell positioning on the scaffold surface. Surface micropatterning combined with the application of an external stimulus was used to influence cell alignment on the substrate (covered in chapters 5 and 6). Directional contraction will be important to produce a functional *in vitro* pump since aligned cardiomyocytes generate more force⁴².

7.1 Manufacturing scaffolds and investigating mechanical compatibility and biocompatibility

7.1.1 General discussion and conclusions

Polymer films are required that can be coupled to cells in order to provide restorative forces against cardiomyocyte contractions. To achieve this, the physical properties of the biomaterial must be such that attached cardiomyocytes experience no loss of mechanical function i.e. the elasticity of the substrate-cell construct remains as close as possible to that of native tissue as previously achieved by the Whitesides' group⁸¹. PDMS was used to manufacture elastomeric membranes ranging from 50-1000 μm thickness and mechanical characterisation was used to show that the Young modulus values of these membranes are within the range of native tissue and biomaterials currently used in the field of cardiac tissue engineering (~ 1 MPa) (chapter 3)¹⁴¹.

Polymer films must exhibit surface chemistry that is compatible with cardiomyocytes directly, or capable of being functionalised such that ECM derivatives can be readily attached. PDMS is inherently hydrophobic and does not promote cell adhesion¹⁰¹. Previous work has demonstrated that the derivatisation of PDMS to promote cell adhesion can be achieved by plasma polymerisation. Deposition of ppAAm (92 nm) on the PDMS surface following light oxygen etching successfully reduced surface hydrophobicity and was best suited to cultivating cells compared to untreated and oxygen etched PDMS surfaces.

7.1.2 Future development

The correct mechanical properties of biomaterials used for cardiac tissue engineering remain unknown. Thus a range of PDMS membranes were manufactured in chapter 3. The next stage of this work would require investigating the effect of membrane thickness on cardiomyocyte function. Previous work has demonstrated that the contractile force of PDMS membrane/ cardiomyocyte engineered construct is defined by membrane thickness⁸¹. Initial experiments should focus on three parameters: membrane thickness, surface area and cell density. Once established, it will be a simple geometric exercise to design sheets capable of biomimetic function.

7.2 Control of cell positioning on PDMS using micropatterning and external stimulation

7.2.1 General discussion and conclusions

Cell alignment on the PDMS surface is required to generate directional contraction and maximise overall contractile force. Therefore, the format of the PDMS membrane should provide a directional template for cell alignment and guide for cardiomyocyte contraction/ restoration. Surface micropatterning of PDMS was used to control cell positioning and was achieved by selective deposition of ppAAm (92 nm)/ ECM protein onto PDMS through a microstencil. Results demonstrated that pattern geometry could control site specific cell attachment (covered in chapter 5). The micropatterning technique achieved micron scale

resolution over a macro scale and could be modified to create co-culture patterns. Latter work involving the assembly of the *in vitro* pump will require forming PDMS tubes with cardiomyocytes attached. The results in chapter 5 demonstrated that PDMS sheets could be manually rolled to form radially cell patterned tubes capable of holding fluid. The application of constant uniaxial strain to micropatterned PDMS surfaces acts as an independent stimulus to influence cell positioning. Results in chapter 6 demonstrated that substrate strain incorporated with surface micropatterning can be used to control site and alignment-specific cell attachment.

7.2.2 Future development

Combining the techniques developed in this thesis, future development will focus on the assembly and testing of an *in vitro* circulation system. Assembly of the *in vitro* pump will first require the PDMS tube with cardiomyocytes attached to generate contractile forces that are capable of generating volume changes to drive fluid movement. The best route to achieve this must be investigated. For example, it has already been demonstrated that co-cultures can be created on micropatterned PDMS surfaces. It may be necessary to use fibroblast co-cultures with cardiomyocytes to spontaneously form new ECM to host multilayers. These multilayer sheets could then be rolled and secured as already demonstrated for single layers in chapter 5, with the prospect of generating greater contractile force.

The BOSE bioreactor system has been developed to accommodate a tubular structure and suspension culture of the engineered construct. Additionally, the BOSE is biodynamic; it can apply tension simultaneously with pulsatile flow. Commercially available cerebrospinal fluid (CSF) flow control valves (as used with ventriculoperitoneal shunts) should be incorporated to direct one way flow through the pumping system. These valves are equipped with standard connector ports of internal diameter 1mm and external diameter 2 mm and are supplied in a sterile state. The engineered construct should either be mounted directly on to the valve ports, or will be attached via a suitable catheter. Once mounted, electrical pacing should be incorporated since previous studies have demonstrated how electrical stimulation is required for further development and spatial-temporal organization of sarcomeric proteins^{72,77}. Electrical pacing should be achieved using a C-Pace pulse generator (C-pace 100, IonOptix, Milton MA) which has already been specialised to deliver electrical stimuli to cardiomyocytes attached to tubular structures within the bioreactor. Once the structure is mounted within the bioreactor chamber using custom made fixtures and cells are being stimulated electrically, initial experiments should evaluate the contractility of the cardiomyocyte cell layer/PDMS membrane combination under isometric and isotonic contraction. Classic pharmacology active molecules (e.g. adrenaline, beta-blockers) could be added to the bathing solution to investigate tissue response. Electrical pacing could also be manipulated to either apply a fixed contractile force, which will be measured (isometric contraction) or to apply a

suitable distraction force, the tube deformation that that will occur from the resulting contraction could be quantified using the video extensometer described in 3.2.5. Once the contractility of the engineered construct is determined, the geometric variables can be used to design pumping tubes capable of developing specific internal pressures and volume displacement.

References

1. Mason, C. & Dunnill, P. A brief definition of regenerative medicine. *Regen Med* 3, 1-5 (2008).
2. Stock, U.A. & Vacanti, J.P. Tissue engineering: current state and prospects. *Annual review of medicine* 52, 443-451 (2001).
3. Levenberg, S. & Langer, R. Advances in Tissue Engineering. Vol. 61 113-134 (2004).
4. Chien, K.R. Regenerative medicine and human models of human disease. *Nature* 453, 302-305 (2008).
5. Novosel, E.C., Kleinhans, C. & Kluger, P.J. Vascularization is the key challenge in tissue engineering. *Advanced Drug Delivery Reviews* 63, 300-311 (2011).
6. Bouten, C.V.C., *et al.* Substrates for cardiovascular tissue engineering. *Advanced Drug Delivery Reviews* 63, 221-241 (2011).
7. Moorman, A., Webb, S., Brown, N.A., Lamers, W. & Anderson, R.H. Development of the heart: (1) Formation of the cardiac chambers and arterial trunks. *Heart* 89, 806-814 (2003).
8. Manabe, I., Shindo, T. & Nagai, R. Gene Expression in Fibroblasts and Fibrosis. *Circulation Research* 91, 1103-1113 (2002).
9. Banerjee, I., Yekkala, K., Borg, T.K. & Baudino, T.A. Dynamic Interactions between Myocytes, Fibroblasts, and Extracellular Matrix. *Annals of the New York Academy of Sciences* 1080, 76-84 (2006).
10. Macchiarelli, G., *et al.* A micro-anatomical model of the distribution of myocardial endomysial collagen. *Histol Histopathol* 17, 699-706 (2002).

11. Kanzaki, Y., *et al.* Three-Dimensional Architecture of Cardiomyocytes and Connective Tissue in Human Heart Revealed by Scanning Electron Microscopy. *Circulation* 122, 1973-1974 (2010).
12. Lutgens, E., *et al.* Chronic myocardial infarction in the mouse: cardiac structural and functional changes. *Cardiovasc Res* 41, 586-593 (1999).
13. Shirani, J., Pick, R., Roberts, W.C. & Maron, B.J. Morphology and significance of the left ventricular collagen network in young patients with hypertrophic cardiomyopathy and sudden cardiac death. *J Am Coll Cardiol* 35, 36-44 (2000).
14. Ahuja, P., Sdek, P. & MacLellan, W.R. Cardiac Myocyte Cell Cycle Control in Development, Disease, and Regeneration. *Physiological Reviews* 87, 521-544 (2007).
15. Akins, R.E. Can Tissue Engineering Mend Broken Hearts? *Circulation Research* 90, 120-122 (2002).
16. Guilak, F., *et al.* Control of Stem Cell Fate by Physical Interactions with the Extracellular Matrix. *Cell Stem Cell* 5, 17-26 (2009).
17. Engler, A.J., Sen, S., Sweeney, H.L. & Discher, D.E. Matrix Elasticity Directs Stem Cell Lineage Specification. *Cell* 126, 677-689 (2006).
18. Engler, A.J., *et al.* Embryonic cardiomyocytes beat best on a matrix with heart-like elasticity: scar-like rigidity inhibits beating. *J Cell Sci* 121, 3794-3802 (2008).
19. Jacot, J.G., McCulloch, A.D. & Omens, J.H. Substrate Stiffness Affects the Functional Maturation of Neonatal Rat Ventricular Myocytes. *Biophysical Journal* 95, 3479-3487 (2008).
20. DeForest, C.A. & Anseth, K.S. Advances in Bioactive Hydrogels to Probe and Direct Cell Fate. *Annual Review of Chemical and Biomolecular Engineering* 3, 421-444 (2012).

21. Young, J.L. & Engler, A.J. Hydrogels with time-dependent material properties enhance cardiomyocyte differentiation in vitro. *Biomaterials* 32, 1002-1009 (2011).
22. Driessen, N.J.B., Mol, A., Bouten, C.V.C. & Baaijens, F.P.T. Modeling the mechanics of tissue-engineered human heart valve leaflets. *Journal of Biomechanics* 40, 325-334 (2007).
23. Engelmayr, G.C., *et al.* Accordion-like honeycombs for tissue engineering of cardiac anisotropy. *Nat Mater* 7, 1003-1010 (2008).
24. Chen, Q.-Z., Harding, S.E., Ali, N.N., Lyon, A.R. & Boccaccini, A.R. Biomaterials in cardiac tissue engineering: Ten years of research survey. *Materials Science and Engineering: R: Reports* 59, 1-37 (2008).
25. Rubart, M., Soonpaa, M.H., Nakajima, H. & Field, L.J. Spontaneous and evoked intracellular calcium transients in donor-derived myocytes following intracardiac myoblast transplantation. *The Journal of Clinical Investigation* 114, 775-783 (2004).
26. Koh, G.Y., *et al.* Stable fetal cardiomyocyte grafts in the hearts of dystrophic mice and dogs. *The Journal of Clinical Investigation* 96, 2034-2042 (1995).
27. Soonpaa, M.H., Koh, G.Y., Klug, M.G. & Field, L.J. Formation of nascent intercalated disks between grafted fetal cardiomyocytes and host myocardium. *Science* 264, 98-101 (1994).
28. Reinecke, H., Zhang, M., Bartosek, T. & Murry, C.E. Survival, Integration, and Differentiation of Cardiomyocyte Grafts. *Circulation* 100, 193-202 (1999).
29. Li, R.-K., Mickle, D.A.G., Weisel, R.D., Zhang, J. & Mohabeer, M.K. In Vivo Survival and Function of Transplanted Rat Cardiomyocytes. *Circulation Research* 78, 283-288 (1996).
30. Scorsin, M., *et al.* Comparison of the effects of fetal cardiomyocyte and skeletal myoblast transplantation on postinfarction left ventricular function. *J Thorac Cardiovasc Surg* 119, 1169-1175 (2000).

31. Catalina, P., *et al.* Human ESCs predisposition to karyotypic instability: Is a matter of culture adaptation or differential vulnerability among hESC lines due to inherent properties? *Mol Cancer* 7, 76 (2008).
32. Shambloott, M.J., *et al.* Human embryonic germ cell derivatives express a broad range of developmentally distinct markers and proliferate extensively in vitro. *Proceedings of the National Academy of Sciences* 98, 113-118 (2001).
33. Thomson, J.A., *et al.* Embryonic Stem Cell Lines Derived from Human Blastocysts. *Science* 282, 1145-1147 (1998).
34. Kehat, I., *et al.* Human embryonic stem cells can differentiate into myocytes with structural and functional properties of cardiomyocytes. *The Journal of Clinical Investigation* 108, 407-414 (2001).
35. Mummery, C., *et al.* Differentiation of Human Embryonic Stem Cells to Cardiomyocytes. *Circulation* 107, 2733-2740 (2003).
36. Beqqali, A., Kloots, J., Ward-van Oostwaard, D., Mummery, C. & Passier, R. Genome-wide transcriptional profiling of human embryonic stem cells differentiating to cardiomyocytes. *Stem Cells* 24, 1956-1967 (2006).
37. Snir, M., *et al.* Assessment of the ultrastructural and proliferative properties of human embryonic stem cell-derived cardiomyocytes. *Am J Physiol Heart Circ Physiol* 285, H2355-2363 (2003).
38. Xue, T., *et al.* Functional integration of electrically active cardiac derivatives from genetically engineered human embryonic stem cells with quiescent recipient ventricular cardiomyocytes: insights into the development of cell-based pacemakers. *Circulation* 111, 11-20 (2005).
39. Kehat, I., *et al.* Electromechanical integration of cardiomyocytes derived from human embryonic stem cells. *Nat Biotechnol* 22, 1282-1289 (2004).
40. Laflamme, M.A., *et al.* Cardiomyocytes derived from human embryonic stem cells in pro-survival factors enhance function of infarcted rat hearts. *Nat Biotechnol* 25, 1015-1024 (2007).

41. Kofidis, T., *et al.* In vitro engineering of heart muscle: Artificial myocardial tissue. *The Journal of Thoracic and Cardiovascular Surgery* 124, 63-69 (2002).
42. van Luyn, M.J.A., *et al.* Cardiac tissue engineering: characteristics of in unison contracting two- and three-dimensional neonatal rat ventricle cell (co)-cultures. *Biomaterials* 23, 4793-4801 (2002).
43. Zimmermann, W.-H., *et al.* Tissue Engineering of a Differentiated Cardiac Muscle Construct. *Circulation Research* 90, 223-230 (2002).
44. Xiang, Z., Liao, R., Kelly, M.S. & Spector, M. Collagen-GAG scaffolds grafted onto myocardial infarcts in a rat model: a delivery vehicle for mesenchymal stem cells. *Tissue Eng* 12, 2467-2478 (2006).
45. Zhong, *et al.* Formation of Collagen–Glycosaminoglycan Blended Nanofibrous Scaffolds and Their Biological Properties. *Biomacromolecules* 6, 2998-3004 (2005).
46. Prabhakaran, M.P., Venugopal, J., Kai, D. & Ramakrishna, S. Biomimetic material strategies for cardiac tissue engineering. *Materials Science and Engineering: C* 31, 503-513 (2011).
47. Grover, C.N., Cameron, R.E. & Best, S.M. Investigating the morphological, mechanical and degradation properties of scaffolds comprising collagen, gelatin and elastin for use in soft tissue engineering. *Journal of the Mechanical Behavior of Biomedical Materials* 10, 62-74 (2012).
48. Shimizu, T., *et al.* Fabrication of Pulsatile Cardiac Tissue Grafts Using a Novel 3-Dimensional Cell Sheet Manipulation Technique and Temperature-Responsive Cell Culture Surfaces. *Circulation Research* 90, e40-e48 (2002).
49. Kubo, H., Shimizu, T., Yamato, M., Fujimoto, T. & Okano, T. Creation of myocardial tubes using cardiomyocyte sheets and an in vitro cell sheet-wrapping device. *Biomaterials* 28, 3508-3516 (2007).
50. Ott, H.C., *et al.* Perfusion-decellularized matrix: using nature's platform to engineer a bioartificial heart. *Nat Med* 14, 213-221 (2008).

51. Robinson, K.A., *et al.* Extracellular matrix scaffold for cardiac repair. *Circulation* 112, I135-143 (2005).
52. Singelyn, J. & Christman, K. Injectable Materials for the Treatment of Myocardial Infarction and Heart Failure: The Promise of Decellularized Matrices. *Journal of Cardiovascular Translational Research* 3, 478-486 (2010).
53. Huang, Y.-C., Khait, L. & Birla, R.K. Contractile three-dimensional bioengineered heart muscle for myocardial regeneration. *Journal of Biomedical Materials Research Part A* 80A, 719-731 (2007).
54. Bursac, N., *et al.* Cardiac muscle tissue engineering: toward an in vitro model for electrophysiological studies. *American Journal of Physiology - Heart and Circulatory Physiology* 277, H433-H444 (1999).
55. Kim, B.-S. & Mooney, D.J. Development of biocompatible synthetic extracellular matrices for tissue engineering. *Trends in Biotechnology* 16, 224-230 (1998).
56. Zammaretti, P. & Jaconi, M. Cardiac tissue engineering: regeneration of the wounded heart. *Current Opinion in Biotechnology* 15, 430-434 (2004).
57. Shin, M., Ishii, O., Sueda, T. & Vacanti, J.P. Contractile cardiac grafts using a novel nanofibrous mesh. *Biomaterials* 25, 3717-3723 (2004).
58. Ishii, O., Shin, M., Sueda, T. & Vacanti, J.P. In vitro tissue engineering of a cardiac graft using a degradable scaffold with an extracellular matrix-like topography. *The Journal of Thoracic and Cardiovascular Surgery* 130, 1358-1363 (2005).
59. Fozdar, D.Y., Soman, P., Lee, J.W., Han, L.-H. & Chen, S. Three-Dimensional Polymer Constructs Exhibiting a Tunable Negative Poisson's Ratio. *Advanced Functional Materials* 21, 2712-2720 (2011).
60. Ozawa, T., *et al.* Optimal biomaterial for creation of autologous cardiac grafts. *Circulation* 106, I176-182 (2002).

61. Zong, X., *et al.* Electrospun fine-textured scaffolds for heart tissue constructs. *Biomaterials* 26, 5330-5338 (2005).
62. Dobner, S., Bezuidenhout, D., Govender, P., Zilla, P. & Davies, N. A synthetic non-degradable polyethylene glycol hydrogel retards adverse post-infarct left ventricular remodeling. *J Card Fail* 15, 629-636 (2009).
63. Fujimoto, K.L., *et al.* Synthesis, characterization and therapeutic efficacy of a biodegradable, thermoresponsive hydrogel designed for application in chronic infarcted myocardium. *Biomaterials* 30, 4357-4368 (2009).
64. Wang, T., *et al.* Novel thermosensitive hydrogel injection inhibits post-infarct ventricle remodelling. *Eur J Heart Fail* 11, 14-19 (2009).
65. Chen, Q.Z., *et al.* Characterisation of a soft elastomer poly(glycerol sebacate) designed to match the mechanical properties of myocardial tissue. *Biomaterials* 29, 47-57 (2008).
66. Pêgo, A.P., *et al.* In vivo behavior of poly(1,3-trimethylene carbonate) and copolymers of 1,3-trimethylene carbonate with D,L-lactide or ϵ -caprolactone: Degradation and tissue response. *Journal of Biomedical Materials Research Part A* 67A, 1044-1054 (2003).
67. McDevitt, T.C., Woodhouse, K.A., Hauschka, S.D., Murry, C.E. & Stayton, P.S. Spatially organized layers of cardiomyocytes on biodegradable polyurethane films for myocardial repair. *Journal of Biomedical Materials Research Part A* 66A, 586-595 (2003).
68. Alperin, C., Zandstra, P.W. & Woodhouse, K.A. Polyurethane films seeded with embryonic stem cell-derived cardiomyocytes for use in cardiac tissue engineering applications. *Biomaterials* 26, 7377-7386 (2005).
69. Fujimoto, K.L., *et al.* An Elastic, Biodegradable Cardiac Patch Induces Contractile Smooth Muscle and Improves Cardiac Remodeling and Function in Subacute Myocardial Infarction. *Journal of the American College of Cardiology* 49, 2292-2300 (2007).

70. Hidalgo-Bastida, L.A., *et al.* Cell adhesion and mechanical properties of a flexible scaffold for cardiac tissue engineering. *Acta Biomaterialia* 3, 457-462 (2007).
71. Tandon, N., Marsano, A., Cannizzaro, C., Voldman, J. & Vunjak-Novakovic, G. Design of electrical stimulation bioreactors for cardiac tissue engineering. *Conf Proc IEEE Eng Med Biol Soc* 2008, 3594-3597 (2008).
72. Fink, C., *et al.* Chronic stretch of engineered heart tissue induces hypertrophy and functional improvement. *FASEB J* 14, 669-679 (2000).
73. Radisic, M., *et al.* Functional assembly of engineered myocardium by electrical stimulation of cardiac myocytes cultured on scaffolds. *Proc Natl Acad Sci U S A* 101, 18129-18134 (2004).
74. Gupta, V. & Grande-Allen, K.J. Effects of static and cyclic loading in regulating extracellular matrix synthesis by cardiovascular cells. *Cardiovascular Research* 72, 375-383 (2006).
75. Akhyari, P., *et al.* Mechanical stretch regimen enhances the formation of bioengineered autologous cardiac muscle grafts. *Circulation* 106, 1137-142 (2002).
76. Tandon, N., *et al.* Electrical stimulation systems for cardiac tissue engineering. *Nat. Protocols* 4, 155-173 (2009).
77. Martherus, R.S., Zeijlemaker, V.A. & Ayoubi, T.A. Electrical stimulation of primary neonatal rat ventricular cardiomyocytes using pacemakers. *Biotechniques* 48, 65-67 (2010).
78. Radisic, M., *et al.* Functional assembly of engineered myocardium by electrical stimulation of cardiac myocytes cultured on scaffolds. *Proceedings of the National Academy of Sciences* 101, 18129-18134 (2004).
79. Costa, K.D., Lee, E.J. & Holmes, J.W. Creating alignment and anisotropy in engineered heart tissue: role of boundary conditions in a model three-dimensional culture system. *Tissue Eng* 9, 567-577 (2003).

-
80. Feinberg, A.W., *et al.* Muscular Thin Films for Building Actuators and Powering Devices. *Science* 317, 1366-1370 (2007).
 81. Cowan, C.A., *et al.* Derivation of Embryonic Stem-Cell Lines from Human Blastocysts. *New England Journal of Medicine* 350, 1353-1356 (2004).
 82. Lue, S.J., *et al.* Sorption, diffusion, and perm-selectivity of toluene vapor/nitrogen mixtures through polydimethylsiloxane membranes with two cross-linker densities. *Journal of Membrane Science* 349, 321-332 (2010).
 83. Claycomb, W.C., *et al.* HL-1 cells: A cardiac muscle cell line that contracts and retains phenotypic characteristics of the adult cardiomyocyte. *P Natl Acad Sci USA* 95, 2979-2984 (1998).
 84. Burridge, P.W., *et al.* Improved Human Embryonic Stem Cell Embryoid Body Homogeneity and Cardiomyocyte Differentiation from a Novel V-96 Plate Aggregation System Highlights Interline Variability. *STEM CELLS* 25, 929-938 (2007).
 85. Dixon, J.E., Dick, E., Rajamohan, D., Shakesheff, K.M. & Denning, C. Directed Differentiation of Human Embryonic Stem Cells to Interrogate the Cardiac Gene Regulatory Network. *Mol Ther* (2011).
 86. Zelzer, M., *et al.* Investigation of cell-surface interactions using chemical gradients formed from plasma polymers. *Biomaterials* 29, 172-184 (2008).
 87. Cuypers, P.A., *et al.* The Adsorption of Prothrombin to Phosphatidylserine Multilayers Quantitated by Ellipsometry. *Journal of Biological Chemistry* 258, 2426-2431 (1983).
 88. Li, Z. & Guan, J. Hydrogels for Cardiac Tissue Engineering. *Polymers* 3, 740-761 (2011).
 89. Chen, Q.-Z., *et al.* Characterisation of a soft elastomer poly(glycerol sebacate) designed to match the mechanical properties of myocardial tissue. *Biomaterials* 29, 47-57 (2008).

-
90. Stella, J.A., *et al.* Tissue-to-cellular level deformation coupling in cell micro-integrated elastomeric scaffolds. *Biomaterials* 29, 3228-3236 (2008).
91. Simpson, T.R.E., Parbhoo, B. & Keddie, J.L. The dependence of the rate of crosslinking in poly(dimethyl siloxane) on the thickness of coatings. *Polymer* 44, 4829-4838 (2003).
92. Abou-Hussein, R., Wu, S., Zhang, L. & Mark, J. Effects of Some Structural Features of Poly(dimethylsiloxane) on its Unusually High Gas Permeabilities. *Journal of Inorganic and Organometallic Polymers and Materials* 18, 100-103 (2008).
93. Miao, L., Jianren, S., Ying, S., Christopher, B. & Quanfang, C. Thickness-dependent mechanical properties of polydimethylsiloxane membranes. *Journal of Micromechanics and Microengineering* 19, 035028 (2009).
94. Roylance, D. Mechanical Properties of Materials. (http://www.yarbis.yildiz.edu.tr/web/userCourseMaterials/canpolat_33671fa8cc73bc3e041fb9bf28893abc.pdf, 2008).
95. Mata, A., Fleischman, A. & Roy, S. Characterization of Polydimethylsiloxane (PDMS) Properties for Biomedical Micro/Nanosystems. *Biomedical Microdevices* 7, 281-293 (2005).
96. Wilson, S.K., Hunt, R. & Duffy, B.R. The rate of spreading in spin coating. *Journal of Fluid Mechanics* 413, 65-88 (2000).
97. Venugopal, J.R., *et al.* Biomaterial strategies for alleviation of myocardial infarction. *Journal of The Royal Society Interface* 9, 1-19 (2012).
98. Hidalgo-Bastida, L.A. University of Nottingham (2008).
99. Aldred, N., Wills, T., Williams, D.N. & Clare, A.S. Tensile and dynamic mechanical analysis of the distal portion of mussel (*Mytilus edulis*) byssal threads. *Journal of The Royal Society Interface* 4, 1159-1167 (2007).

100. Liu, M., Sun, J., Sun, Y., Bock, C. & Chen, Q. Thickness-dependent mechanical properties of polydimethylsiloxane membranes. *Journal of Micromechanics and Microengineering* 19, 35028-35031 (2009).
101. Ma, M. & Hill, R.M. Superhydrophobic surfaces. *Current Opinion in Colloid & Interface Science* 11, 193-202 (2006).
102. De Silva, M.N., Desai, R. & Odde, D.J. Micro-Patterning of Animal Cells on PDMS Substrates in the Presence of Serum without Use of Adhesion Inhibitors. *Biomedical Microdevices* 6, 219-222 (2004).
103. De Silva, M.N., Paulsen, J., Renn, M.J. & Odde, D.J. Two-step cell patterning on planar and complex curved surfaces by precision spraying of polymers. *Biotechnology and Bioengineering* 93, 919-927 (2006).
104. Eddington, D.T., Puccinelli, J.P. & Beebe, D.J. Thermal aging and reduced hydrophobic recovery of polydimethylsiloxane. *Sensors and Actuators B: Chemical* 114, 170-172 (2006).
105. Ferguson, G.S., Chaudhury, M.K., Biebuyck, H.A. & Whitesides, G.M. Monolayers on disordered substrates: self-assembly of alkyltrichlorosilanes on surface-modified polyethylene and poly(dimethylsiloxane). *Macromolecules* 26, 5870-5875 (1993).
106. Bodas, D. & Khan-Malek, C. Hydrophilization and hydrophobic recovery of PDMS by oxygen plasma and chemical treatment--An SEM investigation. *Sensors and Actuators B: Chemical* 123, 368-373 (2007).
107. Kim, H.T. & Jeong, O.C. PDMS surface modification using atmospheric pressure plasma. *Microelectronic Engineering* 88, 2281-2285 (2011).
108. Efimenko, K., Wallace, W.E. & Genzer, J. Surface Modification of Sylgard-184 Poly(dimethyl siloxane) Networks by Ultraviolet and Ultraviolet/Ozone Treatment. *Journal of Colloid and Interface Science* 254, 306-315 (2002).
109. Maheshwari, N., Kottantharayil, A., Kumar, M. & Mukherji, S. Long term hydrophilic coating on poly(dimethylsiloxane) substrates for microfluidic applications. *Appl Surf Sci* 257, 451-457 (2010).

-
110. Bodas, D. & Khan-Malek, C. Formation of more stable hydrophilic surfaces of PDMS by plasma and chemical treatments. *Microelectron. Eng.* 83, 1277-1279 (2006).
 111. Barbier, V., *et al.* Stable Modification of PDMS Surface Properties by Plasma Polymerization: Application to the Formation of Double Emulsions in Microfluidic Systems. *Langmuir* 22, 5230-5232 (2006).
 112. Kühn, G., Retzko, I., Lippitz, A., Unger, W. & Friedrich, J. Homofunctionalized polymer surfaces formed by selective plasma processes. *Surface and Coatings Technology* 142–144, 494-500 (2001).
 113. Hamerli, P., Weigel, T., Groth, T. & Paul, D. Surface properties of and cell adhesion onto allylamine-plasma-coated polyethylenterephthalat membranes. *Biomaterials* 24, 3989-3999 (2003).
 114. Stalgren, J.J., Eriksson, J. & Boschkova, K. A comparative study of surfactant adsorption on model surfaces using the quartz crystal microbalance and the ellipsometer. *J Colloid Interface Sci* 253, 190-195 (2002).
 115. Sadhu, V.B., *et al.* Surface Modification of Elastomeric Stamps for Microcontact Printing of Polar Inks. *Langmuir* 23, 6850-6855 (2007).
 116. Toworfe, G.K., Composto, R.J., Adams, C.S., Shapiro, I.M. & Ducheyne, P. Fibronectin adsorption on surface-activated poly(dimethylsiloxane) and its effect on cellular function. *J. Biomed. Mater. Res. Part A* 71A, 449-461 (2004).
 117. Harvey, P.A. & Leinwand, L.A. Cellular mechanisms of cardiomyopathy. *The Journal of Cell Biology* 194, 355-365 (2011).
 118. Bhatia, S.N., Yarmush, M.L. & Toner, M. Controlling cell interactions by micropatterning in co-cultures: hepatocytes and 3T3 fibroblasts. *J Biomed Mater Res* 34, 189-199 (1997).
 119. Altomare, L. & Fare, S. Cells response to topographic and chemical micropatterns. *J Appl Biomater Biomech* 6, 132-143 (2008).

120. Bai, H.J., Shao, M.L., Gou, H.L., Xu, J.J. & Chen, H.Y. Patterned Au/poly(dimethylsiloxane) substrate fabricated by chemical plating coupled with electrochemical etching for cell patterning. *Langmuir* 25, 10402-10407 (2009).
121. Frimat, J.P., *et al.* A microfluidic array with cellular valving for single cell co-culture. *Lab Chip* 11, 231-237 (2011).
122. Nakanishi, J., Takarada, T., Yamaguchi, K. & Maeda, M. Recent advances in cell micropatterning techniques for bioanalytical and biomedical sciences. *Analytical Sciences* 24, 67-72 (2008).
123. Chen, T.H., Chuang, Y.J., Chieng, C.C. & Tseng, F.G. A wettability switchable surface by microscale surface morphology change. *J Micromech Microeng* 17, 489-495 (2007).
124. Goubko, C.A. & Cao, X.D. Patterning multiple cell types in co-cultures: A review. *Mat Sci Eng C-Mater* 29, 1855-1868 (2009).
125. Gu, Z. & Tang, Y. Enzyme-assisted photolithography for spatial functionalization of hydrogels. *Lab Chip* 10, 1946-1951 (2010).
126. Hook, A.L., Thissen, H. & Voelcker, N.H. Surface manipulation of biomolecules for cell microarray applications. *Trends Biotechnol* 24, 471-477 (2006).
127. Inglis, D.W. A method for reducing pressure-induced deformation in silicone microfluidics. *Biomicrofluidics* 4(2010).
128. DiBartolomeo, F.J. & Trinkle, C.A. High Throughput Continuous Fabrication of Large Surface Area Microstructured Pdms. *Imece 2009: Proceedings of the Asme International Mechanical Engineering Congress and Exposition, Vol 12, Pts a and B*, 193-194 1039 (2010).
129. Huang, N.F., *et al.* A matrix micropatterning platform for cell localization and stem cell fate determination. *Acta Biomaterialia* 6, 4614-4621 (2010).

130. Shin, H. Fabrication methods of an engineered microenvironment for analysis of cell-biomaterial interactions. *Biomaterials* 28, 126-133 (2007).
131. Goessl, A., Garrison, M.D., Lhoest, J.B. & Hoffman, A.S. Plasma lithography--thin-film patterning of polymeric biomaterials by RF plasma polymerization I: Surface preparation and analysis. *J Biomater Sci Polym Ed* 12, 721-738 (2001).
132. Frimat, J.P., *et al.* Plasma stencilling methods for cell patterning. *Anal Bioanal Chem* 395, 601-609 (2009).
133. Gigout, A., Jolicoeur, M. & Buschmann, M.D. Low calcium levels in serum-free media maintain chondrocyte phenotype in monolayer culture and reduce chondrocyte aggregation in suspension culture. *Osteoarthritis and Cartilage* 13, 1012-1024 (2005).
134. Ahmed, W.W., *et al.* Myoblast morphology and organization on biochemically micro-patterned hydrogel coatings under cyclic mechanical strain. *Biomaterials* 31, 250-258 (2010).
135. Bao, G. & Suresh, S. Cell and molecular mechanics of biological materials. *Nat Mater* 2, 715-725 (2003).
136. Kurpinski, K., Chu, J., Hashi, C. & Li, S. Anisotropic mechanosensing by mesenchymal stem cells. *Proceedings of the National Academy of Sciences* 103, 16095-16100 (2006).
137. Park, J.S., *et al.* Differential effects of equiaxial and uniaxial strain on mesenchymal stem cells. *Biotechnol Bioeng* 88, 359-368 (2004).
138. Gopalan, S.M., *et al.* Anisotropic stretch-induced hypertrophy in neonatal ventricular myocytes micropatterned on deformable elastomers. *Biotechnology and Bioengineering* 81, 578-587 (2003).
139. Ben-Porath, I. & Weinberg, R.A. When cells get stressed: an integrative view of cellular senescence. *The Journal of clinical investigation* 113, 8-13 (2004).

140. Fudge, D., *et al.* The Intermediate Filament Network in Cultured Human Keratinocytes Is Remarkably Extensible and Resilient. *PLoS ONE* 3, e2327 (2008).
141. Starr, D.A. & Han, M. ANChors away: an actin based mechanism of nuclear positioning. *J Cell Sci* 116, 211-216 (2003).
142. Brown, X.Q., Ookawa, K. & Wong, J.Y. Evaluation of polydimethylsiloxane scaffolds with physiologically-relevant elastic moduli: interplay of substrate mechanics and surface chemistry effects on vascular smooth muscle cell response. *Biomaterials* 26, 3123-3129 (2005).

Appendix

1 Media and Supplements

1.1. Media A

Dulbecco's modified Eagle's Medium (DMEM) (GibcoBRL, UK)	500 ml
L-Glutamine (GibcoBRL, UK) (200mM)	5 ml
Antibiotic/antimycotic solution (containing penicillin (10000 units), streptomycin (10000 µg) and amphotericin B (125 µg) in 0.85 % w/v saline (GibcoBRL, UK)	5 ml
Foetal calf serum (FCS) (heat –inactivated (56°C for 1 hour)) (Sigma-Aldrich, Poole, UK)	50 ml
Non-essential amino acids (NEAA) (Sigma-Aldrich, Poole, UK)	5 ml

All supplements were passed through a 0.2 µm filter in to the medium. Complete medium was stored at 4°C.

1.2 Media B

Claycomb medium (JRH Biosciences, USA)	500 ml
Norepinephrine (Sigma-Aldrich, Poole, UK) (10 mM)	5 ml
L-Glutamine (GibcoBRL, UK) (200 mM)	5 ml
Antibiotic/antimycotic solution (containing penicillin (10000 units)),	

streptomycin (10000 µg) and amphotericin B (125 µg) in 0.85 % w/v saline

(GibcoBRL, UK) 5 ml

FCS (heat –inactivated (56°C for 1 hour)) (Sigma-Aldrich, Poole, UK) 50 ml

All supplements were passed through a 0.2 µm filter in to the medium. Complete medium was stored at 4°C.

1.3 Media C

Dulbecco's modified Eagle's medium –Ham's F-12 medium

(DMEM-F12) (GibcoBRL, UK) 500 ml

KnockOut serum replacement (Sigma-Aldrich, Poole, UK) 75 ml

β-mercaptoethanol (β-ME) (Sigma-Aldrich, Poole, UK) (10 mM) 5 ml

Non-essential amino acids (NEAA) (Sigma-Aldrich, Poole, UK) 5 ml

GlutaMAX (Sigma-Aldrich, Poole, UK) (200 mM) 5 ml

Basic fibroblast growth factor (bFGF) (Sigma-Aldrich, Poole, UK) 2 µg

1.4 Phosphate buffered saline (PBS) (0.01 M pH 7.4)

PBS (Dulbecco's A) tablets (Oxoid, UK) 1 tablet

Made up to 100 ml in distilled water and heat sterilized.

1.5 Ethylenediaminetetraacetic acid (EDTA) stock solution (2 %)

EDTA (Sigma, UK) 0.5 g

Made up to 25 ml PBS (see 1.4)

1.6 Trypsin/EDTA solution

Trypsin (Sigma, UK) 2.5 % 10 ml

EDTA (2%) 1 ml

Made up to 100 ml with PBS (see 1.4), filter sterilised and stored - 20°C

1.7 Freezing medium (Sigma-Aldrich, Poole, UK)

Dimethyl Sulphoxide (DMSO) 2 ml

FCS (heat-inactivated (56°C for 1h)) 18 ml

Passed through a 0.2 µm filter and used immediately.

2 Other Solutions

2.1 Triton-X 100 solution (0.1 % v/v)

Triton-X 100 (Sigma-Aldrich, Poole, UK) 20 µl

PBS to 20 ml

2.2 Poly vinyl acetate (PVA) solution (30 %)

PVA (Sigma-Aldrich, Poole, UK) 300 g

Distilled water 1 L

Stirred at room temperature overnight and filtered before use.

3 General cell maintenance

3.1 Cryopreservation

Cells were maintained in an actively growing state to ensure optimum health and good recovery prior to storage. Cells were detached from the culture vessel (minimum cell density: 5×10^6 cells/ ml) before being re-suspended in freezing medium (appendix 1.7). The cell suspension was subsequently aliquot in to cryogenic storage vials and placed into an isopropanol-containing cryo-container (Mr Frosty, Sigma, Poole, UK), before being 'stepped-frozen'- by placement into a -80 °C freezer for 24 hours, after which the vials were transferred to liquid nitrogen for further long-term storage.

3.2 Cell revival from storage

Cells were removed from storage and immediately placed into a water bath (37 °C) until thawed. Immediately after thawing, the cell suspension was slowly introduced into a T75 cm² flask containing complete, pre-warmed media. Cells were incubated for 24 hours before the medium was changed to remove the DMSO from culture.

3.3 Trypan blue exclusion assay

Viable cell counts were performed using the trypan blue exclusion technique by means of a 0.22µm sterile filtered 0.5 % (w/v) trypan blue solution and a haemocytometer. An equal ratio of cell suspension: trypan blue were mixed to create a homogenous solution and transferred onto a haemocytometer. The cells within 5 separate squares were counted under a light-inverted microscope. The average cell number per square was determined and multiplied by 10⁴ to give the final cell density (cells/ml). Non-viable cells stained blue due to the loss of their membrane integrity, allowing trypan blue to pass into the cell. Viable cells remained colourless.

4 Standard curve derivation

4.1 Alamar blue assay

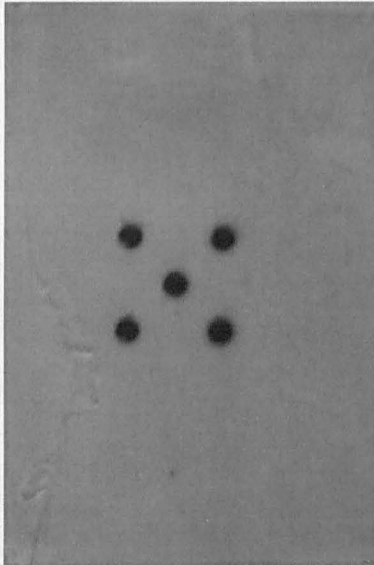
Alamar Blue reagent (Invitrogen, Paisley, UK)	25 ml
Hanks Balanced Salt Solution (HBSS)	225 ml

Cell suspensions were created into 2 ml aliquots using the Alamar Blue solution containing the following cell densities in 10^4 cells/ml: 100, 50, 25, 12.5, 6.25, 3.125, 1.5625, 0. Cell suspensions were plated in to tissue culture treated 6-well plates and incubated for 90 minutes. Subsequently, cells were analysed fluorometrically (ex 560 nm/ emm 590 nm) using an Infinite™ M200 plate reader (Tecan). Triplicates of each cell density were used. Cell number vs. Average relative fluorescence units (RFU) was plotted to derive the line equation and correlation co-efficient ($y=0.212x +2778.9/ R^2= 0.9671$). The line equation was used to extrapolate cell numbers at specific time points for cell culture experiments.

5 Sample Preparation for CMS testing on BOSE

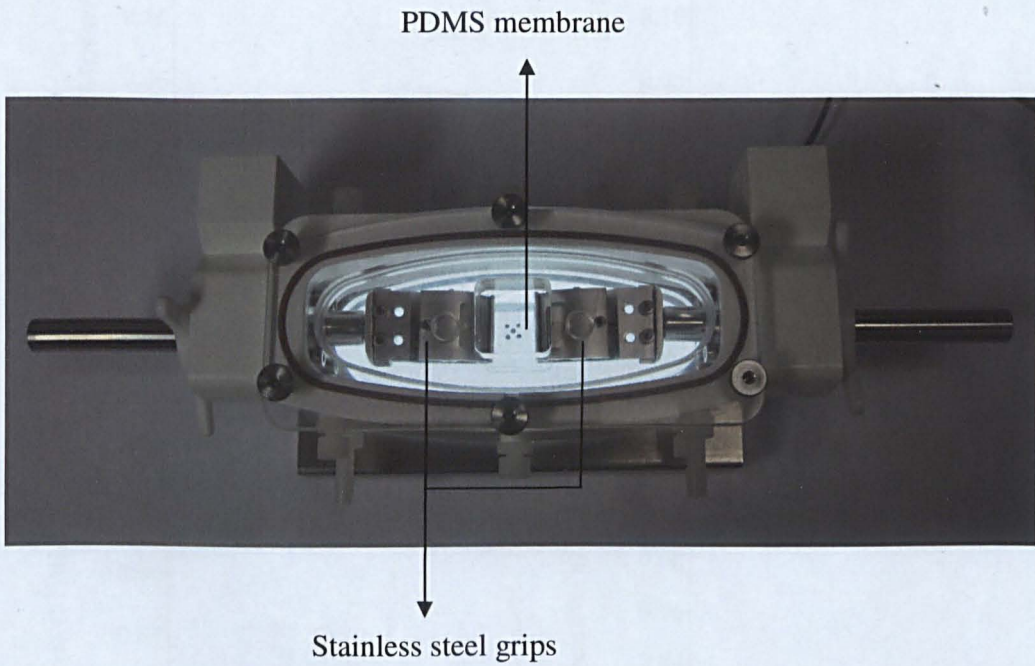
5.1 Membrane Preparation

The image below shows the five dot dice pattern marked on a PDMS membrane using permanent marker. The extensometer was used to measure tensile strain by monitoring the distance between the five dots.



5.2 Fatigue bath containing PDMS membrane

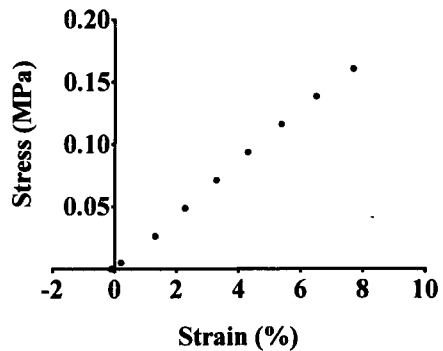
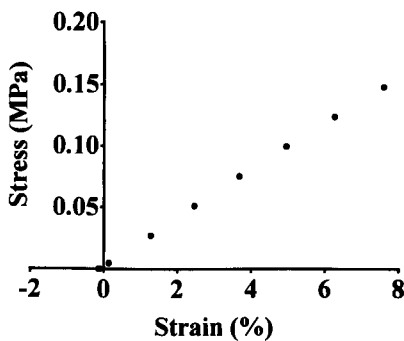
Image showing a PDMS membrane held between two tensile grips inside the fatigue bath used for cyclic testing on the BOSE bioreactor.



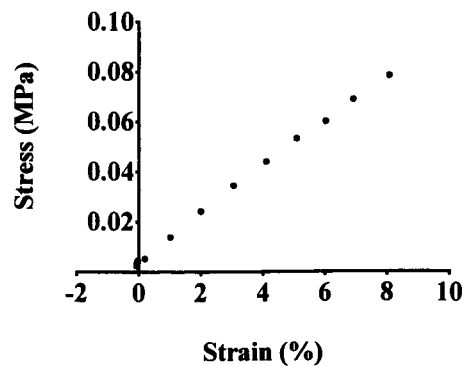
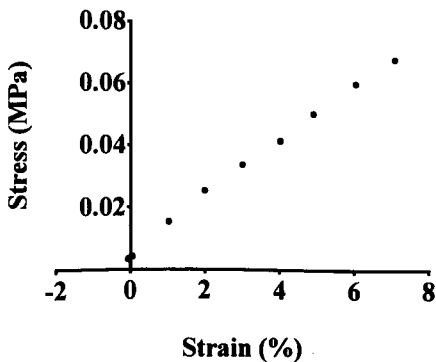
5.3 Stress-strain plots of PDMS membranes subjected to uniaxial tension

Below is the stress-strain curves of four membranes spin coated at A) 250 rpm and B) 2000 rpm, subjected to uniaxial tension at a strain rate of 1 mm/30 seconds. Each membrane was stretched within its linear elastic region. The gradient of these stress-strain curves was measured automatically using Q800 software to obtain the Young modulus of each PDMS membrane.

A. 250 rpm



B. 2000 rpm



5.4 Cyclic mechanical strain of PDMS membrane spin coated at 2000 rpm (10 s duration)

Scatter line graph showing PDMS membrane of $47\ \mu\text{m}$ thickness being subjected to cyclic mechanical strain (CMS), triangular waveform at 1 Hz, 0-10 % for a 10 s duration, the membrane was subjected to CMS for a total duration of 72 hours.

Inset, an illustration of the physical effect on a PDMS membrane during one cycle.

